MONTANA STATE UNIVERSITY

Heat transfer from a horizontal bundle of tubes in an air fluidized bed
by William James Bartel

A thesis submitted to the Graduate Faculty in partial fulfillment of the requirements for the degree of Doctor of Philosophy in Chemical Engineering
Montana State University
© Copyright by William James Bartel (1971)

Abstract:
Growth characteristics of sheep from birth to maturity and the evaluation of the genetic and phenotypic relationships between growth traits with lifetime lamb and wool production were studied using data from 302 Rambouillet, 338 Targhee and 175 Columbia ewes born between I960 and 1976. The Brody (1945) growth model was used for the derivation of growth parameters mature weight (A) and maturing rate (k). The Fitzhugh and Taylor (1971) equation-free model was used for the estimation of growth statistics; Absolute Growth Rate (AGR), Relative Growth Rate (RGR) and Absolute Maturing rate (AMR) for five intervals from birth to 18 mo. Genetic and phenotypic parameters were estimated by half-sib intraclass correlation using Harvey (1977) leastsquares method for each breed and for the pooled data. Targbees were superior to Rambouillet and Columblas for weight of lamb at weaning (ATWW) and efficiency index (El). ATWW was the lifetime yearly average of kg of lamb weaned and El was ATWW per unit of ewes mature weight (A). Columblas were superior for yearly average grease wool produced (ATFP). Age at maturity was estimated on 39 mo, 38 mo and 41 mo for Rambouillets, Targbees and Colimbias, respectively. Columblas had the highest A and the smallest k, Targbees matured the fastest. Ewes born twins had the highest El. From the pooled data, heritabillty estimates of average total of lambs born (ATLB), average total of lambs weaned (ATLW), average total weight of lambs weaned (ATWW), average total grease fleece produced (ATFP) and El were .43±.15, .33±..15, .11±>15, 68±..16 and .15±,15, respectively. Genetic correlation, between ATWW and A, indicated that ewes with hlgft additive genetic potential for ATWW will have high genetic potential for larger A. The genetic correlation between ATWW and k was zero. For the three Fitzhugh and Taylor (1971) growth statistics, highest her! ta bill ties were obtained for the weanlng-12 mo interval: AGR2 (.80+.16), RGR2 (.76+.16) and AMR2 (.81+.16). RGR2 had the highest positive genetic correlations with ATWW (.95+.81), El (.77+.S2) and ATFP (.39+.19) among growth statistics. Inclusion of AGR2 and RGR2 in the construction of selection indexes would improve accuracy of selection for ATWW, ATFP and El. However, the contributions of A and k were inferior to AGR2 and RGR2. The use of any of the growth traits studied in selection indexes for improvement of ATFP and El simultaneously gave no advantage in improving efficiency of selection.

HEAT TRANSFER FROM A HORIZONTAL BUNDLE OF TUBES IN AN AIR FLUIDIZED BED

by

WILLIAM JAMES BARTEL

A thesis submitted to the Graduate Faculty in partial fulfillment of the requirements for the degree

of

DOCTOR OF PHILOSOPHY

in

Chemical Engineering

Approved:

Lloyd Berg
Head, Major Department

William E. Jennett
Chairman, Examining Committee

Henry L. Parsons
Graduate Dean

MONTANA STATE UNIVERSITY
Bozeman, Montana

August, 1971

ACKNOWLEDGEMENT

The author wishes to acknowledge the assistance of the Chemical Engineering staff at Montana State University for the helpful suggestions made throughout the duration of this research project. Appreciation is also expressed to the members of his Graduate Committee for their time spent in reviewing this thesis and in performing miscellaneous chores related to the project.

Special thanks go to Dr. William E. Genetti, Graduate Adviser, who made so many helpful contributions throughout the entire project, from the design of the equipment through the correlation of the data.

Financial assistance for the study was obtained from a number of sources, including a joint Idaho Nuclear Corporation-Associated Western University Fellowship during the first year, and from an NDEA fellowship and a departmental Teaching Assistantship during the last two years.

TABLE OF CONTENTS

	Page
INTRODUCTION	1
THEORY AND PREVIOUS RELATED RESEARCH	6
The Mechanism of Fluidization	6
Heat Transfer between Fluidized Beds and Surfaces	14
EXPERIMENTAL PROGRAM	20
EXPERIMENTAL EQUIPMENT	27
Fluidizing System	27
Electrical System	29
Heater and Tube Assemblies	31
Equipment Drawings	34
EXPERIMENTAL PROCEDURE	45
Determination of Minimum Fluidizing Velocities	45
Calibration of Air Line Gate Valves	47
Determination of Thermocouple Location on Tubes	48
Procedure for a Typical Run	50
CALCULATIONS	54
PERFORMANCE OF INDIVIDUAL TUBE BUNDLES	62
Bare Tubes	66
Finned Tubes	69
Performance Curves for Bare Tubes	75
Performance Curves for 1/8 inch Finned Tubes	79
Performance Curves for 3/8 inch Finned Tubes	88
Performance Curves for 5/8 inch Finned Tubes	93
Performance Curves for 7/8 inch Finned Tubes	98
COMPARATIVE PERFORMANCE OF ALL TUBE BUNDLES	103
Comparative Performance Curves	107
Kinetic Analogy	116

TABLE OF CONTENTS (Continued)

	Page
CORRELATION	119
Model used for Correlation	119
Redefining Heat Transfer Coefficient	125
Correlation for Expanded Bundle or for Single Horizontal Tube	135
Final Correlation for all Experimental Data	141
MISCELLANEOUS RELATED STUDIES	145
Optimum Fin Length for an Overall Available Diameter	145
Effect of Particle Surface Area on Heat Transfer Coefficients	149
CONCLUSIONS	156
RECOMMENDATIONS FOR FURTHER STUDY	161
BIBLIOGRAPHY	163
NOMENCLATURE	165

LIST OF FIGURES

Figure		Page
1	Schematic Drawing of Equipment	34
2	Details of Fluidizing Column	35
3	Column and Supporting Mechanism	36
4	Details of Micarta Plate	37
5	Tubes Assembled in Micarta Plate	38
6	Details of Bed Thermocouples and Pressure Taps	39
7	Details of a Typical Bare Tube	40
8	Details of a Typical Finned Tube	41
9	Details of Electrical Heater	42
10	Tube and Heater Assembly	43
11	Tube Surface Area	44
12	Comparison of Experimental and Theoretical Minimum Air Velocities	46
13	Bypass Valve Settings	49
14	Nomenclature used with Bare Tubes	73
15	Nomenclature used with Finned Tubes	74
16	Performance of Bare Tubes - Particles	76
17	Performance of Bare Tubes - No Particles	77
18	Comparison of Experimental Data with Correlations from Literature	78
19	Performance of 0.125" Finned Tubes	80
20	Performance of 0.125" Finned Tubes.	81

LIST OF FIGURES (Continued)

Figure		Page
21	Performance of 0.125" Finned Tubes	82
22	Performance of 0.125" Finned Tubes	83
23	Performance of 0.125" Finned Tubes - Small Particles	84
24	Performance of 0.125" Finned Tubes - Medium Particles	85
25	Performance of 0.125" Finned Tubes - Large Particles	86
26	Performance of 0.125" Finned Tubes - No Particles	87
27	Performance of 0.375" Finned Tubes - Small Particles	89
28	Performance of 0.375" Finned Tubes - Medium Particles	90
29	Performance of 0.375" Finned Tubes - Large Particles	91
30	Performance of 0.375" Finned Tubes - No Particles	92
31	Performance of 0.625" Finned Tubes - Small Particles	94
32	Performance of 0.625" Finned Tubes - Medium Particles	95
33	Performance of 0.625" Finned Tubes - Large Particles	96
34	Performance of 0.625" Finned Tubes - No Particles	97
35	Performance of 0.875" Finned Tubes - Small Particles	99
36	Performance of 0.875" Finned Tubes - Medium Particles	100
37	Performance of 0.875" Finned Tubes - Large Particles	101
38	Performance of 0.875" Finned Tubes - No Particles	102
39	Summary of Coefficients Based on Total Area - Small Particles	108
40	Summary of Coefficients Based on Total Area - Large Particles	109

LIST OF FIGURES (Continued)

Figure		Page
41	Summary of Coefficients Based on Bare Tube Area - Small Particles	110
42	Summary of Coefficients Based on Bare Tube Area - Large Particles	111
43	q/ΔT versus Fin Height - Small Particles	112
44	q/ΔT versus Fin Height - Large Particles	113
45	Effectiveness Factor versus Fin Height - Small Particles	114
46	Effectiveness Factor versus Fin Height - Large Particles	115
47	Analogy of Simplified Kinetic Model Applied to Fin Tubes	116
48	q/ΔT versus Reduced Velocity - Small Particles	117
49	q/ΔT versus Reduced Velocity - Large Particles	118
50	Schematic of Proposed Heat Transfer Mechanism	120
51	Schematic used for deriving Equation for Temperature Profile in Fin	126
52	Solutions to Equation relating q/ΔT to h	131
53	Correlation for Expanded Bundles, with variable $(1 - \epsilon)$	137
54	Average of $(1 - \epsilon)$ Values measured in This Study	138
55	Correlation for Expanded Bundles, with constant $(1 - \epsilon)$	139
56	Correlation for Bundles with all Tube Spacings	143
57	Comparison of Rate of Heat Transfer in a restricted Overall Diameter	146
58	Photomicrographs of Particles	150
59	Comparison of Coefficients for Sand Particles and Glass Particles	151

ABSTRACT

Heat transfer coefficients were measured for heat transfer from a bundle of electrically heated horizontal tubes in a bed of glass particles fluidized with air. The studies were carried out with carbon steel tubes and fins in a clear Plexiglas column, 15.5" wide, 8.125" deep, and 74" high. Bare tubes and serrated finned tubes were studied, and experimental variables included fin height, tube spacing, particle diameter, and air velocity.

Two smaller related studies were also made, including a measurement of the performance of finned tubes arranged into a tightly meshed bundle, and the effect of particle surface area on the heat transfer coefficient.

The results indicated that the rate of heat transfer increased with increasing fin height, but that the performance curves leveled off at a fin height of about one inch, and that little increase in the rate of heat transfer would be gained with longer fins. It was also found that the rate of heat transfer from a bundle of tubes with long fins was almost independent of the spacing between the tubes, but with short fins the rate of heat transfer was quite sensitive to tube spacing. The heat transfer rates with all bundles increased with an increase in the fluidizing air velocity, but in most cases a maximum was reached, and a further increase in air velocity resulted in a decrease in the rate of heat transfer. There was a large increase in the rate of heat transfer between the largest particles (0.0185" diameter) and the medium particles (0.0110" diameter), but there was relatively little difference in the rate between the medium particles and the smallest particles (0.0080" diameter).

The data were correlated into a single equation which relates the heat transfer coefficient to the four experimental variables for all fin heights and tube spacings investigated.

INTRODUCTION

The terms "fluidization" and "fluidized bed" are used to describe the condition in which a bed of particles is suspended in a gas or liquid stream passed upward through the bed. For example, consider a cylindrical column containing a volume of dry sand supported on a porous plate. As air is passed upward through the porous plate the bed will remain static until the air velocity is increased to a rate at which the pressure drop across the bed equals the weight of the solids in the bed. At this point the sand particles will become suspended in the air stream and in its mobility the aerated sand will resemble a liquid of high viscosity. The air velocity at which the first signs of fluidization are detected is known as the "minimum fluidization" velocity. At air velocities close to minimum there is little solids movement. Fine particles are carried to the top of the bed very slowly, while coarse or dense particles settle to the bottom. If the air velocity is increased beyond a critical value, the gas starts to rise in well defined, rapidly moving "pockets" or "bubbles". These are regions of very low solids concentration compared with the surrounding gas-solids mixture which is referred to as the "emulsion" phase. This "bubble" type of fluidization is the kind that is normally encountered in fluidized beds; it is known as "aggregative fluidization". This is the type of fluidization that was observed in all of the runs made in this study.

The earliest recorded applications of fluidized beds occurred in the 16th century when fluidization was used in ore processing. From that time until the early 1900's there were a few limited applications of fluidization in the areas of municipal water purification, using sand filters, and in small scale catalyzed reactions in which a finely divided catalyst was suspended in a gas stream. The first large scale commercial use of fluidization was developed in Germany in 1921 when a patent was awarded to Fritz Winkler for the manufacture of water and producer gas by the gasifaction of powdered coal. The Winkler process was inefficient, however, because of its high oxygen consumption and its large carbon loss by entrainment.

The petroleum industry provided impetus to fluidized bed studies in this country when in 1937 it introduced the process of catalytic cracking. When this process was first developed, the cracking was carried out in a fixed bed of catalyst pellets, and when the pellets became fouled by carbon formed in the reaction, it was necessary to regenerate the catalyst. To do this, the oil feed was stopped and air was introduced to burn the carbon off the catalyst. This intermittent operation was complex and costly. Something simpler was needed. Moving the catalyst continuously between the cracker and a regenerator seemed a likely approach, because in this way conditions would be constant at any given point in the apparatus during the entire operating period. The idea of transporting the pellets between cracker and regenerator with a mechan-

ical conveyor was rejected because of the potential mechanical problems and because of the cost of high speed conveyors. Pneumatic transport of finely powdered catalyst appeared to be the best way to go, so research was initiated in both petroleum research laboratories and university laboratories to work out the details of the system. Remarkably smooth pilot plant operations were obtained almost from the start, and in 1942 the first full scale commercial fluid cracking plant was put into operation.

The highly successful application of fluidization in the petroleum industry led to research into other potential fields of application. Recently a process was developed whereby radioactive waste solutions are converted to a safer solid form by spraying the solution into a hot bed of fluidized granular solids. A portion of the solution is vaporized and passed to an off-gas scrubbing system, while the radioactive component solidifies on the surface of the particles. The particles are gradually withdrawn from the column and transported to underground storage bins.

A similar process is being investigated for producing municipal water by desalting sea water. The salt water would be sprayed into a hot bed of fluidized salt particles where the water would vaporize, pass from the column, and be condensed for use as drinking water. The salt in the sea water solution would be deposited on the salt particles, and granulated salt particles would gradually be withdrawn from the

column as a by-product of the process.

In other applications, fluidization has been used for the roasting of sulfide ores, the drying of powdery materials, and the calcination of limestone. Also, the recent introduction of fluidization into the process of reducing iron oxide has caused some radical changes in this important industry.

In many applications of fluidized beds it is necessary to supply heat to the bed. The walls of the bed are sometimes heated to produce the necessary bed temperature, but more frequently a heated bundle of horizontal or vertical tubes is immersed in the bed.

Heat transfer coefficients for heat transfer from a surface to the fluid in a gas fluidized bed are many times larger than corresponding forced convection coefficients for one phase flow. This increase in heat transfer is attributed to the increased turbulence the fluidized bed creates, as well as to the energy transferred by solids in contact with the surface. Because of the high coefficients it is possible to transfer large amounts of heat with moderate exchanger surface requirements.

Although a number of investigators have studied heat transfer from bundles of bare tubes positioned horizontally or vertically in a fluidized bed, very little research has been performed with finned tube bundles. The surface area added by the fins would greatly increase the rate of heat transfer and allow for a smaller heat exchanger for a given

application. The purpose of this study is to provide some information on how the heat transfer coefficients of horizontal finned tube bundles are affected by the height of the fins and the spacing between the tubes, along with other operating variables.

THEORY AND PREVIOUS RELATED RESEARCH

The theoretical work and previous research in fluidized bed technology can be classified into two broad categories:

1. The mechanism of fluidization
2. Heat transfer between fluidized beds and surfaces

The Mechanism of Fluidization

The study of the behavior of the bubbling action taking place in a fluidized bed begins with the study of a single rising bubble in the bed, through the region of higher solid density called the emulsion phase. Davidson (6) postulated an elegant model which accounted for the movement of both gas and solid and the pressure distribution around rising bubbles. The model postulates three conditions, namely: (1) a gas bubble is solid-free and spherical in shape, (2) as the bubble rises the particles move aside as would an incompressible inviscid fluid, and (3) the gas flows in the emulsion phase as an incompressible fluid. He also included two boundary conditions which state that (a) far from the bubble the undisturbed pressure gradient exists, and (b) the pressure in the bubble is constant.

These postulates and boundary conditions are sufficient to give the flow pattern for solids and for gas, as well as the pressure distribution, in the vicinity of the rising bubble. A mathematical analysis

indicates that the pressure in the upper part of the bubble is higher than the pressure in the surrounding bed, while the pressure in the lower part of the bubble is lower than the bed pressure. Thus, gas flows into the bottom of the bubble and out the top. The theory also indicates that the volume of gas passing through a bubble as it rises in the bed is three times the amount of gas passing through an equal volume in the emulsion phase in the same time. The Davidson model explains the stability of bubbles in that it is the upward flow of gas through the bubble which keeps the roof from collapsing.

Experiments have shown the Davidson model to be essentially correct, with the most noticeable deviation being that the shape of the lower part of the bubble is not spherical as postulated, but is actually concave. The reason for this is that the pressure in the lower part of the bubble is less than in the nearby emulsion phase. The gas is thereby forced into the bubble, resulting in an instability, partial collapse of the bubble, and turbulent mixing behind it. Rowe and Partridge (23) suggested that this is the primary mechanism by which solids mix in a vigorously bubbling bed.

Various experimenters (9, 11, 24), using photographic methods, have shown that the bubble is not quite solid-free as postulated by Davidson, but actually contains 0.2 to 1.0% solids.

The theories and experiments relating to single bubbles must now be related to multi-bubble behavior in ordinary bubbling beds. Many

studies have been conducted to determine how small bubbles coalesce and grow, how large bubbles break up into smaller bubbles, and in general what goes on in a fluidized bed.

Numerous investigators have shown that bubble size increases with gas velocity and with height in any bed. Botterill, George, and Besford (4) showed that at any fixed point in a bed, at least 20 centimeters above the distributor plate, the same number of bubbles will pass the point in any given time interval no matter what the gas flow rate. This indicates that the effect of gas flow rate is to change the size of bubbles passing the point.

Toei, et al. (24) investigated the interaction of two rising bubbles, one trailing the other. X-ray photographs showed that the trailing bubble moves into the wake behind the leading bubble, the trailing bubble is then elongated, and finally is drawn into the leading bubble.

Before a complete model can be postulated for the mechanism of fluidization, it is necessary to determine particle movement as well as bubble movement. Kondukov, et al. (12) plotted the trajectories of radioactive particles and found a very erratic path of the individual particles, showing that they wander everywhere in the bed. There is a definite up-and-down movement, the upward being rapid, the downward being relatively slow. Thus, solids spend most of their time moving downward slowly, but occasionally are swept upward to the top of the bed. Other approaches to the study of particle movement include measuring the

residence time distribution of particles fed and discharged into and from a fluidized bed, and measuring the rate of vertical mixing of solids in terms of the flux of solids across a horizontal plane in the bed. This latter investigation was performed by measuring the change in concentration of tracer within one of the regions in a two-region bed, with one region above the other. Lateral diffusion of solids was studied by Brötz (5) with a shallow rectangular bed in which particles of two different materials were separated by a removable partition. At time zero the partition was removed, and the rate of approach to uniformity of solids was measured.

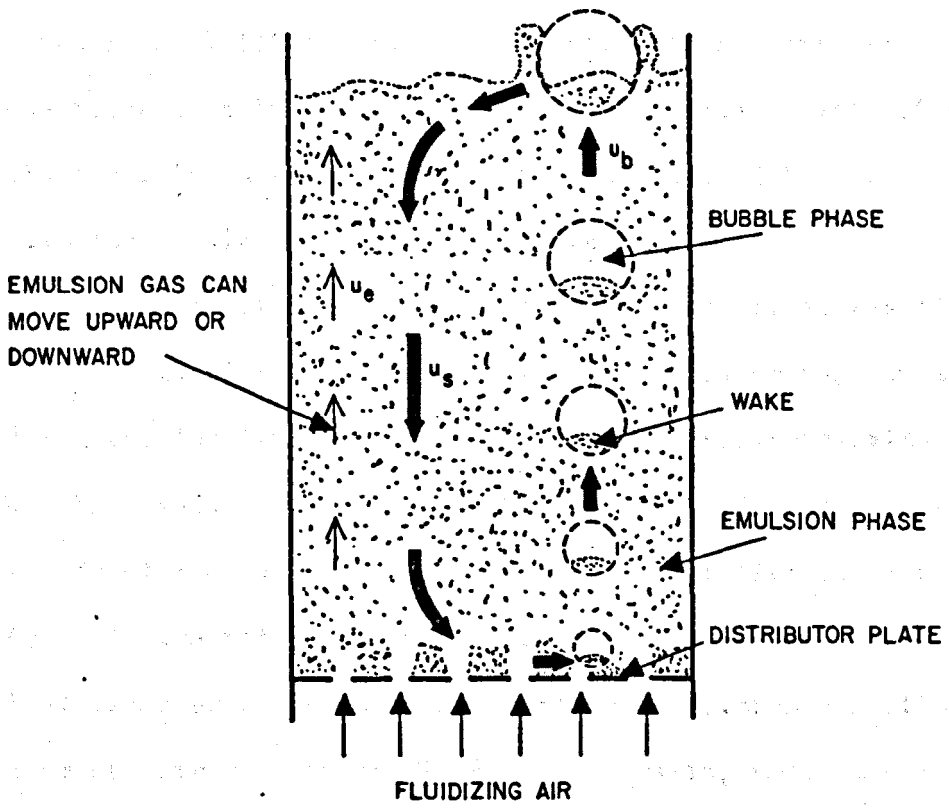
Putting together the available information on bubble and particle movement, the following simplified model of fluidization was postulated (13):

1. Every rising bubble drags behind it a wake of gas and particles.
2. Just above the distributor plate, solid is entrained by rising bubbles to form the bubble wake. This solid is carried up the bed at velocity u_b and is continually exchanged with fresh emulsion solid as it rises. At the top of the bed this wake solid rejoins the emulsion to move down the bed at velocity u_s.
3. The relative velocity between the upward percolating emulsion gas, u_e, and the downward flowing solids, u_s, is given by the minimum fluidizing conditions:

$$u_e = \frac{u_{mf}}{\epsilon_{mf}} - u_s$$

This expression shows that if the downward velocity of solids, u_s, is sufficiently high, as may be the case in vigorously bubbling beds, then since u_{mf}/ϵ_{mf} is constant, u_e may be negative, indicating that the emulsion gas is flowing downward instead of upward. This result seems surprising, but tracer studies in vigorously bubbling beds support this finding.

A simple sketch of the model is shown below:



Despite the many interesting aspects of fluidization, experience so far gained indicates that a wholesale substitution of fixed beds by fluidized beds is by no means in sight. As with most processes and operations there are advantages and disadvantages on both sides. The most important are as follows (14):

Advantages:

1. Owing to the intense agitation in a well-fluidized dense-phase bed, local temperatures and solids distribution are much more uniform than in a fixed bed. This may be important in many chemical and catalytic processes.
2. Since in a fluidized bed particle size is of a smaller order of magnitude than in a fixed bed, the resistance to diffusion through the particle is smaller in a fluidized bed. This, too, may benefit many chemical and catalytic reactions.
3. Fluidization will permit the ready additions of solids to or the withdrawals of solids from the bed. This is an important advantage over the fixed bed, especially where rapid-activity losses are involved. This property of the fluidized system is responsible for the ease with which continuous operation is achieved.
4. Owing to the motion of the particles past internal or external heat transfer surfaces, heat transfer coefficients in fluidized beds are higher than in fixed beds operating under the same conditions. Thus the fluidized bed offers a great advantage where

highly exothermic or endothermic reactions are involved.

5. Although heat transfer coefficients between solid particles and fluid appear to be of the same order of magnitude in both fluidized and fixed beds when both are operating under comparable flow rates, the state of subdivision and heat transfer surfaces are so much greater in the fluidized bed that the rate of solids-fluid heat transfer is actually much higher in the fluidized bed.
6. Because of the high solids-fluid heat transfer rates, fluidized solids lend themselves more readily to recovery of heat from waste solids than do the generally larger solids particles of fixed beds.
7. In many instances fluidization will cause a smaller pressure drop than will fixed bed operation.
8. Fluidization will eliminate catalyst pelleting, an important cost item in many catalytic processes.

Disadvantages:

1. The average flow of the solids and fluids in the single-bed fluidized reactor is concurrent. This has an unfavorable effect on the driving force. In order to approach countercurrent flow, a multicompartment reactor is required. This is much more expensive than a fixed bed.
2. From low height-to-diameter ratios there may result appreciable longitudinal mixing of fluid and solids in the fluidized reactor.

This may lead to low conversion rates and a reduction in selectivity.

3. During a fluidized operation, a catalyst may undergo attrition, or size reduction. Thus the fluidization properties of the material may become different and require adjustment of fluid rates.

4. In the fluidized reactor the fluid velocity must be closely coordinated with the properties of the solids so that adequate fluidization results. Thus the fluidized reactor is in this respect restricted, while the fixed bed offers a great degree of freedom and adjustment of space velocity.

5. Fluidization with gaseous components is possible only if no liquids or waxes will form during the reaction. This is a severe restriction and a great disadvantage as compared with the fixed bed, as experience with the hydrocarbon synthesis has disclosed.

6. In fluidized-operation equipment, erosion may be serious. Special and generally expensive designs may be required to eliminate or minimize wear in reactors and transfer lines.

7. Owing to solids carry-over, known as elutriation, installation for fines recovery may be required.

8. Attrition and formation of fines leads to catalyst losses. These must be replaced in the fluidized unit. The cost involved may be appreciable.

Heat Transfer between Fluidized Beds and Surfaces

In the study of heat transfer between fluidized beds and surfaces, numerous models have been postulated by investigators to explain the large heat transfer coefficients compared to coefficients for forced convection.

Leva, et al. (15), Dow and Jakob (7), and Levenspiel and Walton (16) proposed models in which the scouring action of descending solids on a gas film on the surface is responsible for decreasing the effective film thickness and increasing the rate of heat transfer. The latter two investigators derived a simple expression for the effective film thickness for both streamline and turbulent flow conditions which accounts for the frequency of scouring of the film and its growth rate as given by film growth on flat plates.

In contrast with these thin-layer models, Mickley and Fairbanks (17) viewed the unsteady heating of elements of packets of emulsion phase as the vehicle for heat transfer. These packets are viewed to rest on the surface for a short time, only to be swept away and replaced by fresh emulsion from the main region of the bed. After leaving the surface, the packets break up and dissipate heat to the bulk of the bed.

There have been several extensions, modifications, and additions to the theory presented by Mickley and Fairbanks. A recent modification was proposed by Ziegler, Koppel, and Brazelton (28), and extended by Genetti and Knudsen (8). A particle is viewed to move to the wall

region where it is suddenly bathed by fluid at the wall temperature. It absorbs heat from the gas by unsteady-state conduction while the gas temperature remains unchanged and particle-to-wall contact is ignored. Assuming a rectangular packing for the particles, a gamma function for the residence time distribution of solids in the wall region, they found that the Nusselt number is given by

$$Nu_p = \frac{7.2}{\left(1 + \frac{6k_{air}\bar{t}}{\rho_s C_{ps} D_p^2} \right)^2}$$

where,

Nu_p = hD_p/k_{air} = particle Nusselt number, dimensionless

k_{air} = thermal conductivity of fluidizing air, BTU/Ft-Hr-F$^\circ$

$\bar{t}$ = mean residence time of solids, Hr

ρ_s = density of solids, Lbs/Ft^3

C_{ps} = specific heat of solids, BTU/Lb-F$^\circ$

D_p = mean particle diameter, Ft

In their extended model, Genetti and Knudsen recommended that the expression $10(1 - \epsilon)^{0.5}$ be substituted for the constant 7.2 in the numerator and that the average of the wall temperature and the bulk mean temperature be used for the film temperature. The data in the present study were correlated in the form of the extended model. The correlation and additional discussion of the model are presented on page 119.

An experiment performed by Ziegler and Brazelton (27) confirms a particle mode heat transfer mechanism. These experimenters measured simultaneous heat and mass transfer from a 1.5 inch diameter celite sphere saturated with water. The rates of mass and heat transfer were measured simultaneously when the sphere was placed in an air stream and when the sphere was placed in a fluidized bed. The particles used had negligible absorptivity for the diffusing water and consequently had no capacity for mass transfer. As a result, the only mechanism of importance for transfer of mass was diffusion through the film. Without fluidized particles the transfer of mass and heat are analogous; that is, both types of transfer can be considered as diffusion through the film. If heat is not transferred by a particle mode, mass and heat transfer coefficients would increase by the same factor. If heat is transferred by a particle mode the analogy breaks down and mass and heat transfer would increase by different factors. These experimenters observed increases in heat transfer coefficients from 10 to 20 fold, but mass transfer coefficients only increased by a factor of 1.5 to 2. They concluded that 80 to 95 percent of the heat was transferred by a particle mode.

Previous Research with Horizontal Tubes:

The only previous research found in the literature that was performed with the same type of serrated finned tubes used in the present investigation was reported in a paper by Bartel, Genetti, and Grimmett (2)

in which the effect of fin height, fin thickness, fluidizing air velocity, and particle diameter on the heat transfer coefficient of a single horizontal tube was studied. The present investigation is a continuation of that study.

In an investigation similar to the present study, Petrie, Freeby, and Buckham (22) measured heat transfer coefficients for a horizontal bundle of tubes with continuous helically wound fins. These experimenters used a horizontal bundle of nineteen 0.75 inch diameter aluminum tubes, with condensing steam as the heat source. Three tube bundles were used; one having bare tubes (no fins), another with tubes having 5 fins/inch, and the third with tubes having 11 fins/inch. All of the finned tubes had fins with length equal to 0.4 inch. The bare tube heat transfer data were correlated into a single equation relating the heat transfer coefficient to the experimental variables. The correlation and a comparison with data obtained in the present study are shown on pages 66 and 78. Based on their limited data, the following conclusions were reached by the above investigators:

1. The effectiveness factor for the finned tubes is directly related to the fluidizing velocity. The effectiveness factor is defined on page 60 of the present report.
2. The effectiveness factor for finned tubes is inversely related to the particle diameter.
3. Increasing the number of fins on the tube decreases the effective-

ness of the finned tubes; however, the increased area more than compensates for the decreased effectiveness factor over the range studied.

Another correlation for single horizontal bare tubes in a fluidized bed often cited in the literature is that presented by Vreedenberg (25). His recommended correlation and a comparison with the data obtained in the present study are shown on pages 67 and 78.

Kearns (10), in a two part paper, discussed various aspects of fluidization in a rectangular column containing horizontal tubes. His visual observations indicated that uniform fluidization in the bed and temperature distribution around the horizontal tubes can be inhibited by stagnant "caps" (areas of poor fluidization) on the tops of the tubes, by defluidized regions between horizontal tubes and the bed wall, and by defluidized regions in the corners of the bed. His heat transfer experiments with a 2 inch diameter para-dichlorobenzene cylinder gave heat transfer coefficients on top of a horizontal tube 7.5 times smaller than coefficients at the bottom.

Botterill, et. al. (3) investigated the flow of fluidized solids past arrays of tubes, making both heat transfer and pressure loss studies. They concluded that the presence of a surface disturbs the fluidization and there is a loss in fluid-like properties at the surface, resulting in decreased heat transfer rates. Their experimental observations agreed with those of Kearns, in that they observed a wake behind

each horizontal tube, and the resulting defluidization there reduced the local particle circulation and decreased the local heat transfer coefficient. In the present study no variation in surface temperature around the tube was measured, apparently because the tube wall thickness and the thermal conductivity of the carbon steel were large enough to "conduct away" any circumferential differences in tube surface temperature.

Numerous papers have been published containing information pertaining to heat transfer between the walls of the vessel and the fluidized bed, and for heat transfer from immersed vertical tubes in a bed. This information is summarized by Kunii and Levenspiel (13), and since it is not directly related to the present study it will not be discussed in this report.

EXPERIMENTAL PROGRAM

The primary objective of this investigation was to determine the effect of tube spacing and fin height on the heat transfer coefficient of each tube in a horizontal bundle of seven serrated, or discontinuous, finned tubes. This objective was attained by following the approach outlined below:

I. Determine parameters to be varied

   a. List parameters which might affect heat transfer coefficient of tubes.

   b. Select those parameters which can be varied without unreasonable modification of equipment or materials between runs.

II. Design equipment for maximum flexibility and ease of varying parameters selected in Ib

   a. Choose shape and size of fluidizing column

   b. Design column for easy access to tube bundle, and with positive method of holding tubes in place for different tube orientations.

   c. Provide a rapid means of draining particles from the column and a means of cleaning the column between particle changes.

   d. Determine pipe line sizes, orifice location, and location of pressure measuring devices required in fluidizing system.

   e. Design electrical system to provide measurement of power consumption in each heater, measurement of each tube wall temperature, and measurement of fluidized bed temperature.

   f. Choose tube and heater diameters and determine method of assembly and thermocouple attachment.

III. Determine range of parameters to be varied

a. Select fin heights, fin thicknesses, and fin spacing on each tube.

b. Determine range and number of tube spacings to be investigated for each tube bundle.

c. Choose range of air fluidizing velocities and select particle sizes.

IV. Make preliminary runs

a. Find optimum location of thermocouples on each tube surface.

b. Calibrate air line valve settings with air velocities to improve accuracy of reproducing air flow rates.

V. Make runs to collect data for all desired values of experimental variables

VI. Discuss results and compare experimental data with available data from literature

VII. Correlate data into single equation relating all experimental variables

Determination of parameters to be varied

The parameters which might effect the heat transfer coefficient can be classified in three categories:

Fluidizing Medium:

1. Nature of fluidizing medium (gas or liquid)
2. Particle size
3. Particle shape
4. Particle composition

Operating Conditions:

1. Velocity of fluidizing medium
2. Rate of heat transfer
3. Height of static bed

Equipment Geometry:

1. Diameter of tubes
2. Fin height
3. Geometry of fins on tube
4. Tube spacing in bundle
5. Location of tube bundle in column
6. Shape of column

After consideration of the equipment modifications and time that would be required to investigate the various parameters, it was decided that the following four parameters would be made experimental variables: particle size, velocity of fluidizing medium, fin height, and tube spacing in the bundle. The range of the four variables was chosen as shown in the table below.

TABLE 1. RANGE OF EXPERIMENTAL VARIABLES

Variable	Range
Particle size	0.008, 0.011, and 0.0185 inch diameter
Fluidizing mass velocity	120 to 825 lbs/hr-ft^2 ($G/G_{\text{minimum fluidization}}$ = 2 to 12)
Fin height	bare tubes, 1/8, 3/8, 5/8, and 7/8 inch
Tube spacing in bundle	0.18 to 4.0 inches between fin tips (distance between fin tips is defined on page 74)

All of the other parameters listed in the three categories above were held at some constant value as discussed below or in the sections following:

Fluidizing medium: Air was used as the fluidizing medium. The temperature of the entering air was approximately the same for all runs, so that the physical properties of the entering air were nearly constant.

Particle shape and composition: All particles used in this study were spherical glass beads manufactured by the Minnesota Mining and Manufacturing Company. The particles were not screened before loading into the column; they were used directly as received from the company. The density of the glass is 156 lbs/cu.ft.

Rate of heat transfer: The rate of heat transfer was held constant at about 160 watts per heater. The rate varied slightly among the seven tubes in the bundle, from a low of 150 watts to a high of 162 watts. These values for the heat transfer rate resulted from plugging the heaters directly into the 110 volt AC source.

Height of static bed: The static bed height was 23 inches above the distributor plate for all particle sizes.

Diameter of tubes: The diameter of the bare tubes and the diameter of the center tube for the finned tubes was 0.625 inch O.D. for all of the tubes.

Geometry of fins on tube: For all of the finned tubes the fin thickness was 0.025 inch, the fins were spaced 8 fins/inch on the tube, and the tubes were serrated with the same geometry. The serrated type fins

were chosen instead of continuous, helically wound fins because it was felt that the additional free volume between the serrated fins would allow greater particle movement between the fins, with resulting higher heat transfer coefficients.

Location of tube bundle: The tube bundle was located in the same horizontal position for each run. The location of the bundle was determined by the location of the window in the side of the column. The center tube in the bundle was always located 17 inches above the distributor plate.

Design of equipment

All of the objectives listed under heading II in the experimental program outline on page 20 were achieved in the final design of the column and accessory equipment. Some particulars about the final design are discussed below.

Column: The primary design problem concerned the size and shape of the column. Early in the design studies it was decided that a clear Plexiglas column would be used so the degree of fluidization could be observed, and the tube bundle could be inspected after installation in the column. Since the experimental procedure would require moving the tubes farther and farther apart, the decision was made to use a rectangular column. The rectangular shape would allow all seven tubes in the bundle to be of the same length no matter how far apart the tubes were

spaced. The inside width of the column was chosen as 14 inches, so the tubes could be spaced as far apart as 4 inches between fin tips, even when the tubes with 7/8 inch fins were used. It was desired to keep the fins at least 2 inches from the inside of the column wall to avoid "wall effects". The inside depth of the column was selected as 6 5/8 inches, so 6 1/2 inch long tubes could be used, leaving 1/16 inch between the tube and the micarta plate on both ends of the tube. The height of the column was arbitrarily chosen as 6 feet above the distributor plate to allow ample room for the bed to expand and surge at the highest fluidizing velocities. The column length included 18 inches below the distributor plate to accommodate a bundle of tubes for straightening the air flow.

Tubes and Heaters: One of the principle concerns in designing the tube and heater assembly was to provide sufficient insulation on both ends of the heater so the heat conducted from the ends of the heaters could be considered negligible. It could then be assumed that all of the energy supplied to the heaters was transferred to the bed through the tubes and fins. The heater design used to achieve this objective is shown in Figure 9 on page 42. After completion of construction and start-up of the equipment it was found that the design performed successfully, since after 8 hours of operation the heated portion of the heaters produced tube surface temperatures of between 200 and 250°F, while the portion of the heater protruding through the micarta plate

was only warm to the touch.

As can be seen in the remainder of this report, the objectives listed under headings IV, V, VI, and VII were achieved as outlined in the experimental program.

EXPERIMENTAL EQUIPMENT

The equipment used in this study can be divided into three types of components - those components used in the fluidizing system, in the electrical system, or in the tube and heater assemblies.

Fluidizing System

A schematic drawing of the fluidizing system is shown in Figure 1. The principle component in the system was a 7.5 foot rectangular column with outside dimensions of 15.5" wide by 8.125" deep. The column was constructed of 0.75" thick clear Plexiglas and was fabricated with both solvent and 3/16" bolts spaced at 9" intervals, on all four sides, up the entire length of the column. Four 3" diameter ports were provided on the four sides near the top of the column, and five 2" diameter ports were provided on the top as outlets for the fluidizing air. All of the exit ports were covered with 140 mesh brass wire cloth. A detailed drawing of the column is shown in Figure 2. The column was supported with wooden blocks and angle irons as indicated in Figure 3.

Two micarta plates, 15.5" x 18", were attached to opposite sides of the column to accommodate the tube bundles. Figures 1 through 5 show various details of the plates. The two plates were identical, except that the holes in one plate were drilled only 0.3" deep, while the holes were drilled completely through the other plate.

Air was supplied to the column with a Sutorbilt blower driven by

a 7 1/2 HP Brown-Brockmeyer electrical motor. Air was transported to the column through a 2.5 inch steel pipe. To reduce vibrations, a section of rubber hose was installed between the blower and the pipe entrance, and between the pipe and the entrance to the column. The air flow rate was regulated by adjusting a gate valve in the main line and a gate valve in a 2 inch bypass line through which air was vented to the atmosphere. The air flow rate was measured with an orifice in the main line. Two mufflers, one in the main line and one in the bypass line, were installed to reduce the noise level from the blower.

Components in Fluidizing System:

A. Column

a. Material: 3/4" thick clear Plexiglas

b. Dimensions: 18" below distributor plate
74" above distributor plate
15.5" wide x 8.125" deep (outside dimensions)

c. Distributor Plate: A piece of 140 mesh brass wire cloth, 19.5" x 12.125" sandwiched between two 1/32" thick pieces of steel perforated plate (perforations were 1/32" diameter and 0.2" center-to-center)

d. Particle Drain Pipe: A 1" diameter pipe silver soldered to the distributor plate and extending through the bottom of the column. A quick opening valve was installed on the pipe just below the bottom of the column.

e. Flow Straighteners: Nine 3/4" pipes installed across the column, beneath the distributor plate.

f. Micarta Plates: Two plates attached to opposite sides of the column to hold the tube bundles.

B. Main Air Line

a. Material: steel, schedule 40

b. Dimensions: 2.469" inside diameter, 14 feet long

C. Bypass Air Line

a. Material: steel, schedule 40

b. Dimensions: 2.067" inside diameter, 2 feet long

D. Valves

a. Type: 2 gate valves

b. Location: 1 in main line, 1 in bypass line

E. Orifice

a. Size: 1.5" diameter opening

b. Tap Arrangement: vena contracta

c. Location: main air line

F. Manometers

a. Fluid: water

b. Location: Pressure drop across orifice and pressure drop across tube bundle in bed

G. Pressure Gauge

a. Type: Duragauge, 0 - 30 psi

b. Location: Pressure in column beneath distributor plate

Electrical System

As shown in Figure 1, the lead wires from the electrical heater in

each tube were connected to a wattmeter and then to the electrical power source. The heaters were connected in parallel, and the circuit to the wattmeter was wired in such a manner that the wattage to each of the 7 heaters could be individually indicated on the wattmeter by flipping one of 7 toggle switches. The power was supplied from a 110 volt AC line. The power to each heater under these conditions was approximately 160 watts. When the column was operated without particles, the heaters were connected through a powerstat to reduce the power to about 30 watts per heater. This was necessary to keep the tube surfaces from getting too hot.

The second part of the electrical system consisted of the thermocouples and accessory equipment required for the measurement of the bed and tube wall temperatures. A single thermocouple on each tube surface, as shown in Figure 10, was used to measure the tube temperatures. Three thermocouples were used to measure the bed temperature - one located above the tube bundle, one below the bundle, and one near the center of the bundle. Figure 6 shows the bed thermocouples in place. A reference thermocouple was used to keep a continuous check on the accuracy of the potentiometer readings. The reference thermocouple was located adjacent to the bulb of a mercury thermometer which was registering room temperature. An ice water bath was used as reference for all thermocouples. The lead wires from the 11 thermocouples were plugged into a panel board, which was wired to an eleven position switch box, and then

connected to a potentiometer capable of indicating millivolts to the fourth decimal place.

Components in Electrical System:

A. Heaters

a. Dimensions: 0.495" outside diameter, 9.9" long

b. Electrical rating: 240V, 1000W

c. Source: Watlow Electric Manufacturing Company
St. Louis, Missouri

B. Wattmeter

a. Type: Simpson, Model 1379

b. Range: 0 - 1500 watts

C. Powerstat

Superior Electric Company, Bristol, Connecticut

D. Thermocouples

a. Type: Iron-Constantan (type J)

b. Size: B and S gauge - 30

E. Potentiometer

Model 1197961
Leeds and Northrup Company
Philadelphia, Pennsylvania

Heater and Tube Assemblies

Horizontal bundles of 7 bare tubes and bundles of 7 finned tubes were investigated in this study. Details of the two types of tubes are shown in Figures 7 and 8. Each tube in the bundle was heated with the

type of electrical heater shown in Figure 9. When assembled, the 6.5" heated section was completely covered by the tube, while the insulated ends protruded from the ends of the tube as shown in Figure 10. The longer insulated end was passed through a hole in one of the micarta plates and was held in place with a swagelock as indicated in Figure 5. When the 7 heater and tube assemblies were fastened to the plate, the plate was placed in the window on the side of the column. The shorter insulated protruding ends of the heaters were then pressed into the 0.3" deep holes in the micarta plate on the other side of the column. This arrangement provided lateral support for the tubes when the bed was fluidized, and also ensured that all of the tubes in the bundle were parallel across the column.

A total of 4 different sizes of finned tubes were investigated, with fin heights of 1/8", 3/8", 5/8", and 7/8". The surface areas for the various fin sizes are given in Figure 11. The fin thickness was 0.025" and the fin spacing on the tube was 8 fins per inch for all of the finned tubes investigated.

Components for Heater and Tube Assemblies:

A. Bare Tubes

a. Dimensions: 0.625" outside diameter, 6.5" long

b. Material: carbon steel

B. Finned Tubes

a. Dimensions: 0.625" outside tube diameter, 6.5" long

b. Material: tubes and fins - carbon steel

c. Source: Escoa Corporation
Pryor, Oklahoma

C. Heaters

(Described in section on Electrical System)

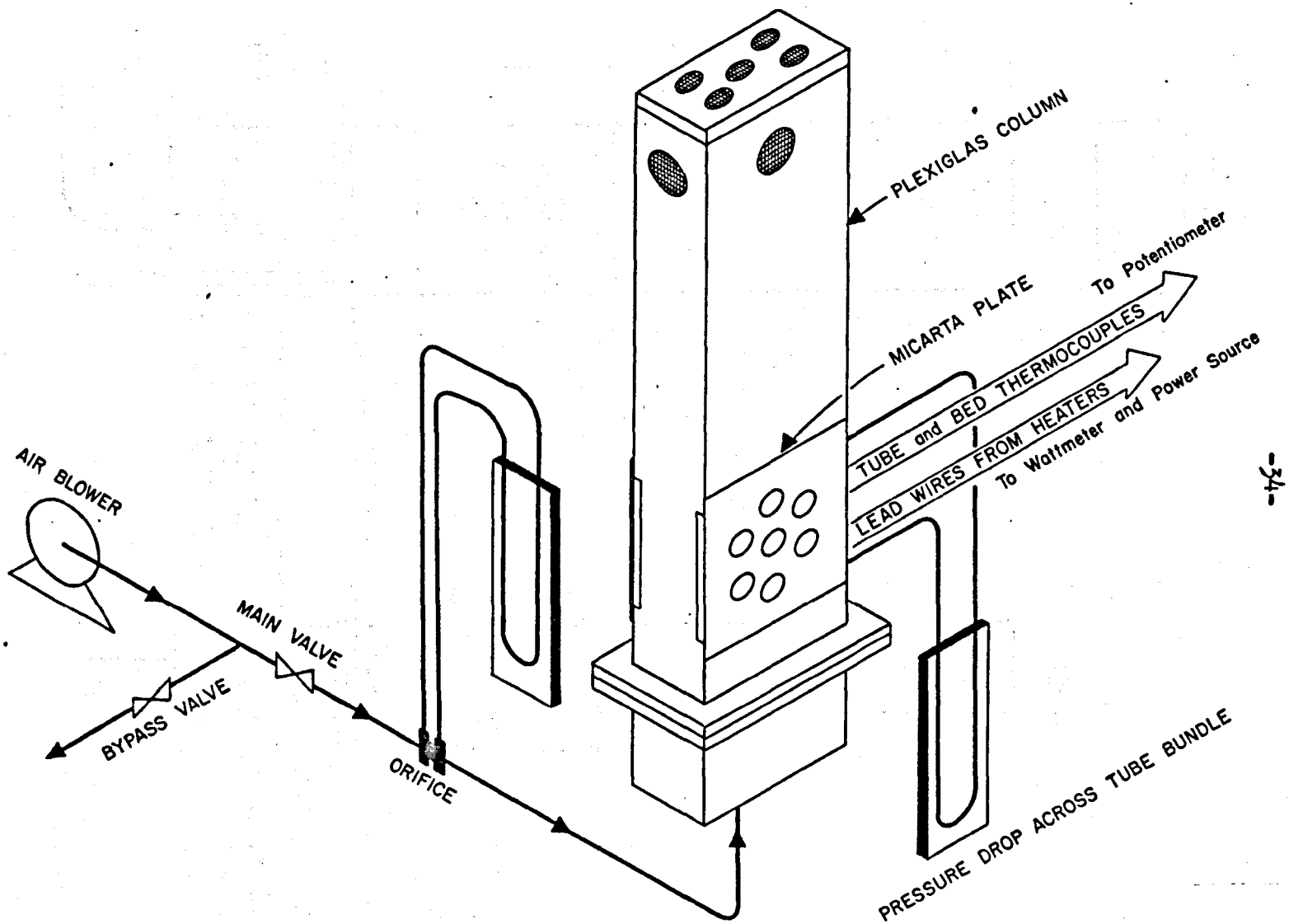


FIGURE I. SCHEMATIC DRAWING OF EQUIPMENT

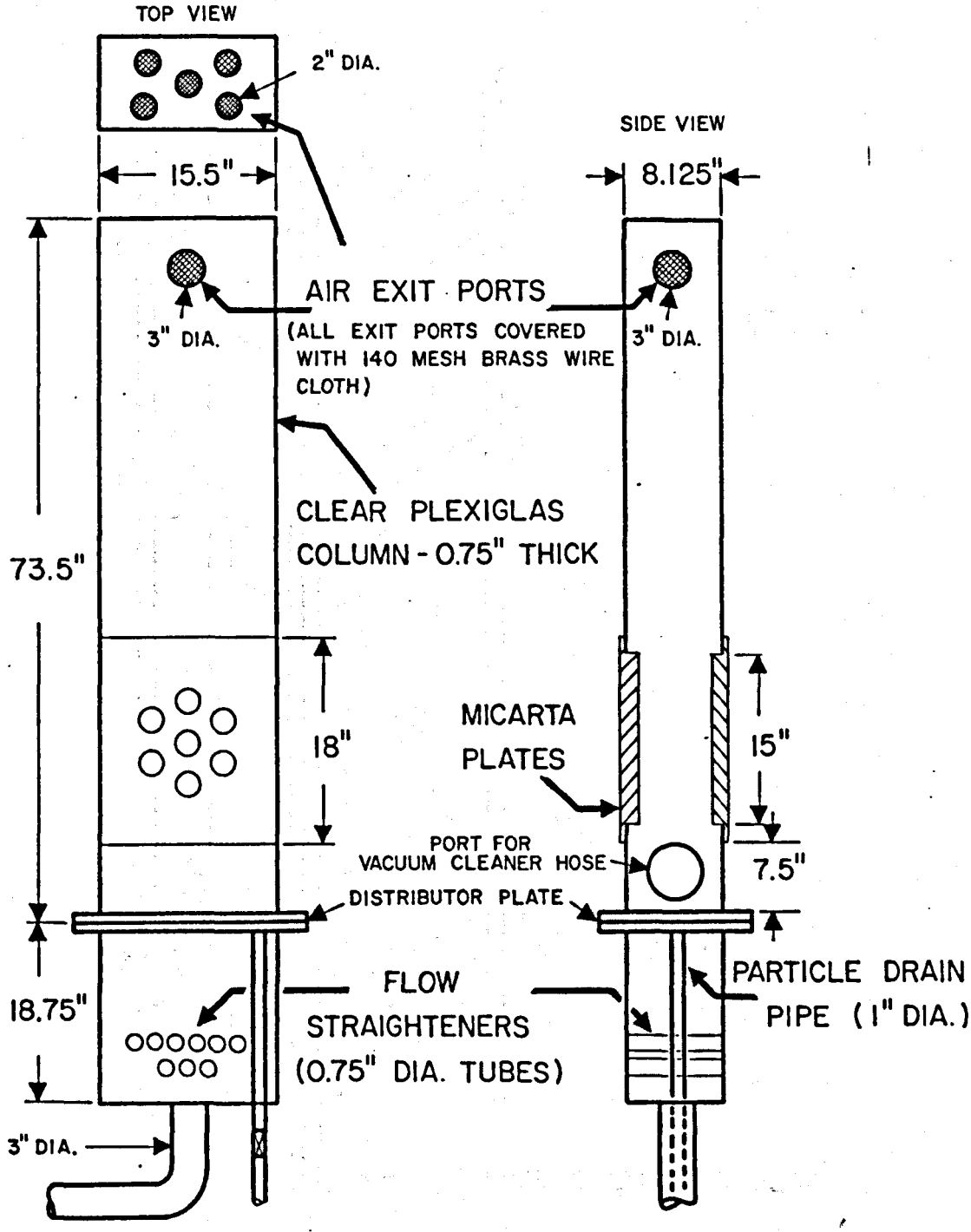


FIGURE 2. DETAILS OF FLUIDIZING COLUMN

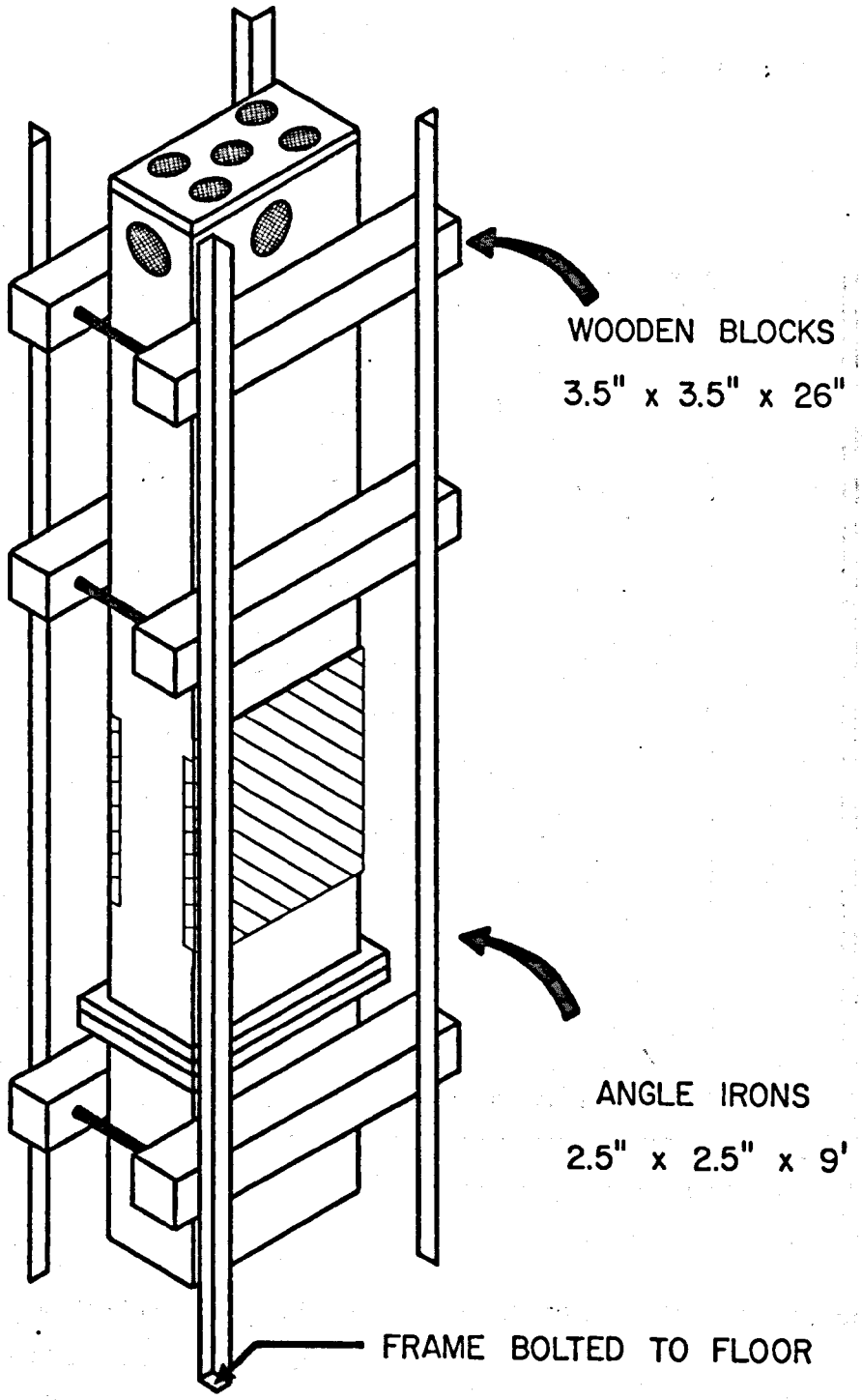
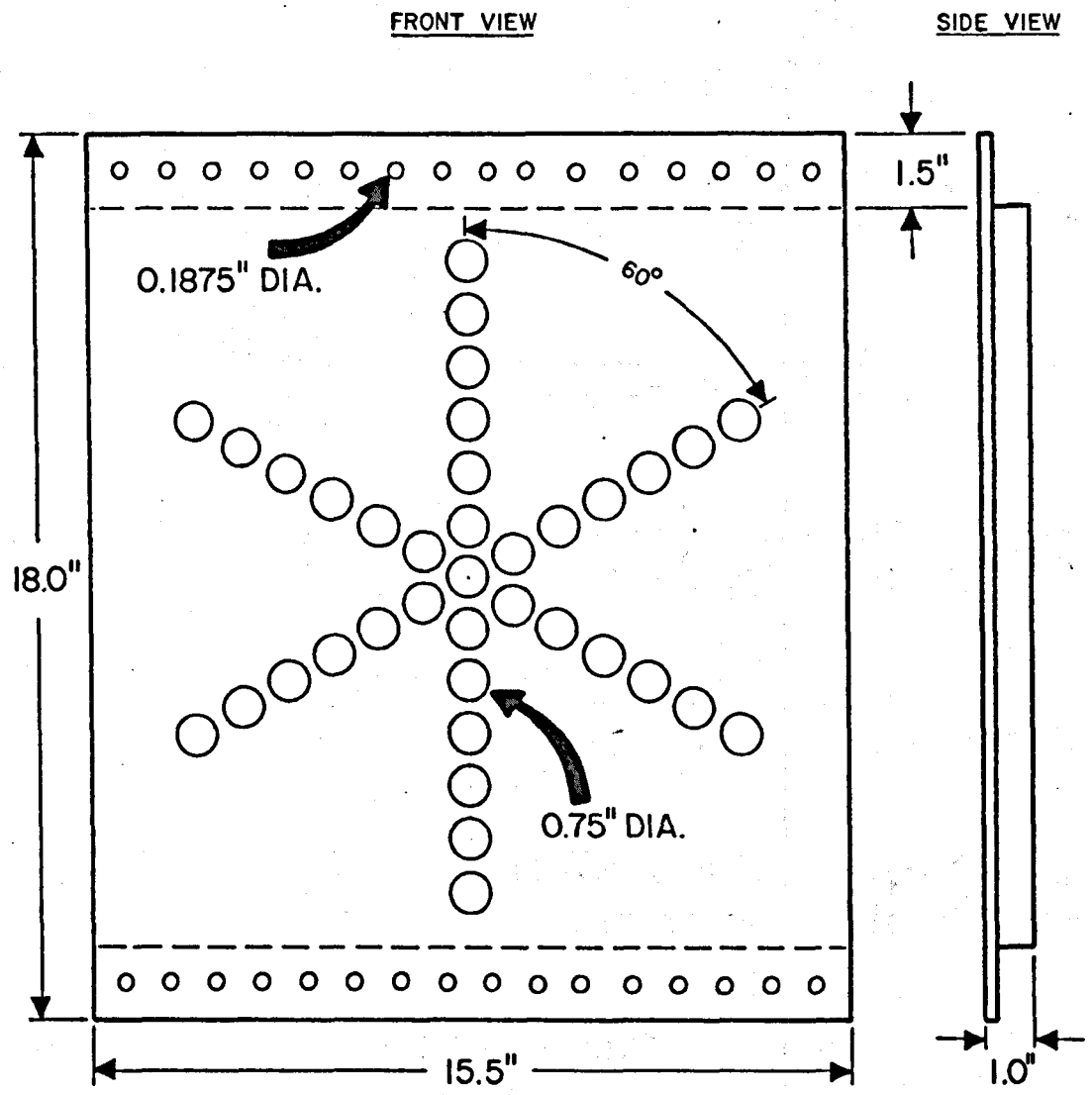


FIGURE 3. COLUMN AND SUPPORTING FRAMEWORK

SCALE ONE-FOURTH



NOTES:

1. Center-to-center distance between adjacent holes on same radial line = 1.0625 inches.
2. Unit assembled by bolting together 0.25" and 0.75" plates.

FIGURE 4. DETAILS OF MICARTA PLATE

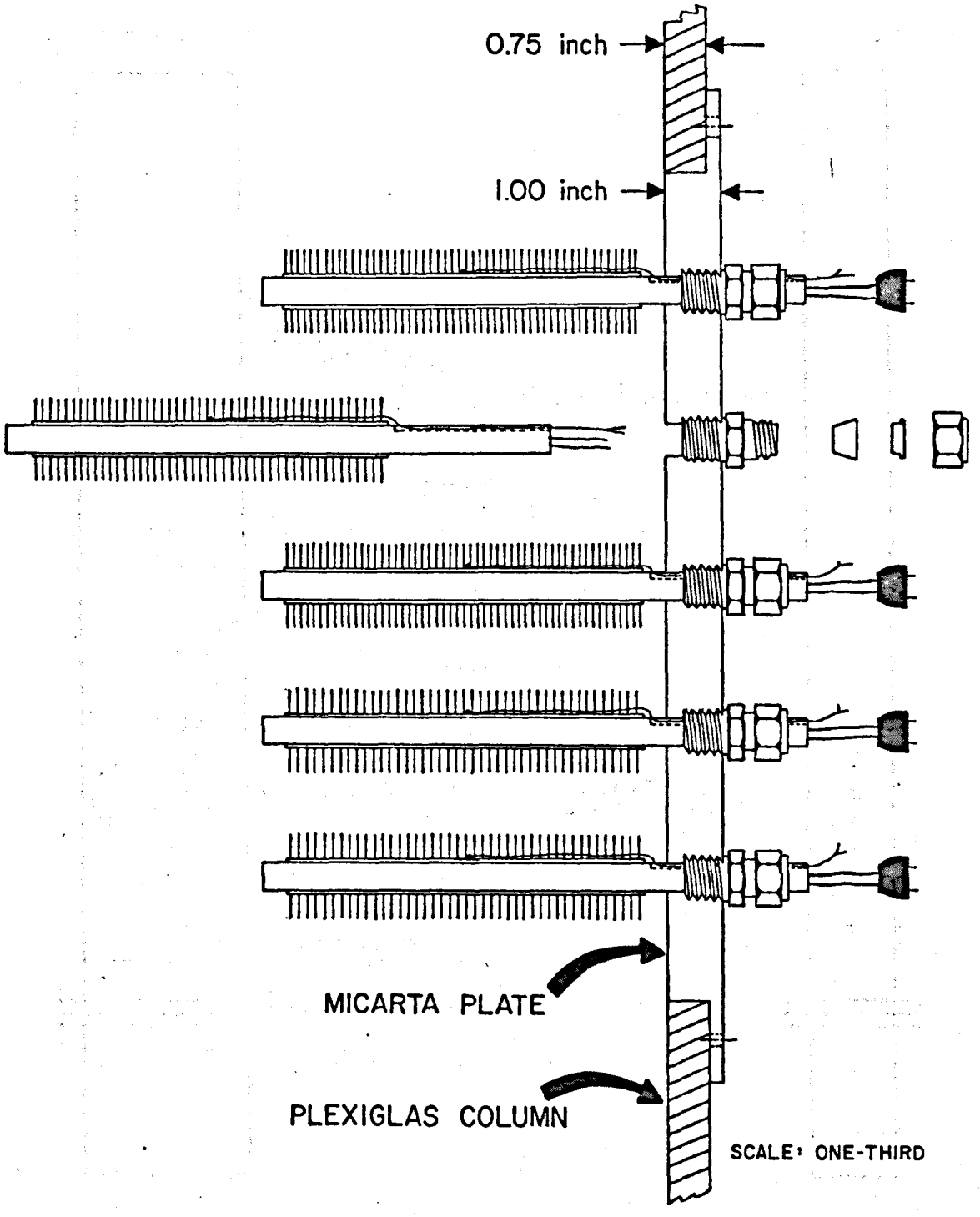


FIGURE 5. TUBES ASSEMBLED IN MICARTA PLATE
(SHOWS 5 OF 7 TUBES IN BUNDLE)

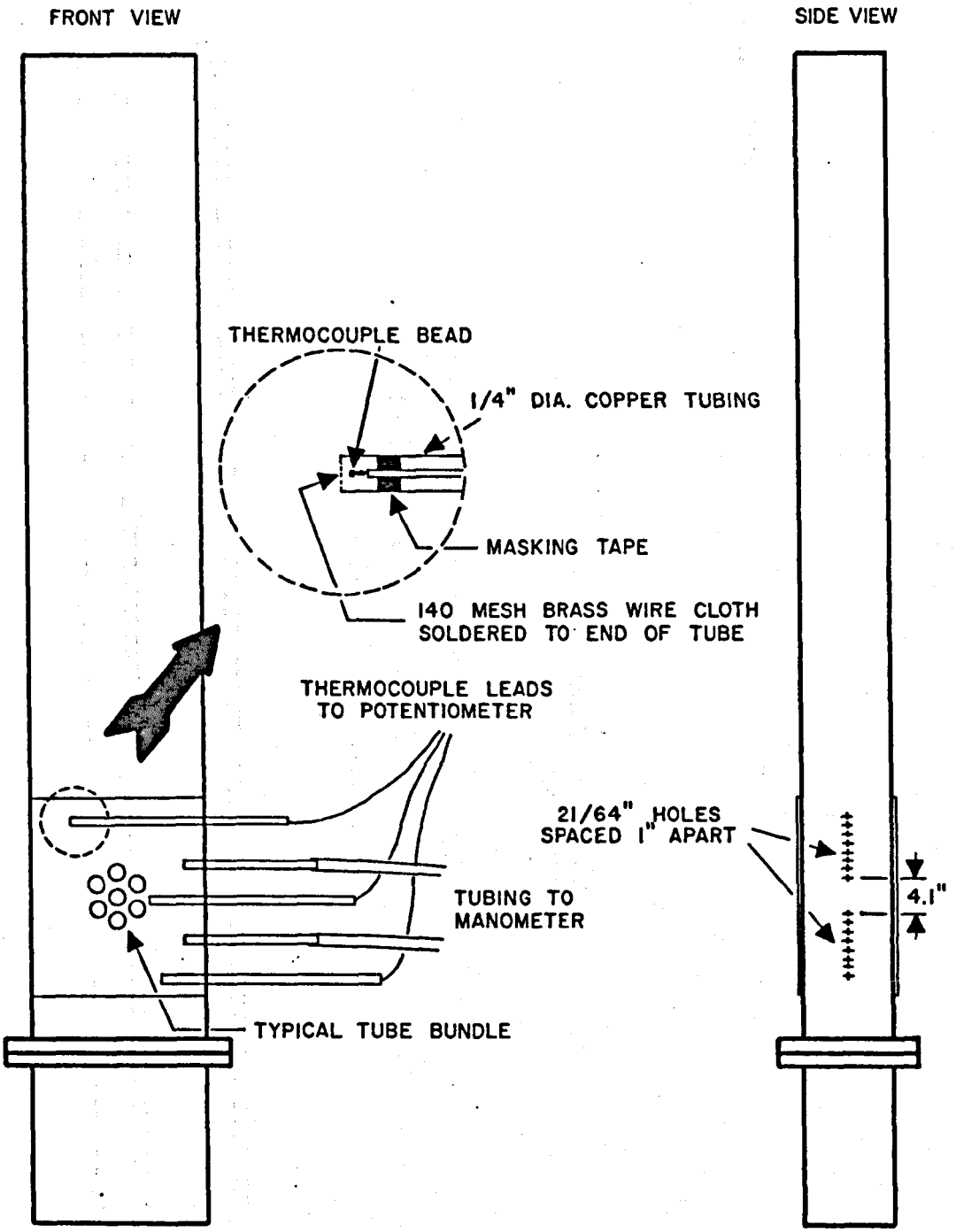
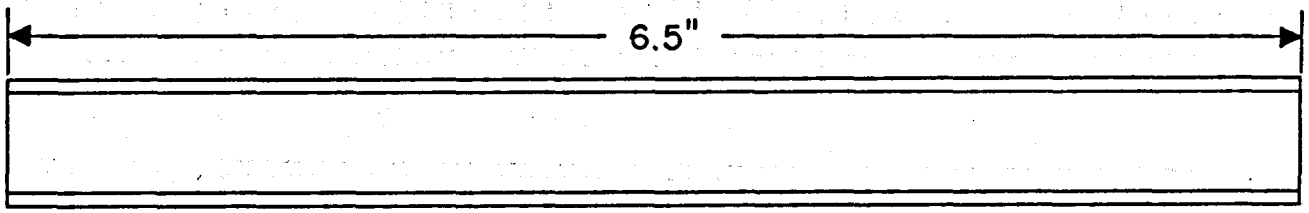


FIGURE 6. DETAILS OF BED THERMOCOUPLES AND PRESSURE TAPS

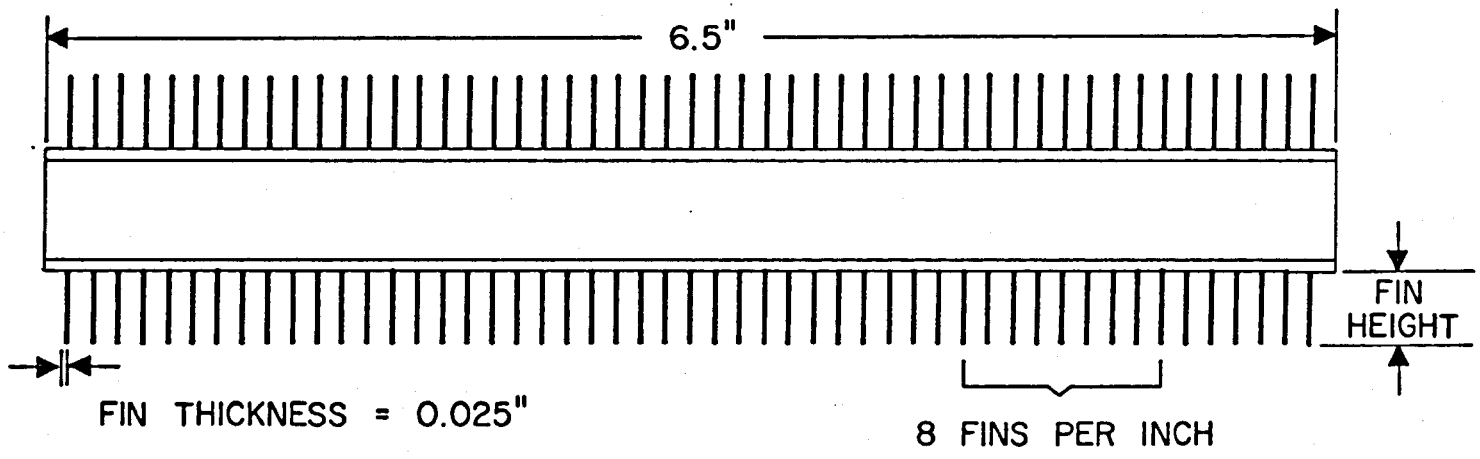


TUBE OUTSIDE DIAMETER = 0.625"
TUBE INSIDE DIAMETER = 0.525"
TUBE WALL THICKNESS = 0.050"

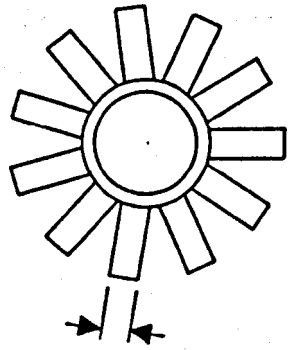
MATERIAL
CARBON STEEL

SCALE: FULL

FIGURE 7. DETAILS OF A TYPICAL BARE TUBE



END VIEW



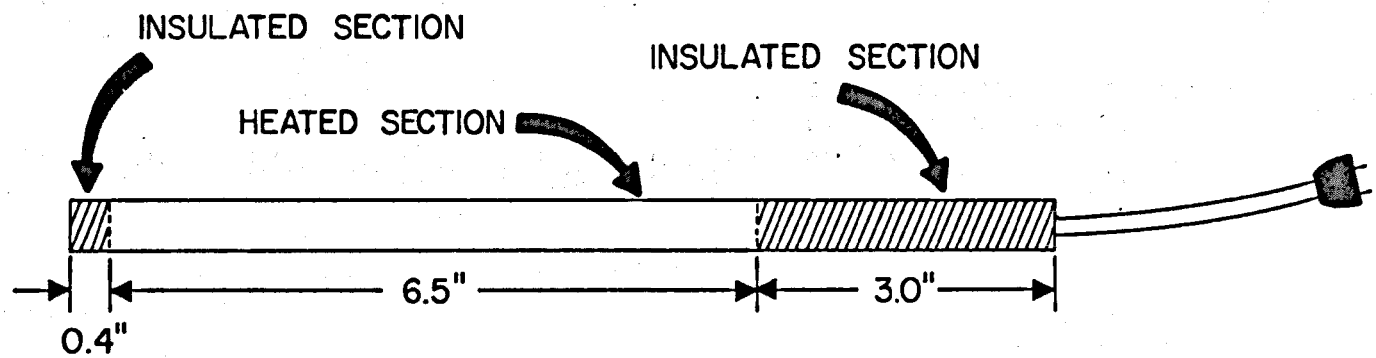
TUBE OUTSIDE DIAMETER = 0.625"
TUBE INSIDE DIAMETER = 0.525"
TUBE WALL THICKNESS = 0.050"

MATERIAL

TUBE - CARBON STEEL
FINS - CARBON STEEL

SCALE: FULL

FIGURE 8. DETAILS OF A TYPICAL FINNED TUBE



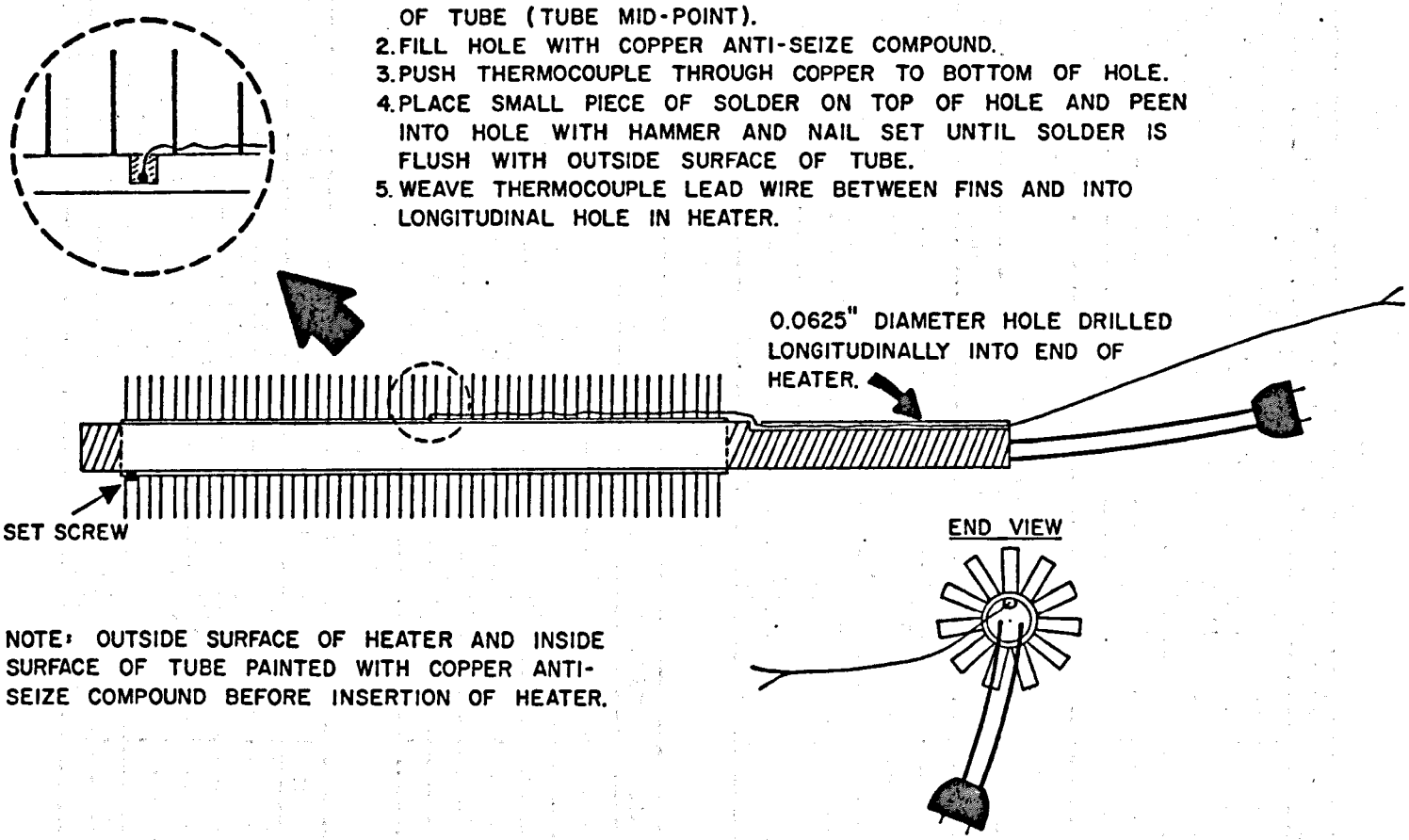
OUTSIDE DIAMETER = 0.495"

SCALE: ONE-HALF

FIGURE 9. DETAILS OF ELECTRICAL HEATER

THERMOCOUPLE ATTACHMENT PROCEDURE

1. DRILL 0.031" DIAMETER HOLE IN TUBE WALL 3.25" FROM END OF TUBE (TUBE MID-POINT).
2. FILL HOLE WITH COPPER ANTI-SEIZE COMPOUND.
3. PUSH THERMOCOUPLE THROUGH COPPER TO BOTTOM OF HOLE.
4. PLACE SMALL PIECE OF SOLDER ON TOP OF HOLE AND PEEN INTO HOLE WITH HAMMER AND NAIL SET UNTIL SOLDER IS FLUSH WITH OUTSIDE SURFACE OF TUBE.
5. WEAVE THERMOCOUPLE LEAD WIRE BETWEEN FINS AND INTO LONGITUDINAL HOLE IN HEATER.



NOTE: OUTSIDE SURFACE OF HEATER AND INSIDE SURFACE OF TUBE PAINTED WITH COPPER ANTI-SEIZE COMPOUND BEFORE INSERTION OF HEATER.

SCALE: ONE-HALF

FIGURE 10. TUBE AND HEATER ASSEMBLY

AREA OF EACH BARE TUBE = 0.0873 FT^2

1/8" FINS

TUBE POSITION	FIN AREA (FT^2)	TUBE AREA (FT^2)	TOTAL AREA (FT^2)
TOP	0.197	0.073	0.270
UPPER RIGHT	0.202	0.073	0.274
LOWER RIGHT	0.199	0.073	0.272
BOTTOM	0.198	0.073	0.271
LOWER LEFT	0.190	0.074	0.263
UPPER LEFT	0.194	0.073	0.267
CENTER	0.195	0.073	0.268

3/8" FINS

TUBE POSITION	FIN AREA (FT^2)	TUBE AREA (FT^2)	TOTAL AREA (FT^2)
TOP	0.530	0.074	0.604
UPPER RIGHT	0.531	0.074	0.605
LOWER RIGHT	0.534	0.074	0.608
BOTTOM	0.529	0.074	0.603
LOWER LEFT	0.538	0.074	0.612
UPPER LEFT	0.527	0.074	0.601
CENTER	0.524	0.074	0.598

5/8" FINS

TUBE POSITION	FIN AREA (FT^2)	TUBE AREA (FT^2)	TOTAL AREA (FT^2)
TOP	0.832	0.075	0.907
UPPER RIGHT	0.827	0.075	0.902
LOWER RIGHT	0.866	0.074	0.940
BOTTOM	0.832	0.075	0.907
LOWER LEFT	0.853	0.074	0.927
UPPER LEFT	0.834	0.075	0.908
CENTER	0.831	0.075	0.905

7/8" FINS

TUBE POSITION	FIN AREA (FT^2)	TUBE AREA (FT^2)	TOTAL AREA (FT^2)
TOP	1.206	0.074	1.281
UPPER RIGHT	1.208	0.074	1.283
LOWER RIGHT	1.304	0.073	1.378
BOTTOM	1.189	0.074	1.263
LOWER LEFT	1.300	0.073	1.373
UPPER LEFT	1.202	0.074	1.276
CENTER	1.200	0.074	1.274

FIGURE II. TUBE SURFACE AREA

EXPERIMENTAL PROCEDURE

Determination of Minimum Fluidizing Velocities

The first experimental work performed in this study was the determination of the minimum fluidizing velocities for the 3 different particle sizes. The minimum velocities were determined by visual observation of the bed, and were then compared with values obtained from a correlation in the literature.

The top of the column was removed, and particles of the desired diameter were poured into the column to the level of the top of the micarta plates, for a total static bed height of 23 inches above the distributor plate. This static bed height was later used for all of the runs made in this study, to ensure that all tubes in the bundle were completely covered with particles in the static condition, regardless of how far apart the tubes were spaced. The blower was then turned on, and the air flow rate to the column was gradually increased until the first sign of bed expansion was detected. The observations were repeated a number of times, from the direction of decreasing air velocity as well as increasing velocity. The experimental minimum fluidizing velocities for the 3 particle sizes are shown in figure 12 where they are compared with theoretical minimum velocities predicted by the Leva correlation. This correlation is found on page 64 of reference (14). Physical properties were evaluated at 75°F.

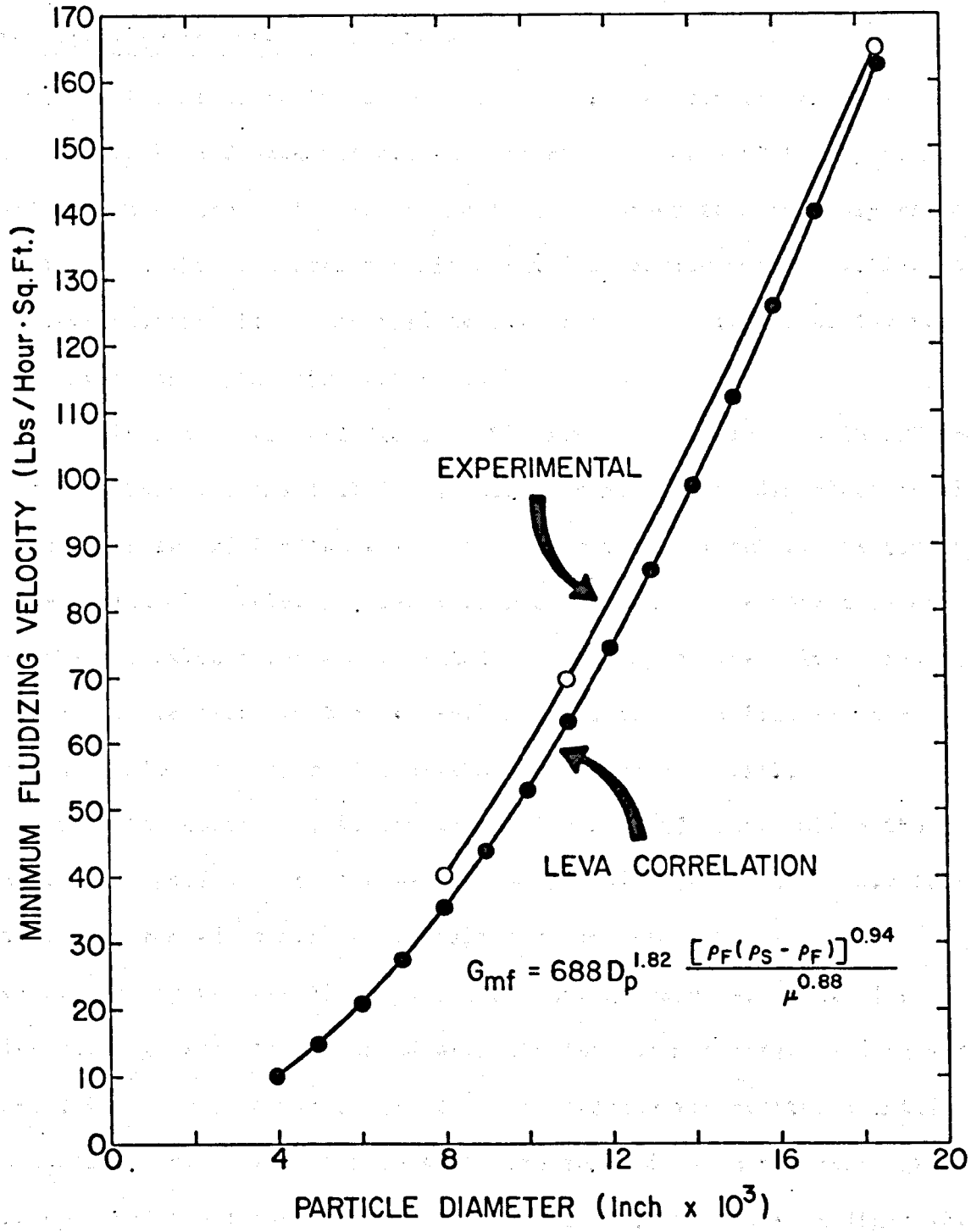


FIGURE 12. COMPARISON OF EXPERIMENTAL AND THEORETICAL MINIMUM AIR VELOCITIES

Calibration of Air Line Gate Valves

The water level in the manometer connected across the orifice in the main air line fluctuated over a wide range because of the "piston-like" action of the particles in the bed. In order to accurately reproduce the same air flow rate for different fin heights and for different tube orientations, it was decided to calibrate the settings of the two gate valves versus the air flow rate.

Two circular cardboard dials of 5" diameter were drawn with 10° angular divisions for the full 360°. Circular holes with diameters equal to the diameters of the two valve stems were then cut out of the center of the dials. The valve handles were removed, the dials were slid down over the two valve stems and cemented to the body of the valves, and the handles were replaced on the valves. A vertical index line was then scratched into each valve stem at the 0° mark on each dial.

After the column was loaded to the level of 23 inches above the distributor plate with particles of the smallest diameter, the air flow rate was increased to minimum fluidization and the manometer reading, read as closely as possible, and valve settings were recorded. The valve settings were then changed slightly and the manometer reading and valve settings were again recorded. This process was continued until the condition of maximum air velocity was reached, with the main valve full open and the bypass valve full closed. The manometer readings were then fed into an orifice computer program and the air flow rates were

found for the various valve settings. The procedure was repeated for the medium and large particles, and the results are shown in Figure 13.

Thus, for example, whenever it was desired to operate at 2 times minimum fluidization with the large particles, the main valve was opened full, and the bypass valve was closed 6 turns plus 40°. The manometer reading was then checked to be sure that the reading was 2.0 inches. It was found that the main valve had to be full open for all of the air flow rates used in this study.

Determination of Thermocouple Location on Tubes

A large number of test runs were made to determine the location and the number of thermocouples required on each tube to accurately measure the tube surface temperature. Thermocouples were attached at two positions along a longitudinal line on the tube surface, the equipment was assembled as described in the next section, and the system was allowed to operate until steady-state conditions were attained. After all thermocouple readings were taken, the tubes were turned through a 10° angle by grasping the portion of the heater protruding through the micarta plate with a pair of pliers. An index mark scratched on the end of each heater and a small circular cardboard dial divided into 10° increments were used to determine the amount of rotation. When the thermocouple readings were again taken, the tubes were rotated through another 10° increment. This procedure was continued until readings had been taken

ALL VALVE SETTINGS IN CHARTS BELOW ARE FOR BYPASS VALVE – MAIN VALVE IS FULL OPEN FOR ALL RUNS

PARTICLE DIAMETER = 0.0185 inch

	MIN. FL.	2 x MIN	3 x MIN	4 x MIN	5 x MIN	6 x MIN
VALVE SETTING	5T+200°	6T+40°	6T+210°	7T	7T+180°	8T+180°
G, lbs/hr·sq.ft.	165	330	495	660	825	990
Δh, inches water	0.5	2.0	4.3	8.0	12.2	17.3

PARTICLE DIAMETER = 0.0110 inch

	MIN. FL.	2 x MIN	3 x MIN	4 x MIN	6 x MIN	9 x MIN
VALVE SETTING	5T+55°	5T+135°	5T+215°	5T+290°	6T+70°	6T+300°
G, lbs/hr·sq.ft.	70	140	210	280	420	630
Δh, inches water	0.09	0.34	0.71	1.35	3.0	7.3

-67-

PARTICLE DIAMETER = 0.0080 inch

	MIN. FL.	3 x MIN	4 x MIN	5 x MIN	8 x MIN	12 x MIN
VALVE SETTING	5T+45°	5T+120°	5T+165°	5T+215°	5T+350°	6T+180°
G, lbs/hr·sq.ft.	40	120	160	200	320	480
Δh, inches water	0.029	0.24	0.40	0.70	1.65	4.2

FIGURE 13. BYPASS VALVE SETTINGS

at 10° increments for the full 360°. From this data, the temperature profile around the tube and across the tube was determined.

The results of this investigation, using all particle diameters and various air flow rates, were that there was no temperature gradient on the tube surface in either the longitudinal or angular directions. In all of the test runs made, the greatest temperature difference between any two points measured on the tube surface was 2 F° when the tube surface temperatures were about 200°F.

Because of the absence of temperature gradients, it was decided that the tube surface temperature could be accurately measured with a single thermocouple attached to the center of each tube. When the equipment was assembled for each run, the tubes were rotated so that the thermocouples were positioned on the top of the tubes. This thermocouple arrangement was used for all of the runs included in this study.

Procedure for a Typical Run

The fin height to be investigated was chosen, thermocouples were attached to each of the 7 tubes, and an electrical heater was inserted into each tube as shown in Figure 10. The tube spacing to be investigated was selected, the 3" protruding portion of each heater was inserted through the proper hole in the micarta plate, and the tube and heater assemblies were fastened loosely to the plate with swagelock fittings as indicated in Figure 5. The plate was then placed in the window on the

side of the column, and the 0.4" protruding ends of the heaters were pressed into the corresponding holes in the micarta plate on the opposite side of the column. The plate was then fastened securely to the column with 3/16" screws along the top and bottom of the plate as shown in figure 4, and with 3 "trunk-lid" type clamps on each side of the plate. Thin rubber sheeting was used as gasket material between the plate and the column to prevent particle leakage. The tubes were then turned so that all of the thermocouples were facing upward, and the swagelocks were tightened to prevent the tubes from turning during operation of the column. Thermocouple and heater leads were plugged into the panel board, and all unoccupied holes in the micarta plate were plugged with 1/2" plugs.

Two 1/4" diameter copper tubes were positioned in the proper tapped holes on the side of the column and were connected with plastic tubing to a water-filled manometer to indicate pressure drop across the tube bundle. Three other 1/4" copper tubes, each containing a thermocouple suspended on the inside of the tube near its end, were inserted through holes in the same side of the column so that the bed temperature could be read near the top of the static bed, in the center of the bed, and near the bottom of the bed. A piece of 140 mesh brass wire cloth was soldered to the ends of all 5 of the copper tubes to prevent particles from entering the tubes. The bed thermocouple positions were the same for all runs made in this study, but the tubes used for pressure drop

measurement were moved when the tube spacing was changed. Thus, one of the pressure tubes was always slightly above the upper tube in the bundle, and the other pressure tube was slightly below the lowest tube in the bundle. Details are given in Figure 6.

The top of the column was removed, and particles with the smallest diameter were poured into the column to the level of 23 inches above the distributor plate. The top was then replaced and held in place with 4 "trunk-lid" type clamps. Thick rubber weather-stripping was used between the top and the top edges of the column to prevent particle leakage at the higher air velocities.

After the two manometers and the wattmeter were zeroed, the air blower was turned on, the main valve was opened full, and the bypass valve was closed 5 turns plus 120°, as indicated in Figure 13, to provide sufficient air for a fluidizing rate of 3 times minimum. The heaters and the potentiometer were then plugged into the electrical outlet, and the column was allowed to operate for 3 hours. At that time steady-state was attained, and the potentiometer, wattmeter, and manometer readings were recorded. The first run was then complete, and the second run was begun by adjusting the bypass valve to the opening indicated in Figure 13. For the second run, and for subsequent changes in air velocity, steady-state was attained in 1 hour. Potentiometer, wattmeter, and manometer readings were again recorded, and the procedure was continued until all of the desired air flow rates had been investigated.

The system was then shut down and the column was prepared for the next particle size by draining the particles through the 1" pipe extending from the distributor plate through the bottom of the column. After the particles were drained, the two small ports on the sides of the column were opened, and a vacuum cleaner hose was inserted to remove the particles clinging to the walls of the column and in the small holes in the perforations in the distributor plate. The ports were then closed and the next particle size was loaded into the column as described above.

After all 3 of the particle sizes had been investigated, the micarta plate was removed, each of the 6 outer tubes was moved outward to the next radial hole, the plate was refastened to the column, and the above procedure was repeated. The tubes were moved outward in subsequent runs until the heat transfer coefficients showed a decrease from the previous tube position. The decrease in coefficient indicated that the outer tubes were getting too close to the column walls, and the difference in the pattern of fluidization near the wall produced "wall effects" which resulted in lower rates of heat transfer. When this condition was reached, the investigation for that particular tube bundle was discontinued, and tubes of the next fin height were assembled and placed in the column in the most clustered tube position. The tubes were then gradually moved farther apart as described above.

CALCULATIONS

Calibration of Gate Valves

As discussed previously on page 47, the gate valves in the main air line and in the bypass line were calibrated to provide greater accuracy in reproducing air flow rates for different tube arrangements. The calibration was performed by setting the valves at various openings, recording the readings on the cardboard dials cemented to the valves, and then reading the water-filled manometer which indicated the pressure drop across the orifice in the main line. A pressure gauge was used to measure the downstream air pressure.

The manometer and pressure gauge readings were entered into a computer program which printed out the air flow rates corresponding to the various valve settings. The following equation was used for the calculations (21):

$$W = \frac{3600\,C\,Y\,S_c}{A_c}\sqrt{\frac{2g_c(p_1 - p_2)\rho_1}{1-\beta^4}} \quad , lb_m/\text{hour-ft}^2$$

where,

C = coefficient of discharge, dimensionless

Y = expansion factor, dimensionless

S_c = cross-sectional area of orifice opening, sq. ft.

A_c = inside cross-sectional area of column, sq. ft.

g_c = dimensional constant, lb_m-ft/lb_f-sec^2

p_1 = pressure at upstream pressure tap, lb_f/ft^2

p_2 = pressure at downstream pressure tap, lb_f/ft^2

ρ_1 = density at upstream temperature and pressure, lb_m/ft^3

β = ratio of orifice diameter to inside pipe diameter, dimensionless

For a square-edged orifice, the expansion factor is given as follows (21):

$$Y = 1 - \left[(p_1 - p_2)/p_1 k_r\right](0.41 + 0.35\beta^4)$$

where,

$$k_r = c_p/c_v$$

The coefficient of discharge is a function of Reynolds number, orifice to pipe diameter, and pressure tap arrangement. The value for C varied for each flow rate and the individual values were found by using complicated empirical equations taken from reference (29).

Since Reynolds number was not known to start with, the computer program contained a loop in which a Reynolds number was assumed, the coefficient of discharge was calculated from the assumed value of Reynolds number, and the air mass flow rate was found. The Reynolds number was then calculated from the flow rate, and if the difference between the assumed and calculated values was greater than 0.1%, the calculated

value was used as the new assumed Reynolds number, and the procedure was repeated. For most flow rates the value of C was close to 0.6. The results of the calibration calculations were shown previously in Figure 13.

Conversion of Potentiometer Readings to Temperatures

All of the thermocouples used on the equipment were connected to a switchbox and then to a potentiometer which indicated millivolts to the fourth decimal place (although this was beyond the accuracy of the thermocouples). The millivolt readings were converted to temperatures with the following equation:

$$T = -0.0733V^2 + 33.94V + 35.12$$

where,

T = temperature, ^{o}F

V = millivolts

This equation was obtained by fitting iron-constantan thermocouple data in reference (26) to a second degree polynomial.

Bed Temperature

As described on page 51, three thermocouples were used to measure the temperature of the fluidized bed. The bed temperature used in the equation for the heat transfer coefficient was the average of the three

bed thermocouple readings:

$$T_{bed} = \frac{T_{upper\ bed} + T_{middle\ bed} + T_{lower\ bed}}{3}$$

In all of the runs made in this study, the largest difference in temperature measured by the three bed thermocouples was 1 F^{o}. In most runs the bed thermocouples indicated temperatures within 0.5 F^{o} of each other.

Tube Wall Temperature

As discussed on page 50, the surface temperature of each tube was measured with a single thermocouple attached to the center of the tube and positioned on the top of the tube when the bed was in operation.

Power to each Tube

The electrical power to each tube heater was measured with a watt-meter and converted to BTU units by multiplying times the appropriate conversion factor:

$$q = \text{watts} \times 3.413\ \text{BTU/Watt-Hr} = \text{BTU/Hr}$$

Area of each Tube

The surface area of each finned tube was found by counting the

number of fins on the tube and multiplying times the area per fin. This was then added to the area of the exposed portion of the center tube to produce the total area, A, of each tube. The areas of the different tubes are tabulated in Figure 11.

Heat Transfer Coefficient for each Tube

The heat transfer coefficient for each tube was calculated from the standard heat transfer equation:

$$h = \frac{q}{A(T_{tube} - T_{bed})} \quad , \quad \frac{BTU}{Hr\text{-}Ft^2\text{-}F^o}$$

Average Heat Transfer Coefficient for Bundle

$$h_{average\ for\ bundle} = \frac{\text{Summation of 7 individual tube coefficients}}{7}$$

Particle Fraction

Parent, Yagol, and Steiner (20) stated that the pressure loss in a fluidized system should be equal to the weight of the solid per unit cross-sectional area of the column. Based on a balance of forces, they gave the relationship for pressure drop as:

$$\Delta P = L_t(1 - \epsilon)(\rho_s - \rho_f)$$

where,

ΔP = pressure drop across bed, lbs/ft^2

L_t = distance between pressure taps, ft

$(1 - \epsilon)$ = particle fraction, dimensionless

ρ_s = density of glass, lbs/ft^3

ρ_f = density of fluidizing air, lbs/ft^3

Since ΔP, L_t, and the densities were known for each run, the equation could be solved for the particle fraction.

Particle Reynolds Number

$$Re_p = D_p G / \mu_f$$

where,

G = air mass velocity, lbs/hr-ft^2

D_p = particle diameter, ft

μ_f = air viscosity at bed temperature, lbs/hr-ft

The air viscosity was calculated for each bed temperature from the following equation:

$$\mu_f = \left[2.45(T_{bed} - 32) + 1538.1\right] 2.688 \times 10^{-5}$$

This equation was obtained by fitting centipoise data to a straight line fit, and then multiplying by conversion factors to convert to the units given above. T_{bed} is in Fahrenheit degrees.

Particle Nusselt Number

$$Nu_p = hD_p/k_f$$

where,

h = heat transfer coefficient, BTU/hr-ft^2-F^o

D_p = particle diameter, ft

k_f = thermal conductivity of fluidizing air at bed temperature, BTU/hr-ft-F^o

The thermal conductivity of the fluidizing air was calculated for each bed temperature from the following equation:

$$k_f = 0.0133 + 0.000024T_{bed}$$

This equation was obtained by fitting thermal conductivity data to a straight line fit. T_{bed} is in Fahrenheit degrees.

Effectiveness Factor

Heat transfer from finned tube exchangers can be represented by the following equation containing an "effectiveness factor":

$$q = h_b A \phi (T_{tube} - T_{bed})$$

where,

q = heat transfer rate for finned tubes, BTU/hr

A = total area of finned tubes, ft^2

h_b = heat transfer coefficient for bare tubes at same operating conditions as for finned tubes, BTU/hr-ft^2-F^o

ϕ = effectiveness factor, dimensionless

The effectiveness factor described in this manner includes the conventional fin efficiency term accounting for temperature gradients within the fins, as well as a term allowing for the decrease in heat transfer caused by the interference with particle movement as the fin height increases.

PERFORMANCE OF INDIVIDUAL TUBE BUNDLES

The first heat transfer coefficients were measured by assembling the bundle of bare tubes and spacing the tubes a distance of 5.3" between centers, with the outer tubes being 2" from the column wall. In this position it could be assumed that the 7 tubes were performing independently and were free of any particle interference caused by neighboring tubes or by "wall effects". The individual tube heat transfer coefficients should have been the same for this tube positioning, but the initial data indicated a difference of about 10% between the highest individual tube coefficient and the lowest coefficient. It was believed that a large part of this difference in the measured coefficients was caused by errors in reading the wattmeter and the potentiometer, and by errors in measuring the tube areas. To determine the magnitude of experimental error that could be expected, an error analysis was performed using the procedure discussed on page 53 of reference (18).

Error Analysis:

Starting with the definition of the heat transfer coefficient,

$$h = q/A\Delta T$$

the approximation form of the total differential becomes

$$\Delta h = (\partial h/\partial q)\Delta q + (\partial h/\partial A)\Delta A + (\partial h/\partial \Delta T)\Delta(\Delta T)$$

Taking the partial derivative of h with respect to q, A, and ΔT,

and substituting in the equation, the total differential becomes

$$\Delta h = (1/A\Delta T)\Delta q + (-q/A^2\Delta T)\Delta A + (-q/A(\Delta T)^2)\Delta(\Delta T)$$

For the bare tubes, with the largest particles and the lowest air rate, the values of the three parameters were as follows:

$$A = 0.0873 \text{ ft}^2$$

$$\Delta T = 80\text{F}^\circ$$

$$q = 513 \text{ BTU/Hr}$$

Substituting these values into the above equation,

$$\Delta h = 0.143\Delta q + 843\Delta A + 0.920\Delta(\Delta T)$$

The minus signs in front of the last two terms were changed to plus so that the maximum value of Δh could be calculated. This was a legal move because Δq, ΔA, and $\Delta(\Delta T)$ are all plus or minus deviations.

Then, assuming that the wattmeter and the potentiometer could be read within an error of plus or minus 2%, and that the tube area could be measured within plus or minus 2%, the following maximum individual errors would result:

$$\Delta q = 2\% \times 513 = 10.2 \text{ BTU/Hr}$$

$$\Delta A = 2\% \times 0.0873 = 0.0017 \text{ ft}^2$$

$$\Delta(\Delta T) = 2\% \times 80 = 1.6 \text{ F}^\circ$$

Substituting these values into the last equation above,

$$\Delta h = 0.143(10.2) + 843(0.0017) + 0.920(1.6)$$

$$= 4.4 \text{ BTU/Hr-ft}^2\text{-F}^\circ$$

Since the measured value of h was 70 BTU/Hr-ft^2-F$^\circ$, the percent

error would be equal to (4.4/70) x 100% = 6%. This is the maximum experimental error that could be expected, and it would occur if the 2% error occurred in all three of the parameters simultaneously and in the directions that would result in the summation of the three terms in the equation. Since the errors in the three parameters could be made in either the positive or negative direction, the maximum experimental error between any two tubes in the bundle would be 12%. This estimate of maximum error is, of course, dependent upon the accuracy of the assumption that the three parameters could be measured within plus or minus 2%.

In the Experimental Program it was stated that the objective of this investigation was to determine the effect of tube spacing and fin height on the heat transfer coefficient of each tube in the bundle. However, with one exception, it was found that the 7 individual tube coefficients were within 15% of each other for all tube bundles at all of the operating conditions studied. Since the error analysis indicated a possible experimental error of 12%, it was decided that the measured differences between tube coefficients could be attributed to experimental error rather than to the position of the tube in the bundle. Therefore, in all of the graphs of Heat Transfer Coefficients versus Air Mass Velocity on the pages following, only the value of the arithmetic average of the 7 individual coefficients was plotted. It should be noted that there was no consistent pattern for the heat transfer coefficient for any particular tube position in the bundle. For example, with some

of the bundles the coefficient for the center tube was consistently higher than the average of the 6 other tubes, while with other bundles the coefficient for the center tube was lower than the average of the other tubes. Also, the 7 individual coefficients in any one bundle sometimes varied in relative magnitude as the operating conditions changed. That is, the coefficient of the tube on the bottom right might be the highest for a given air flow rate, but the coefficient of the tube on top left might be slightly higher at a different air rate. As mentioned, however, the maximum difference between the highest and lowest coefficients in the bundle for any run was always less than 15%. It appeared that each tube had certain inherent characteristics, perhaps resulting from slight differences in thermocouple attachment or from differences in heater to tube contact, which introduced additional error in the coefficients above that expected from the 2% errors in the three parameters. In any case, it was assumed that all of the differences between individual tube coefficients were caused by experimental or inherent errors, and that no differences could be detected resulting from a particular tube location in the bundle.

The one exception mentioned above occurred with the 0.875" fins when the tubes were meshed tightly together so that the fins on adjacent tubes overlapped by 0.78". With the tubes in this position, the coefficient of the center tube was considerably lower than could be expected from experimental error. That study is discussed in detail on page 145.

Performance curves (Average Heat Transfer Coefficient versus Air Mass Velocity) for the individual tube bundles are shown in Figures 16 thru 38 on page 76 thru 102. The expressions "distance between tube surfaces", "distance between fin tips", and "center-to-center distance" used on the graphs are defined in Figures 14 and 15.

Bare Tubes: For bare tubes it was found that the average heat transfer coefficient for the bundle increased when the tubes were moved from the most clustered position (0.4375" between tube surfaces) to the first expanded position (1.50" between tube surfaces). However, there was no additional increase in the average coefficient when the bundle was expanded at 1.0625" increments to the final expanded position of 4.6875" between tube surfaces. This was true for all particle sizes.

To obtain some indication of the accuracy of the measured coefficients in this study, a comparison was made between the experimental data for bare tubes and two correlations from the literature. Petrie, Freeby, and Buckham correlated heat transfer coefficients for an expanded horizontal bundle of bare tubes heated with steam, while Vreedenberg suggested a correlation for a single horizontal bare tube. The two correlations are as follows:

Petrie, Freeby, and Buckham (22):

$$N_{Nu_t} = 14(G/G_{mf})^{0.33}(N_{Pr})^{0.33}(D_t/D_p)^{0.667}$$

where,

N_{Nu_t} = Nusselt number based on tube diameter

G/G_{mf} = reduced fluidizing air mass velocity ratio

N_{Pr} = Prandtl number of the fluidizing air

D_t/D_p = ratio of tube diameter to particle diameter

Fluid properties were arbitrarily determined at a film temperature, defined as the arithmetic average between the bed temperature and the surface temperature of the horizontal tubes.

Vreedenberg (25):

$$N_{Nu_t} = 420(N_{Pr})^{0.33}(GD_t\mu/D_p^3\rho_s\rho g)^{0.33}$$

where,

G = fluidizing air mass velocity, lbs/hr-ft^2

ρ = density of fluidizing gas, lbs/ft^3

ρ_s = apparent particle density of solids, lbs/ft^3

g = gravitational constant, 4.18×10^8 ft/hr^2

μ = viscosity of the fluidizing air, lb/hr-ft

In the Vreedenberg correlation, fluid properties were evaluated at the temperature of the bed.

Since the first correlation is for an expanded bundle and the second is for a single horizontal tube, only the expanded bundle experimental data shown in Figure 16 was compared to the correlations. Since

there is no difference in the measured average coefficient when the tubes are moved from a distance of 0.4375" to 4.6875" between tube surfaces, it can be assumed that the tubes are performing independently in this region and, therefore, the average of the 7 tubes can be compared with the correlation for a single horizontal tube as well as with the correlation for the expanded bundle.

The comparison of the experimental data with the two correlations is shown in Figure 18. Since the experimental data is reasonably close to both correlations, and in much of the graph is closer to either correlation than the two correlations are to each other, it was assumed that the measured coefficients have reasonable values.

For the bare tube bundle, as well as for all of the finned tube bundles, the column was also operated without particles so that the coefficients for forced convection could be measured. The results for the bare tube bundle are plotted in Figure 17. The forced convection data is not compared to literature values because it is felt that this experimental data is not as accurate as the data obtained when particles were used. The reason for this is that the equipment was not designed for measuring coefficients without particles, as the air temperature must be found by averaging the three bed thermocouple readings, rather than by using a thermocouple adjacent to each tube wall. Thus, with the equipment as designed, the same air temperature is used for all 7 tubes, when in reality there is a large temperature gradient in the air from

the area around the lower tube to the area around the upper tube. It was mentioned previously that when particles were used the three bed temperatures were within 1 F^{o} of each other. However, when no particles were used the difference between the upper bed temperature and the lower bed temperature was as large as 40 F^{o}, depending upon the spacing of the tubes. Therefore, when the average of the three bed temperatures was used as the air temperature for all of the tubes, considerable error was introduced into the calculated coefficient for each tube. Hopefully, the errors were balanced out when the average of the 7 individual coefficients was taken, but most likely some error remains in the averaged value. Therefore, in all of the plots of Average Heat Transfer Coefficient versus Air Mass Velocity for the runs where no particles were used, it must be emphasized that the coefficients are not as accurate as those obtained with particles, and that they are presented only to provide a rough indication of how much the heat transfer rate from the bundles increases when particles are used.

Finned Tubes:

0.125" Fins: Performance curves for the bundle of tubes with 0.125" fins are shown in Figures 19 thru 22 for the individual tube spacings; the curves are then summarized for each particle size in Figures 23 thru 25. In these last three figures it is clear that the largest increase in the heat transfer coefficients occurs in the first inch

of bundle expansion; the increases in the coefficients as the bundle is expanded further are relatively small.

It can be seen that the coefficients for the small particles are nearly the same as those for the medium particles and, in fact, in Figures 19 and 21 the curves for the small particles are slightly below those for the medium particles. This is contradictory to what would be expected, and can be explained partly by experimental error and partly by an effect discussed by Nazemi, Lancaster, and Wheelock (19) who stated that small particles sometimes cling together because of van der Waal interparticle adhesive forces, producing an effective diameter larger than the actual particle diameter. This closeness of heat transfer coefficients for the small and medium particles was observed for all of the fin heights investigated.

Some of the performance curves for the 0.125" finned tube bundle, as well as for all of the other bundles, exhibit a maximum value, while other curves are monotonically increasing or decreasing. This behavior is caused by the interaction of two opposing effects taking place in the column as the air velocity is increased. An increase in air velocity will cause an increase in particle circulation, with resulting higher heat transfer rates, while at the same time the increased velocity will cause the bed to expand, resulting in a lower particle fraction in the vicinity of the tubes and lower heat transfer rates. This interaction of the two effects sometimes produces a

maximum in the coefficient curve, while at other times it produces curves that are either increasing or decreasing. This phenomena is discussed in more detail on page 266 of reference (13).

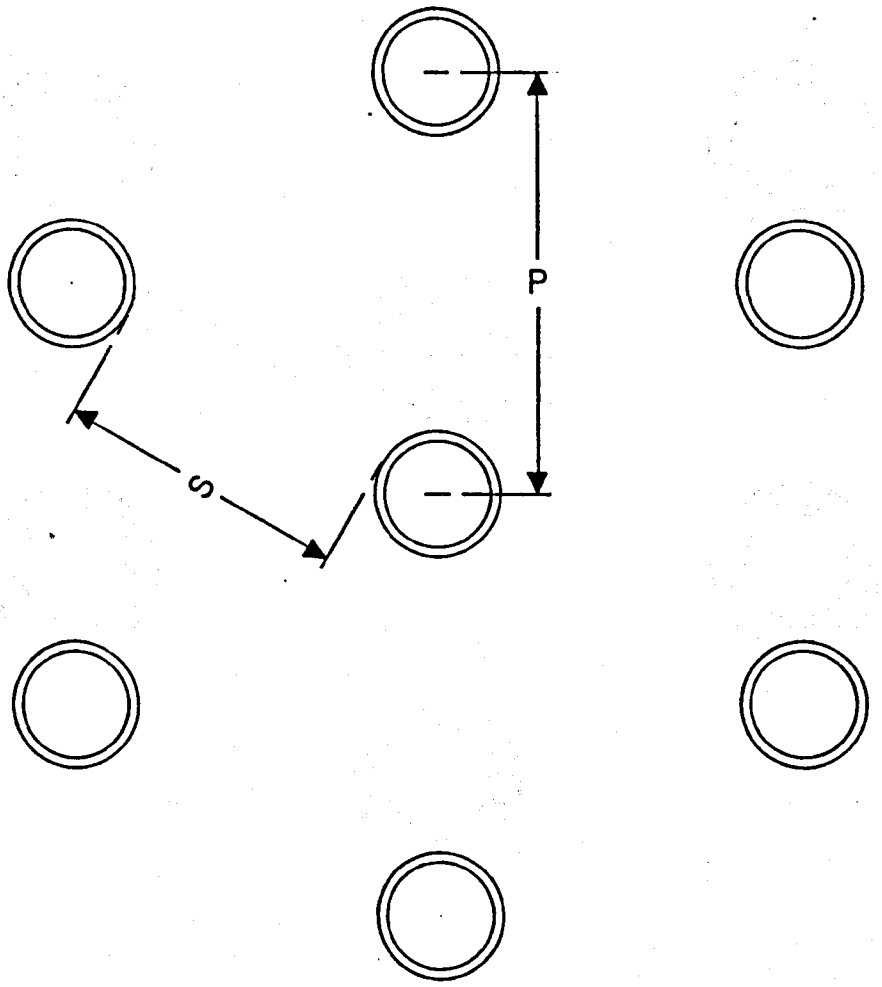
0.375" Fins: Heat transfer coefficients for the 0.375" finned tube bundle were measured only for the most clustered position (0.2188" between fin tips) and for the most expanded position (3.4063" between fin tips). The two curves for each particle size are shown in Figures 27 thru 29.

0.625" Fins: The 0.625" finned tube bundle was investigated at three different spacings (0.25", 1.3125", and 2.375" between fin tips). The curves are shown in Figures 31 thru 33. As in the 0.125" finned tube bundle, the largest increase in heat transfer coefficients took place in the first inch of bundle expansion, while the second expansion resulted in a smaller increase in the coefficients.

0.875" Fins: For all of the previous coefficients measured in this study the bundles were expanded in increments of 1.0625". It was decided that with the 0.875" finned tube bundle the increment of bundle expansion would be cut in half to a distance of 0.5313". To do this, the existing micarta plates were first used and the coefficients were measured at 0.8125" and 2.4063" between fin tips. Two new micarta plates were then fabricated in which the holes for the heaters were offset by 0.5313" from the holes in the original plates. With the

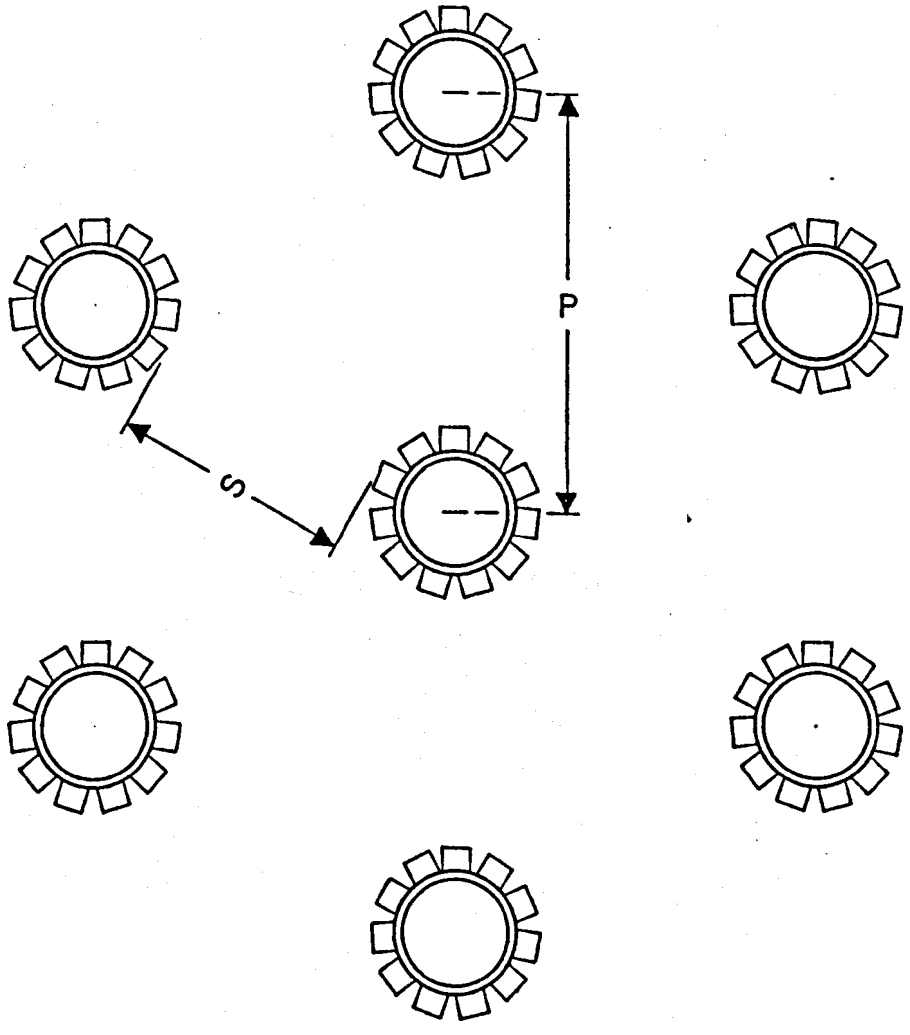
two new micarta plates on the column, the coefficients were then measured at 0.2813" and 1.3438" between fin tips. The performance curves for the four bundle expansions are shown in Figures 35 thru 37. It can be seen that there is only a slight difference in the magnitude of the coefficients for the bundle in any of the four expanded positions.

A second modification was made with the 0.875" finned tube bundle when the tubes were meshed tightly together so that the fins on adjacent tubes overlapped by 0.78" as shown in Figure 57. With the tubes in this arrangement, the average coefficients for the bundle were much lower than the coefficients in any of the four expanded bundle positions. This investigation was made only with the small and medium particles, and the results are shown in Figures 35 and 36. A more detailed discussion of this study is given on page 145.



P = CENTER - TO - CENTER DISTANCE
S = DISTANCE BETWEEN TUBE SURFACES

FIGURE 14. NOMENCLATURE USED WITH BARE TUBES



P = CENTER - TO - CENTER DISTANCE

S = DISTANCE BETWEEN FIN TIPS

FIGURE 15. NOMENCLATURE USED WITH FINNED TUBES

PERFORMANCE CURVES

for

BARE TUBES

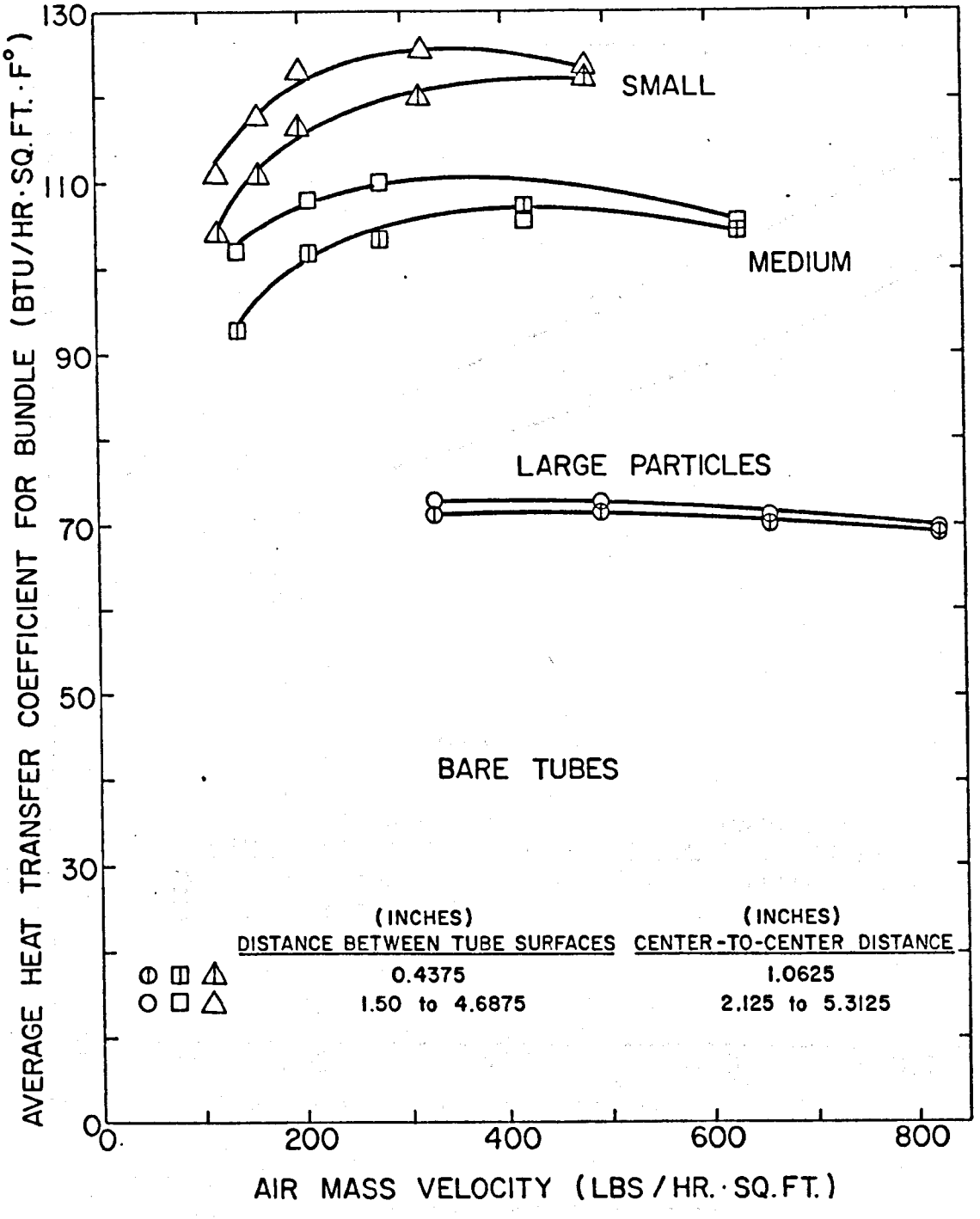


FIGURE 16. PERFORMANCE OF BARE TUBES

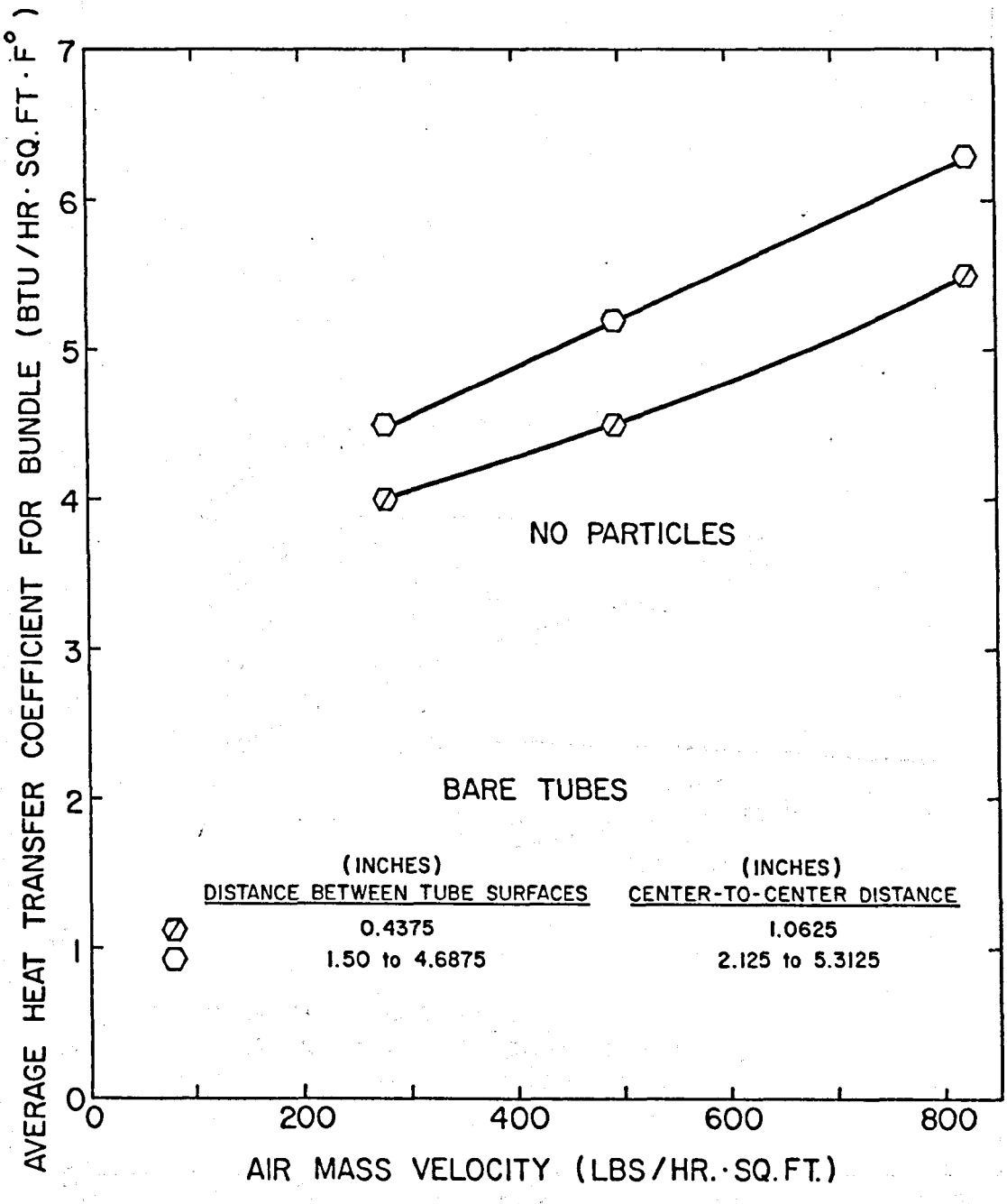


FIGURE 17. PERFORMANCE OF BARE TUBES

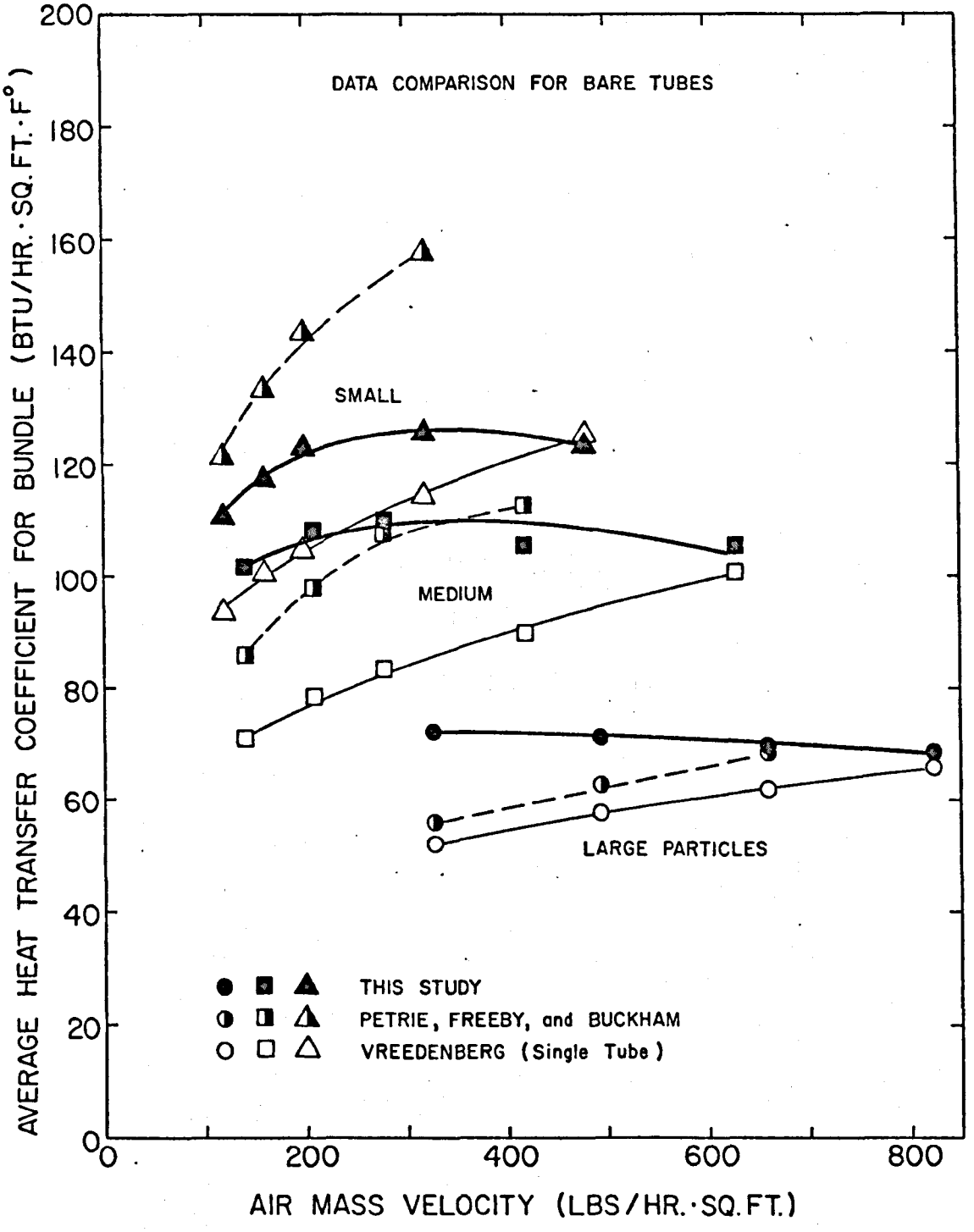


FIGURE 18. COMPARISON OF EXPERIMENTAL DATA WITH CORRELATIONS FROM LITERATURE

PERFORMANCE CURVES

for

1/8 inch FINNED TUBES

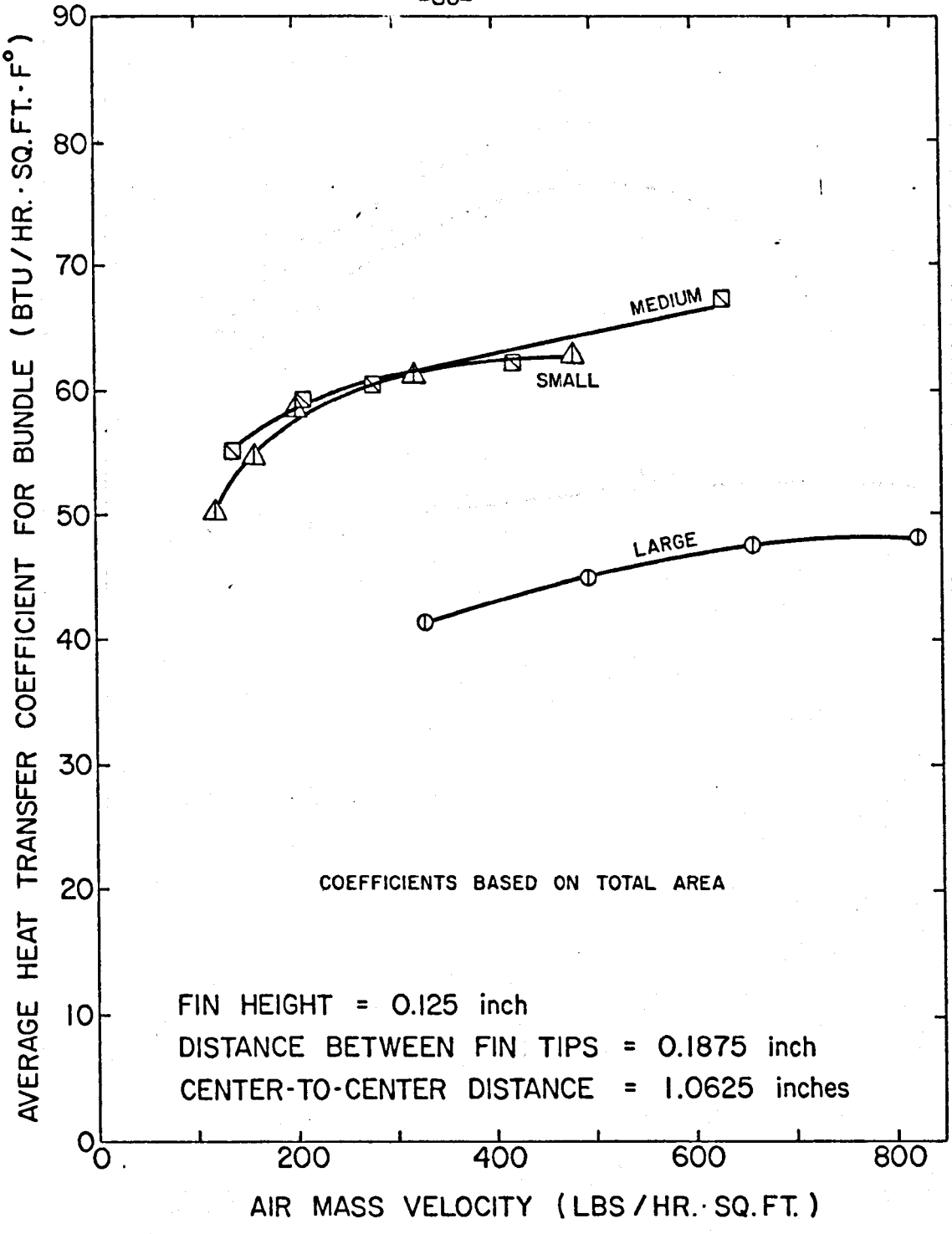


FIGURE 19. PERFORMANCE OF 0.125" FINNED TUBES

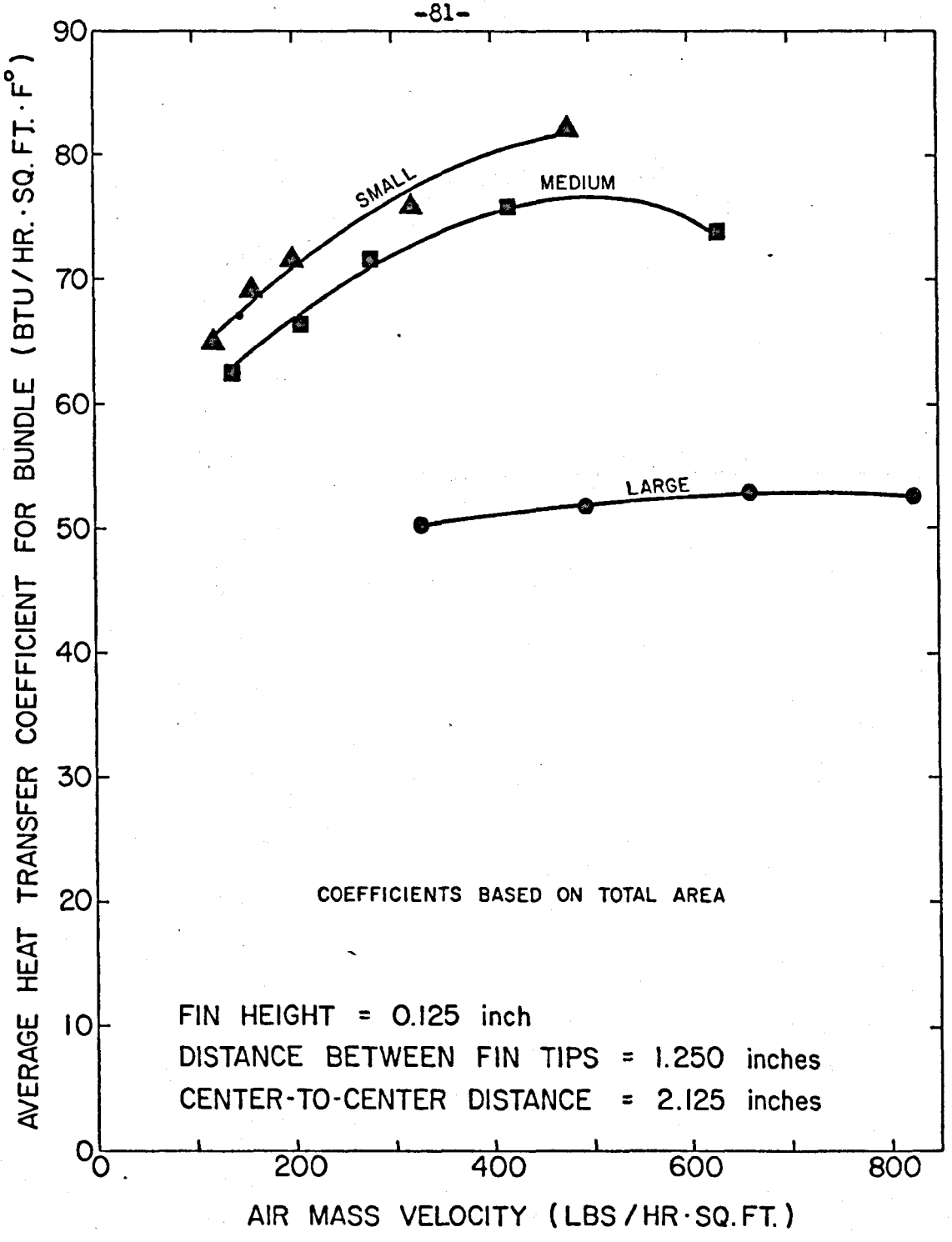


FIGURE 20. PERFORMANCE OF 0.125" FINNED TUBES

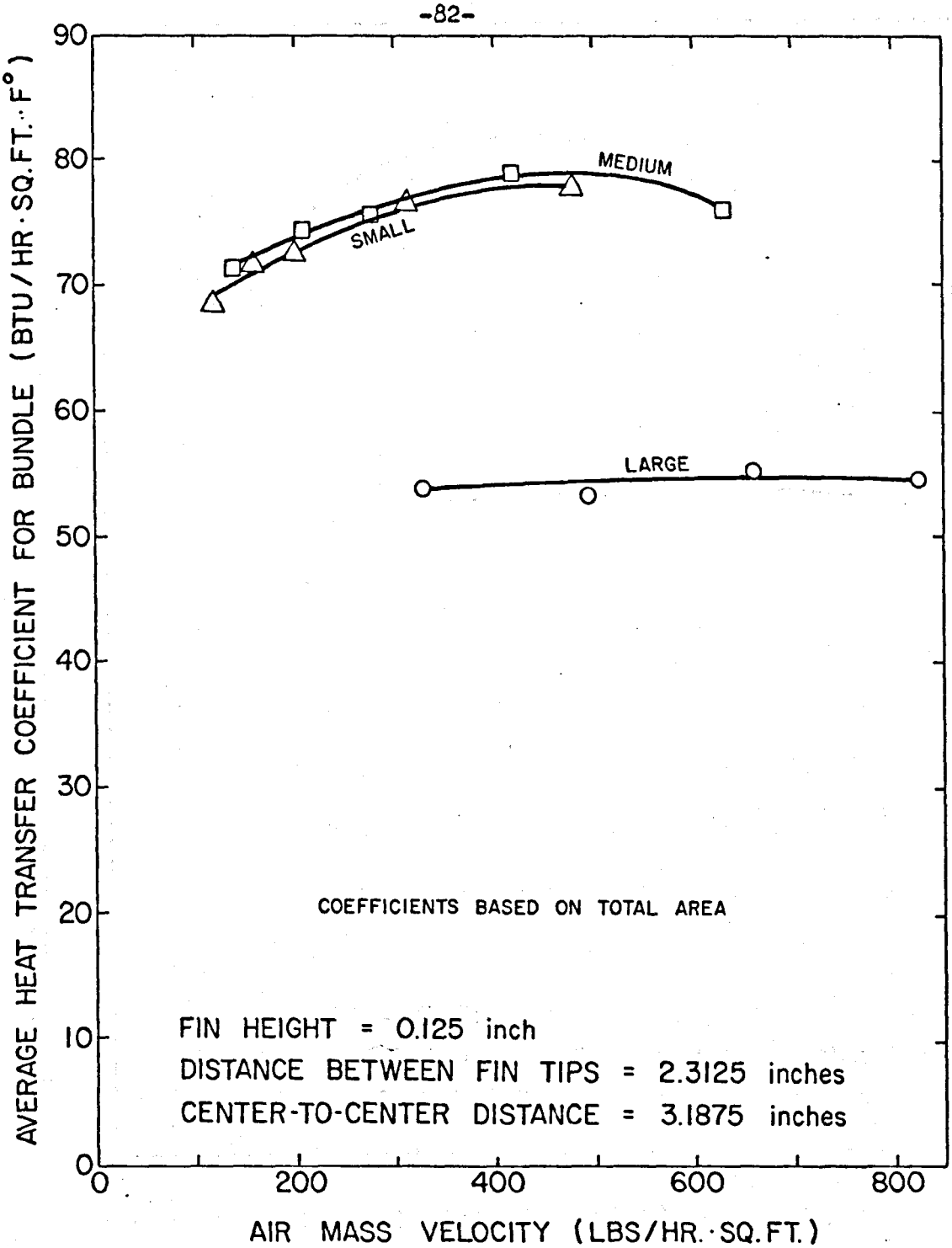


FIGURE 21. PERFORMANCE OF 0.125" FINNED TUBES

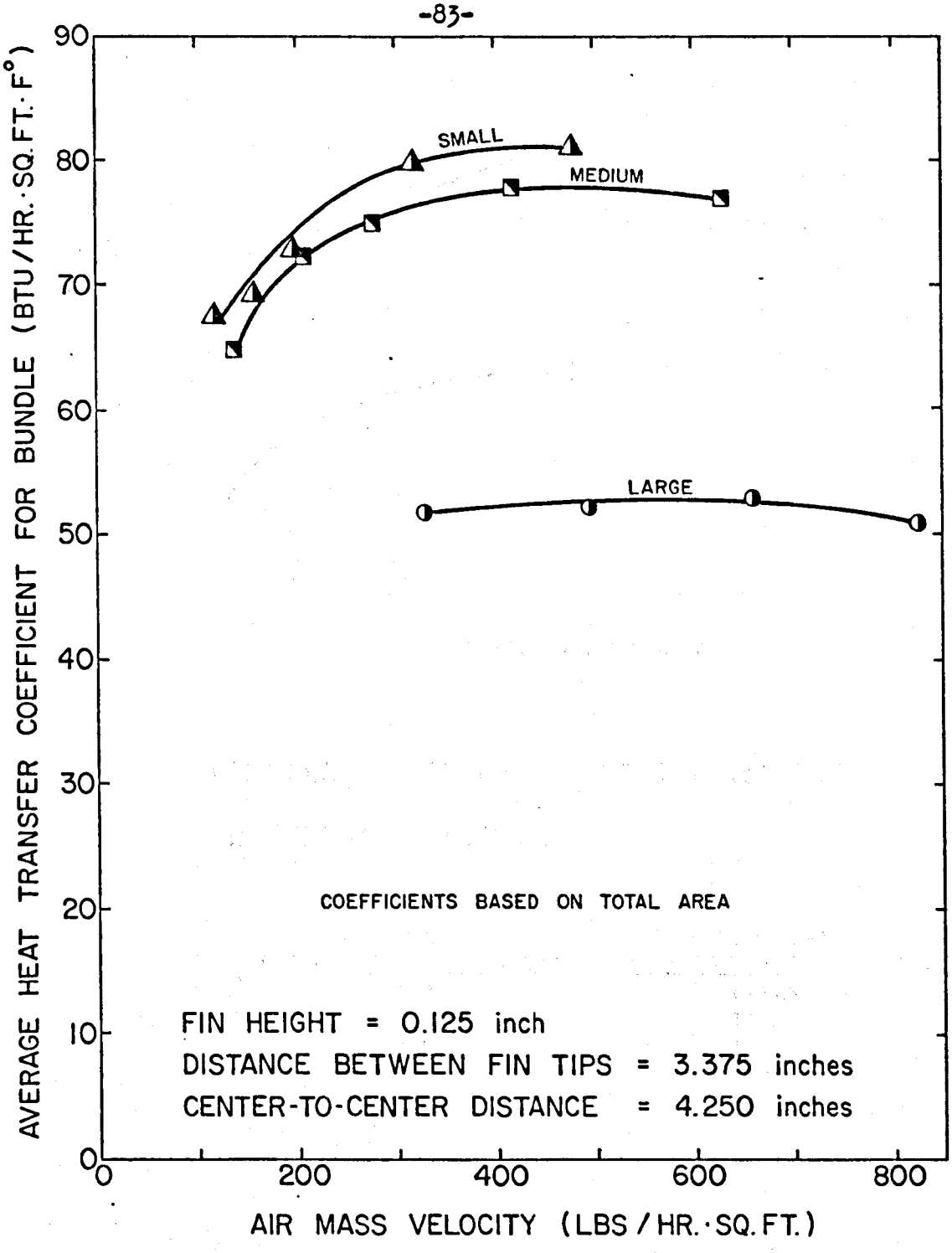


FIGURE 22. PERFORMANCE OF 0.125" FINNED TUBES

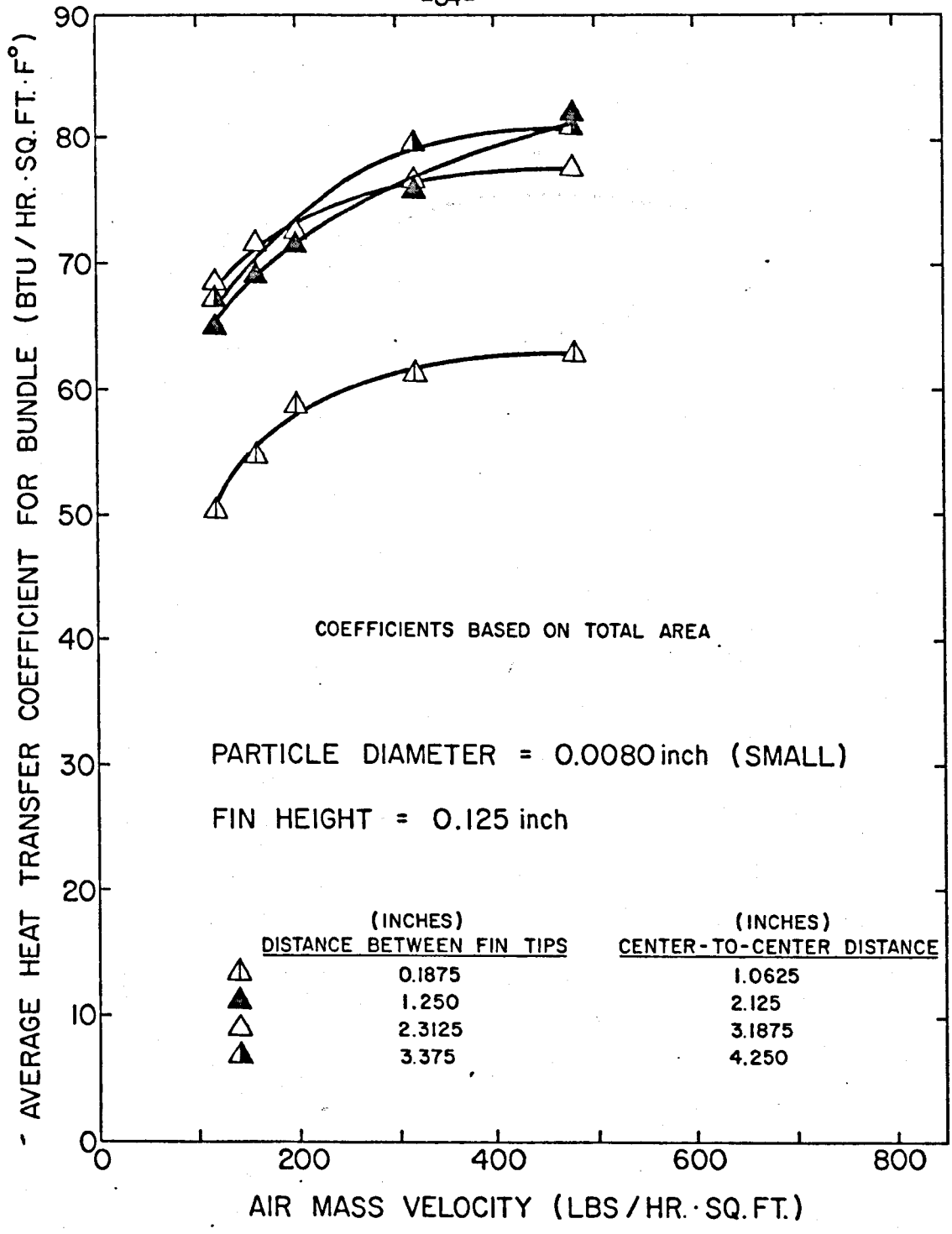


FIGURE 23. PERFORMANCE OF 0.125" FINNED TUBES

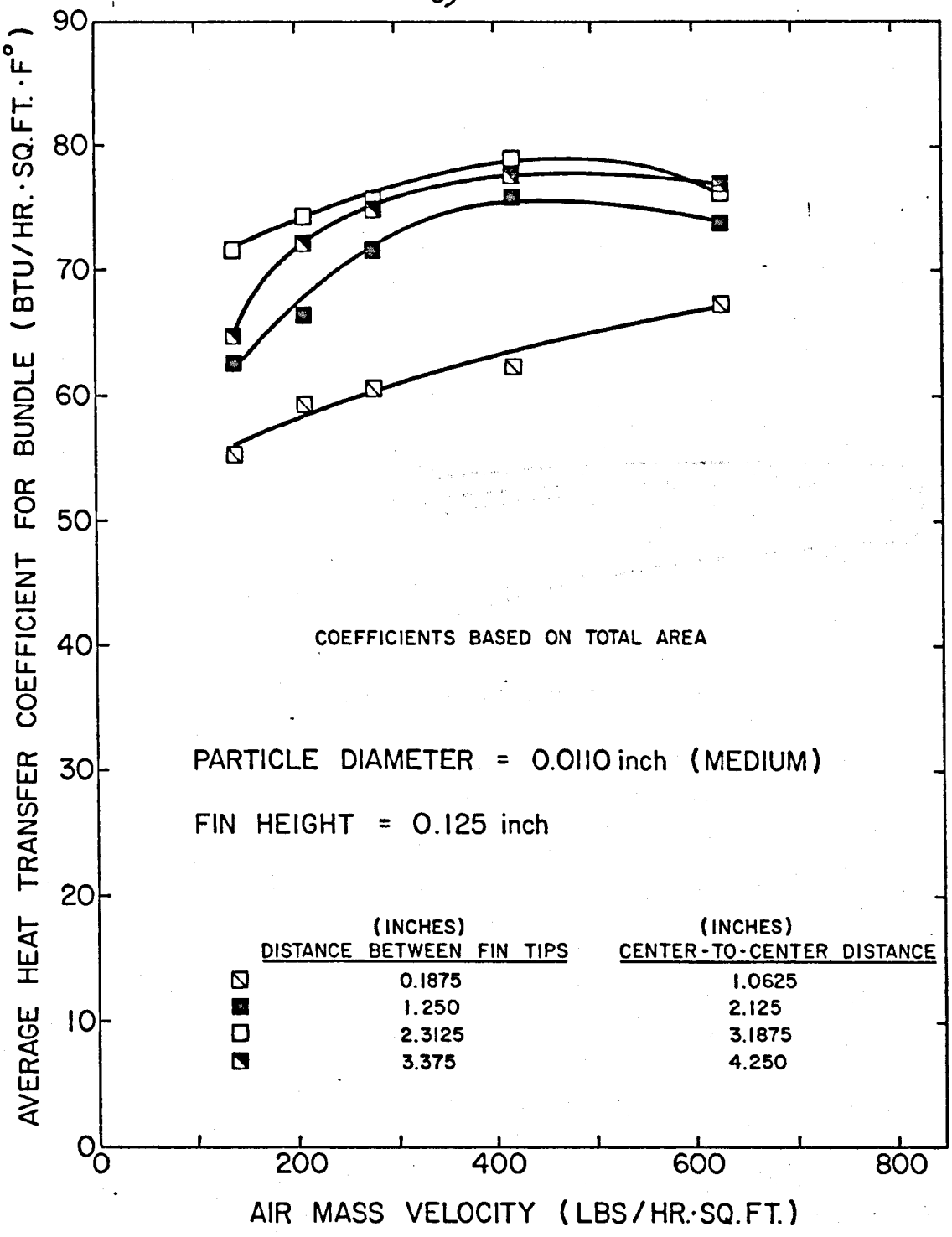


FIGURE 24. PERFORMANCE OF 0.125" FINNED TUBES

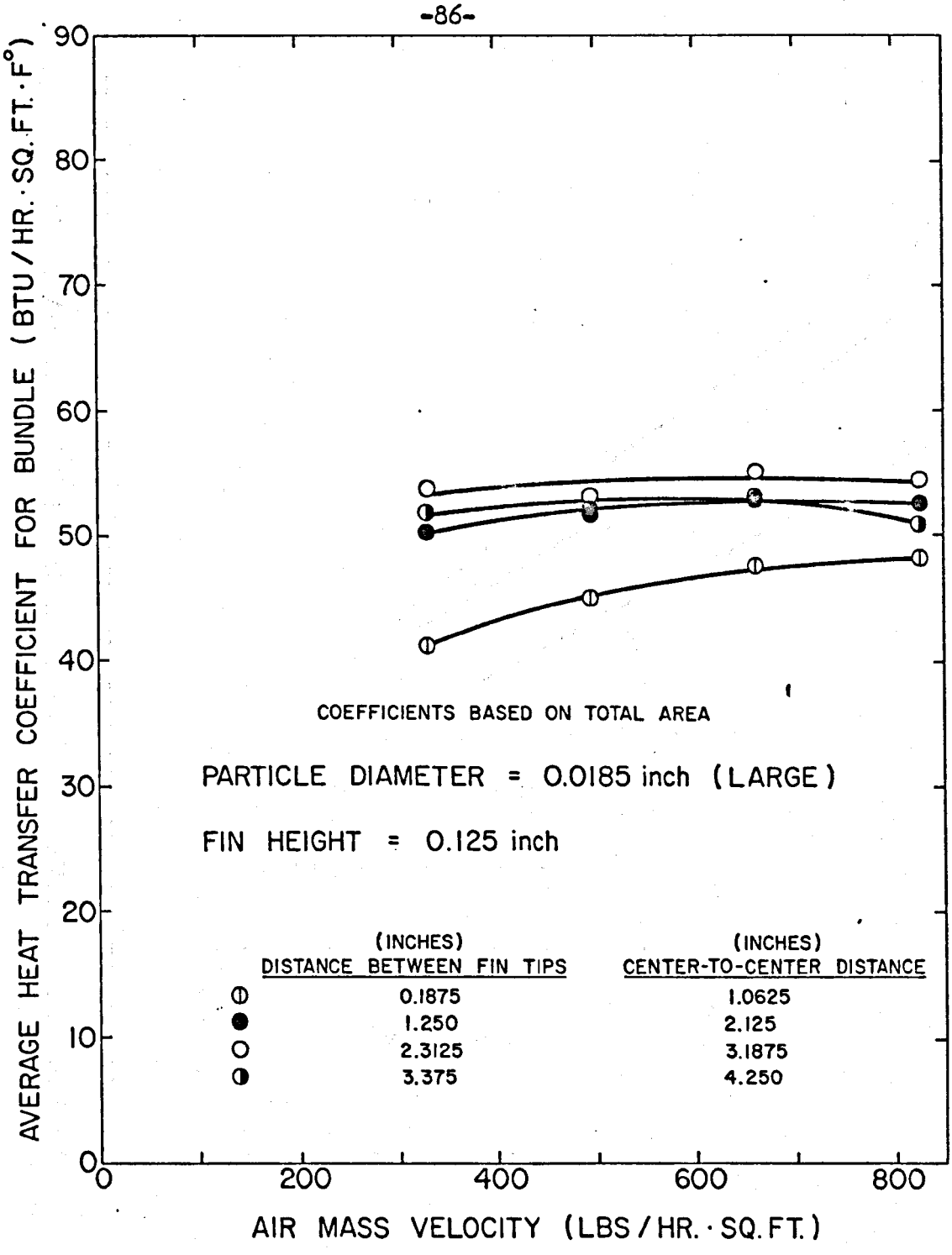


FIGURE 25. PERFORMANCE OF 0.125" FINNED TUBES

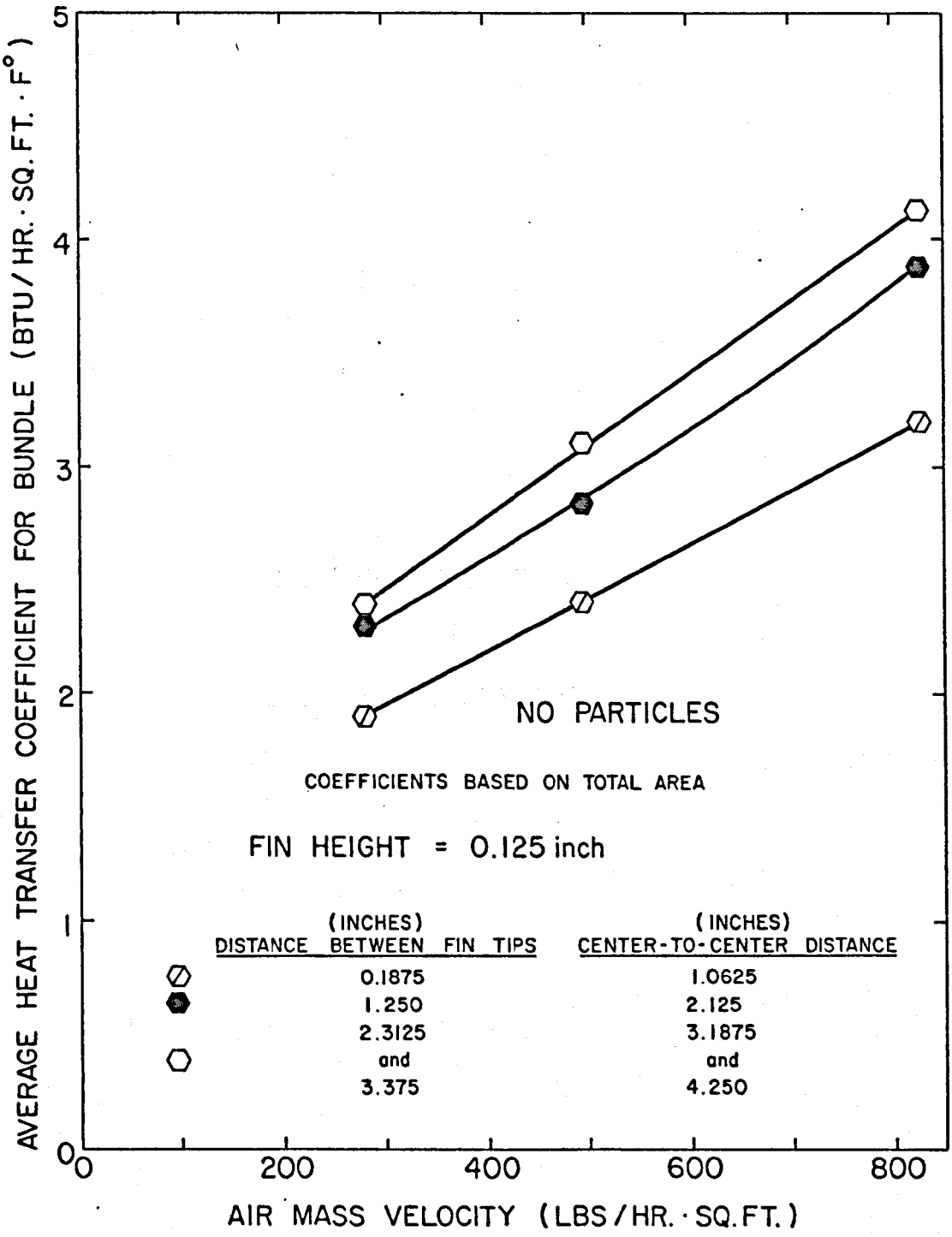


FIGURE 26. PERFORMANCE OF 0.125" FINNED TUBES

PERFORMANCE CURVES

for

3/8 inch FINNED TUBES

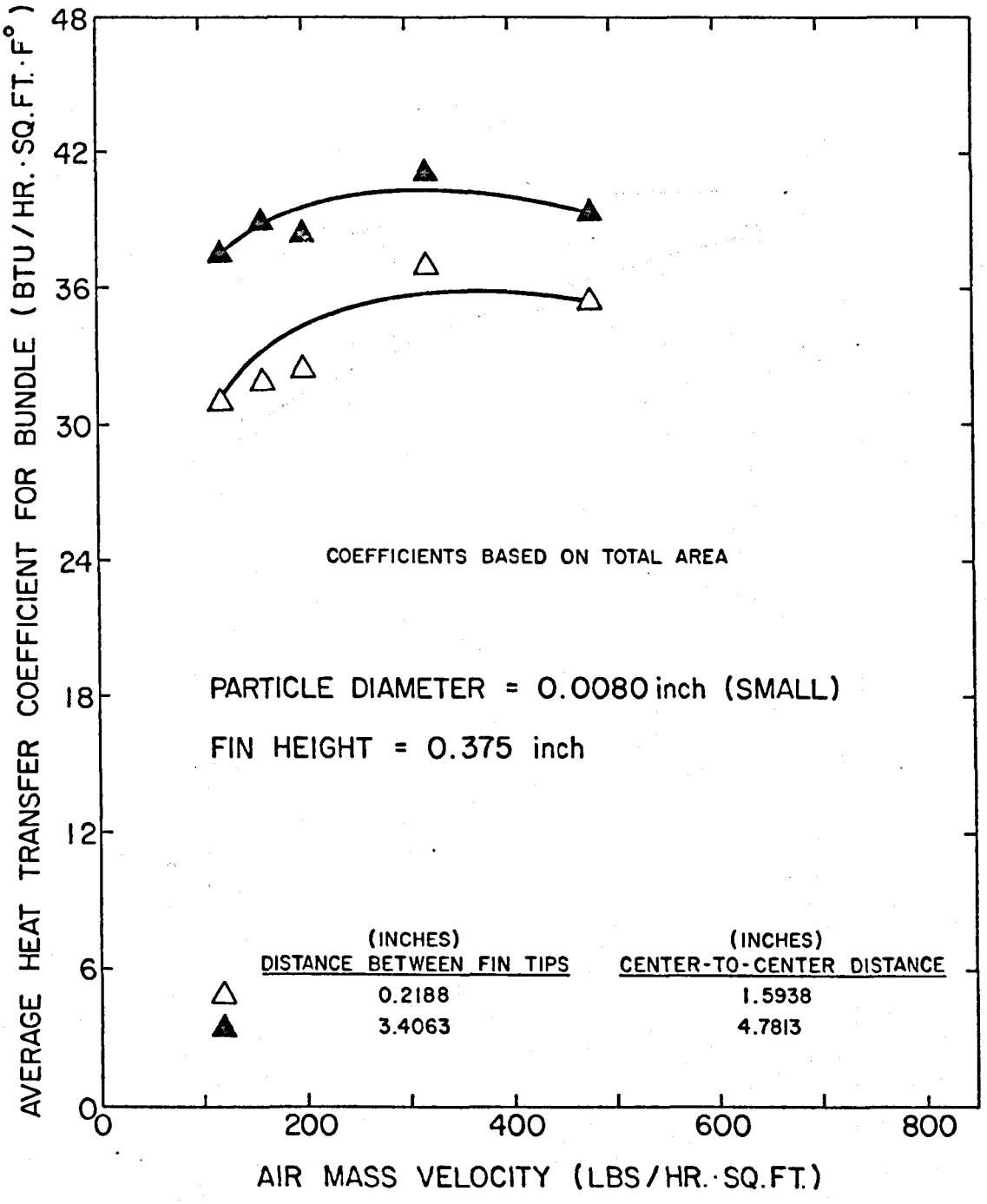


FIGURE 27. PERFORMANCE OF 0.375" FINNED TUBES

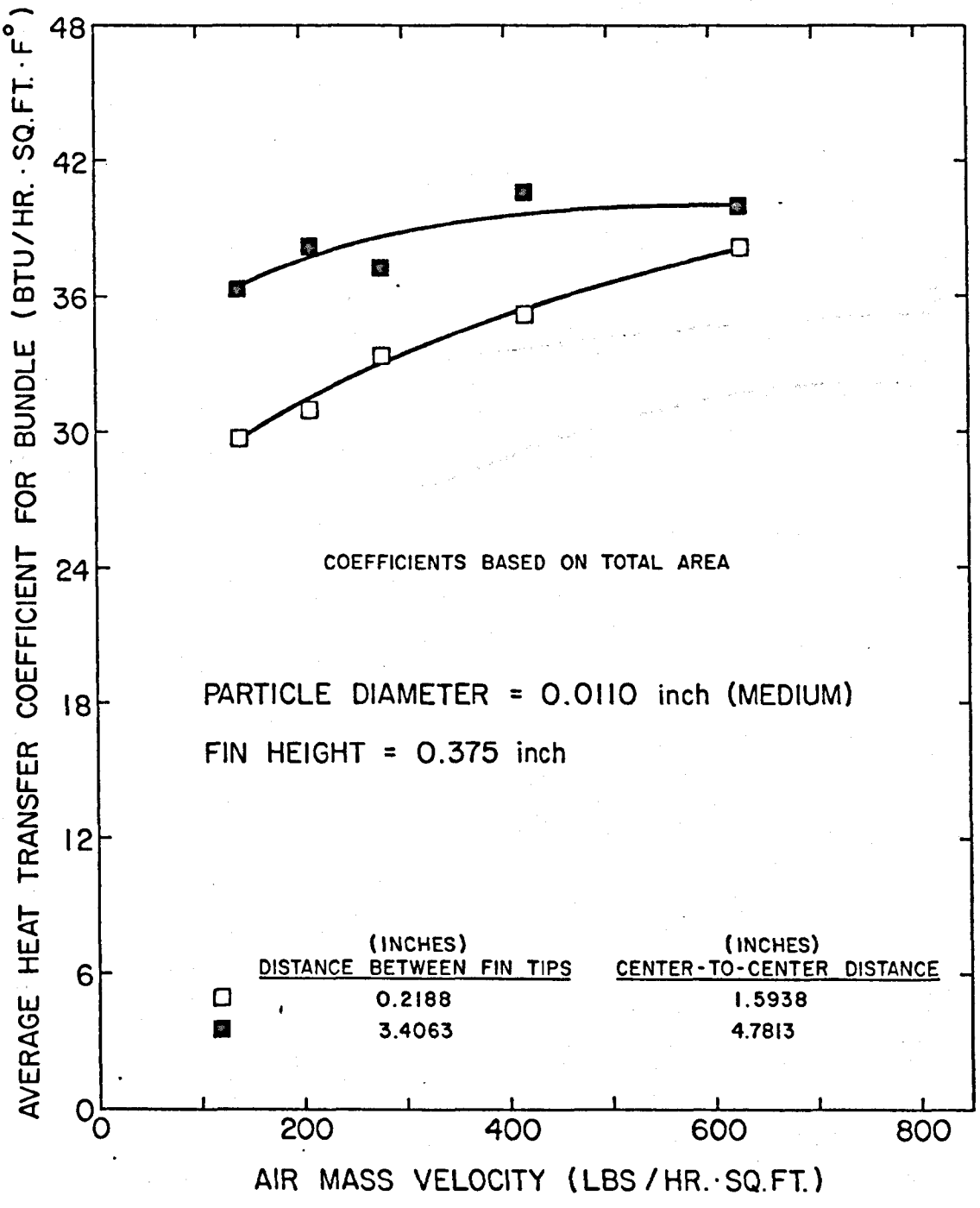


FIGURE 28. PERFORMANCE OF 0.375" FINNED TUBES

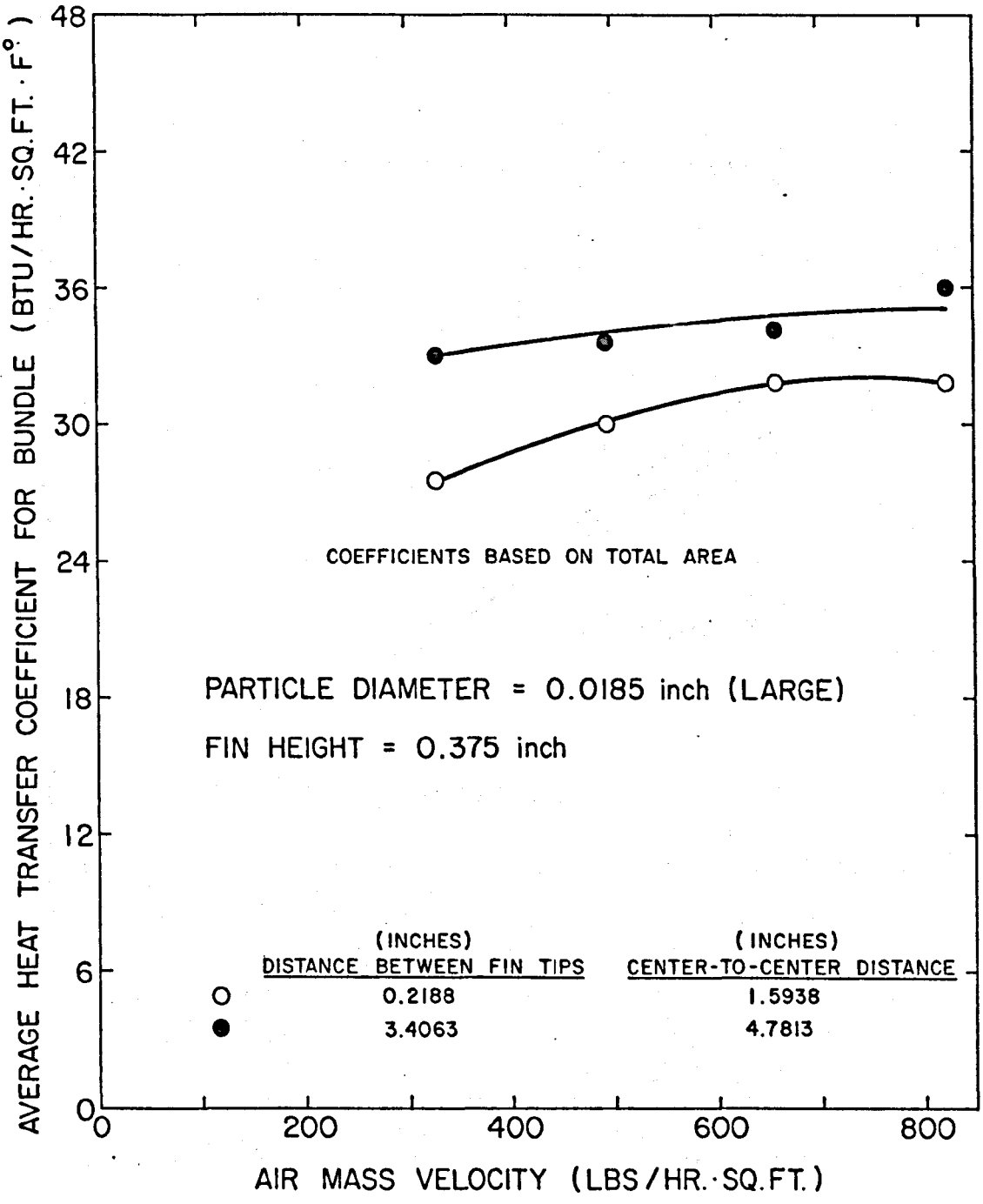


FIGURE 29. PERFORMANCE OF 0.375" FINNED TUBES

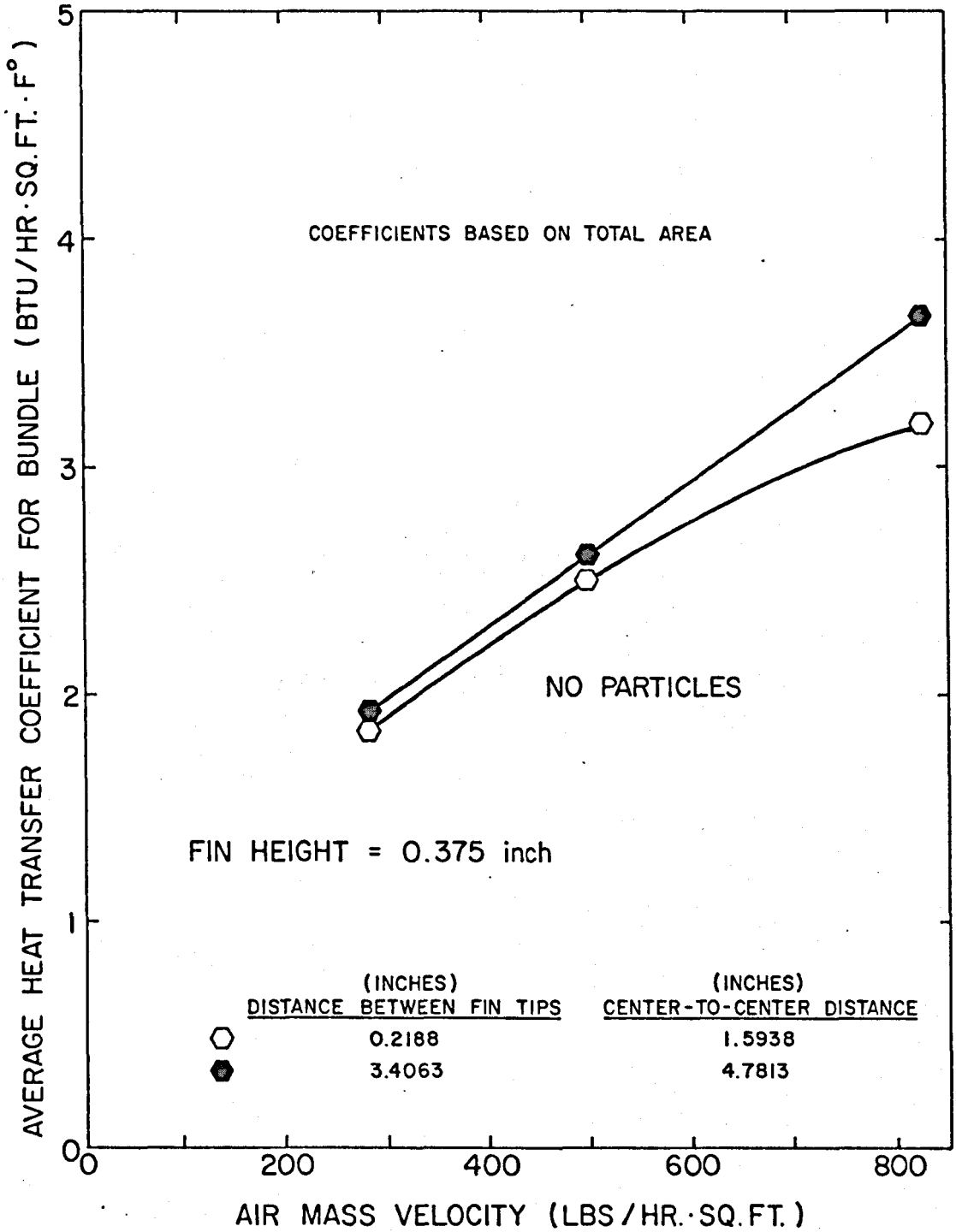


FIGURE 30. PERFORMANCE OF 0.375" FINNED TUBES

PERFORMANCE CURVES
for
5/8 inch FINNED TUBES

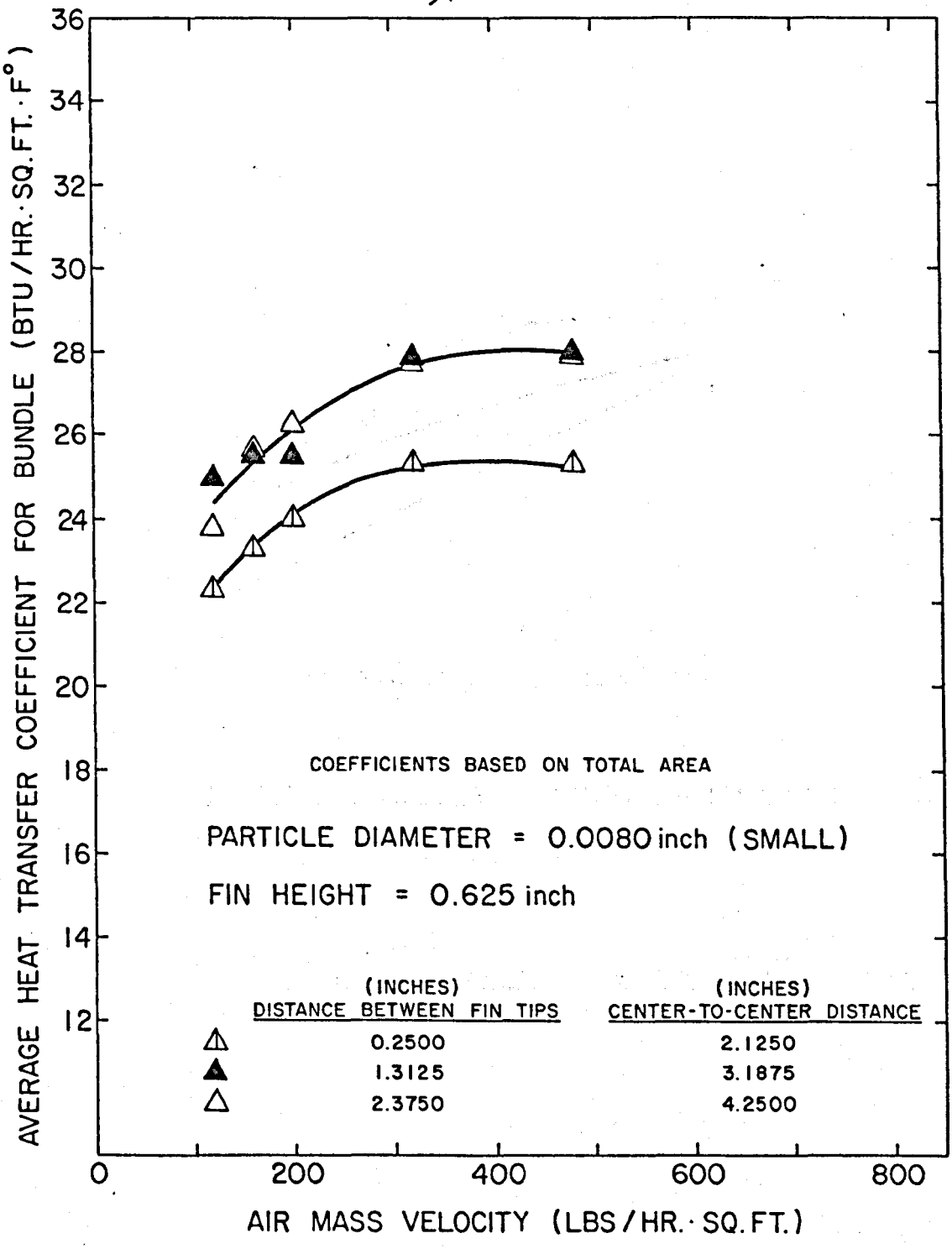


FIGURE 31. PERFORMANCE OF 0.625" FINNED TUBES

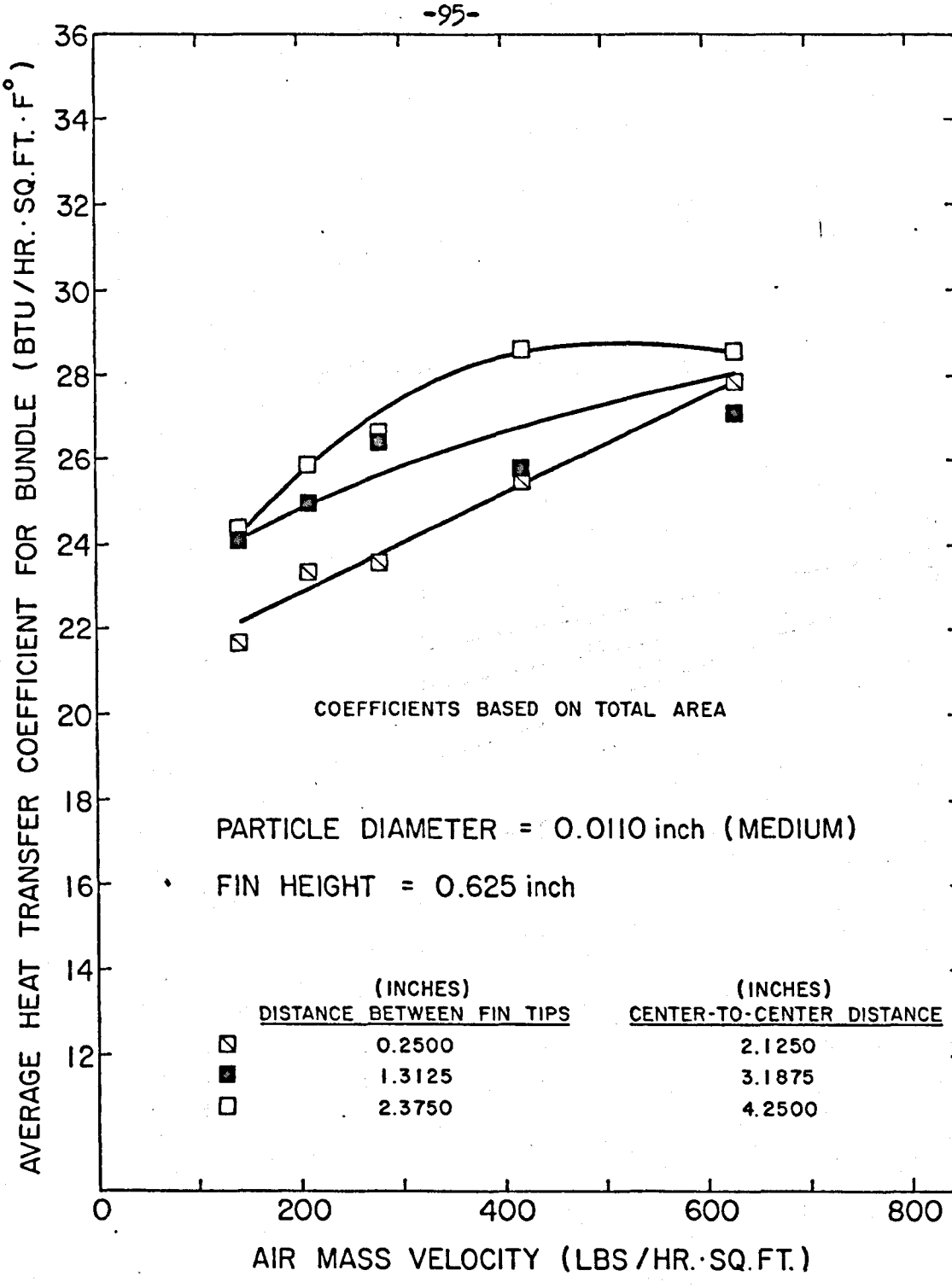


FIGURE 32. PERFORMANCE OF 0.625" FINNED TUBES

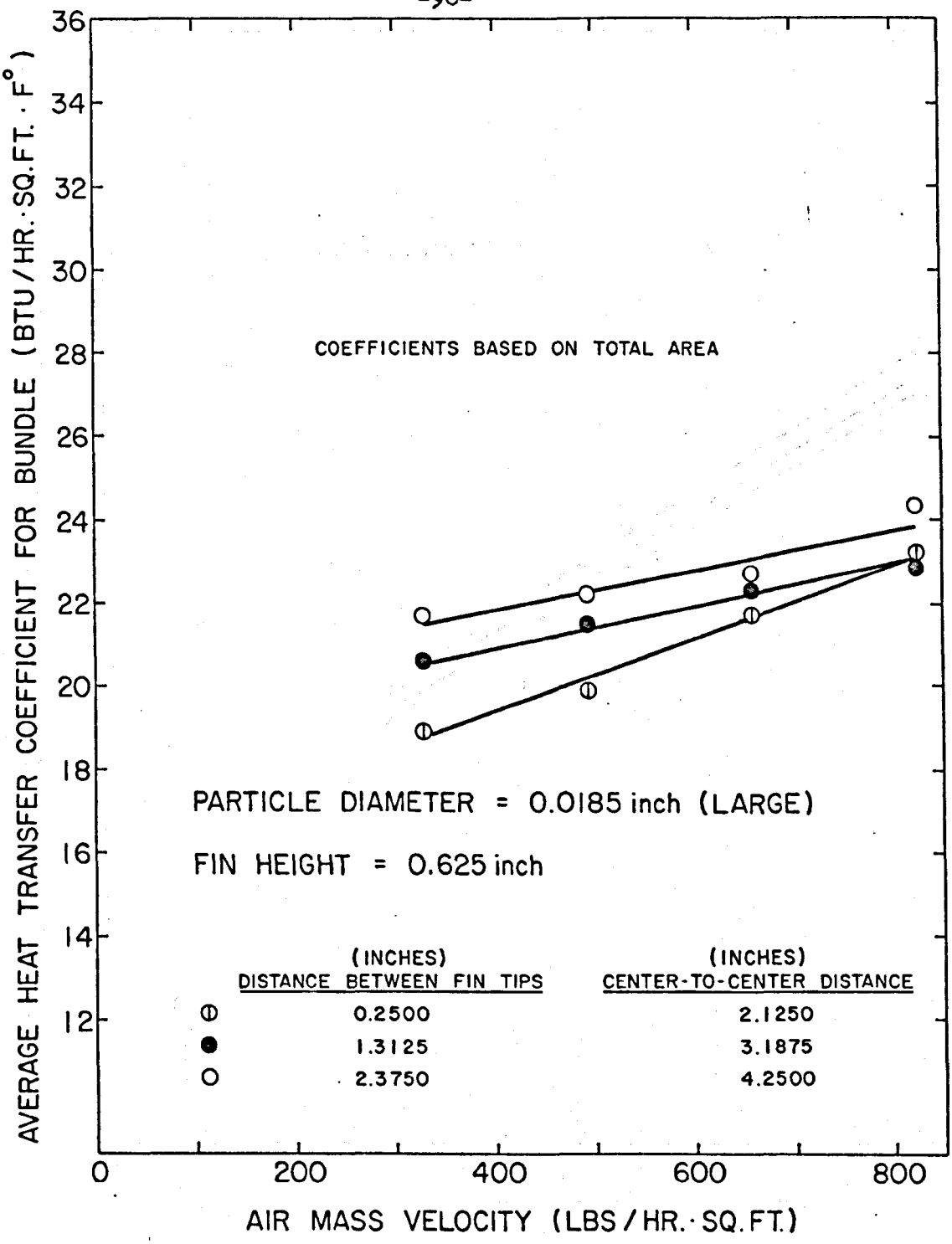


FIGURE 33. PERFORMANCE OF 0.625" FINNED TUBES

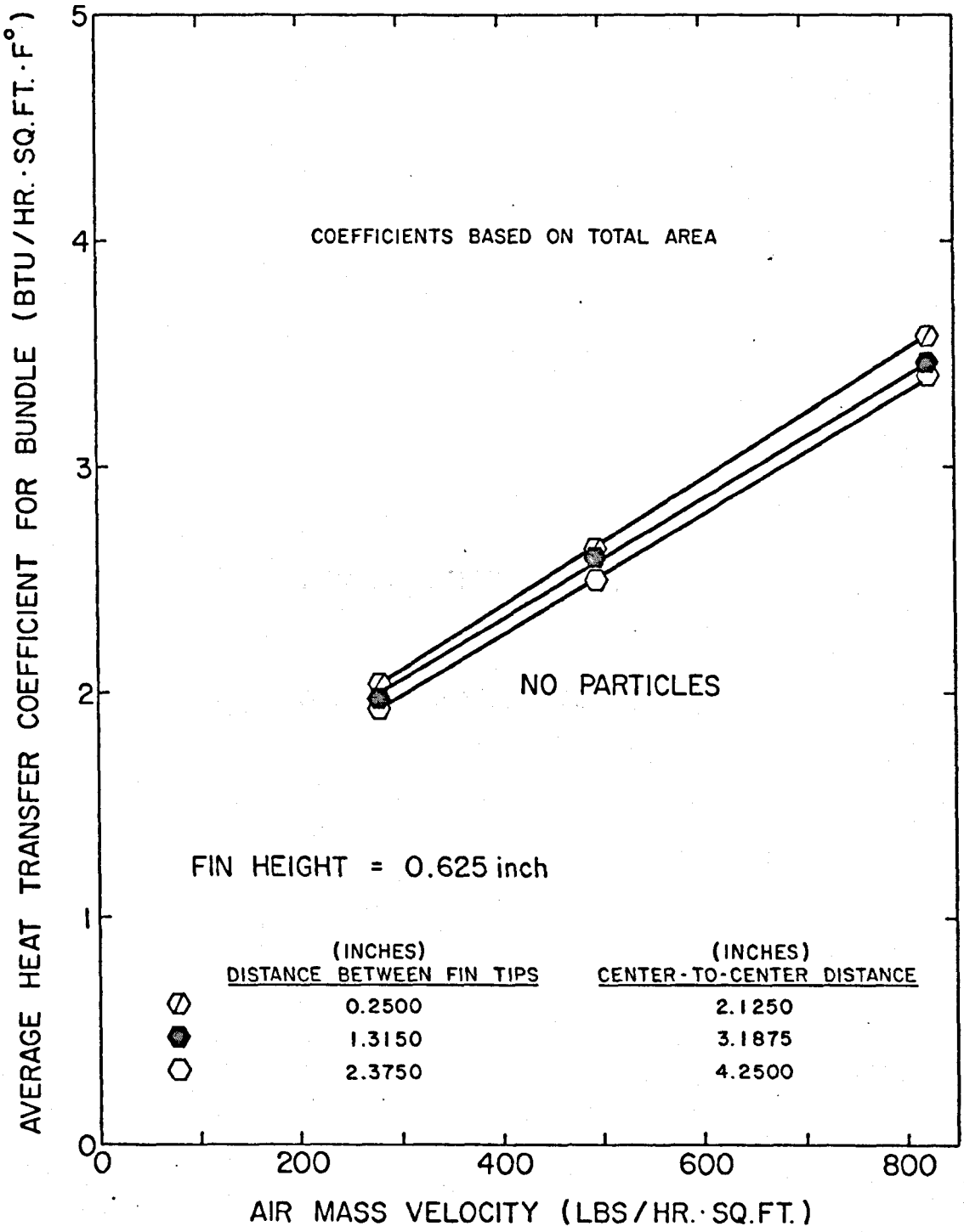


FIGURE 34. PERFORMANCE OF 0.625" FINNED TUBES

PERFORMANCE CURVES

for

7/8 inch FINNED TUBES

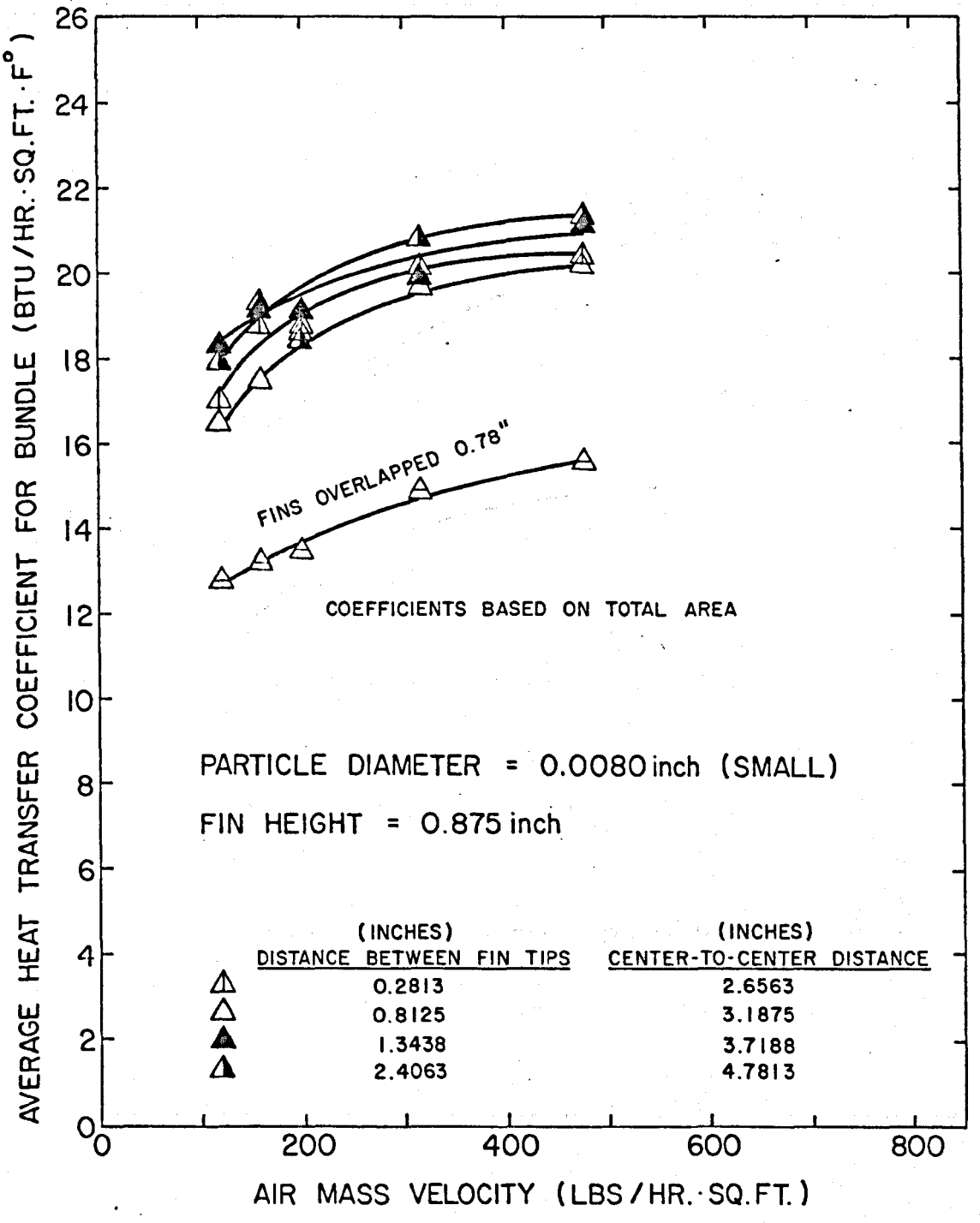


FIGURE 35. PERFORMANCE OF 0.875" FINNED TUBES

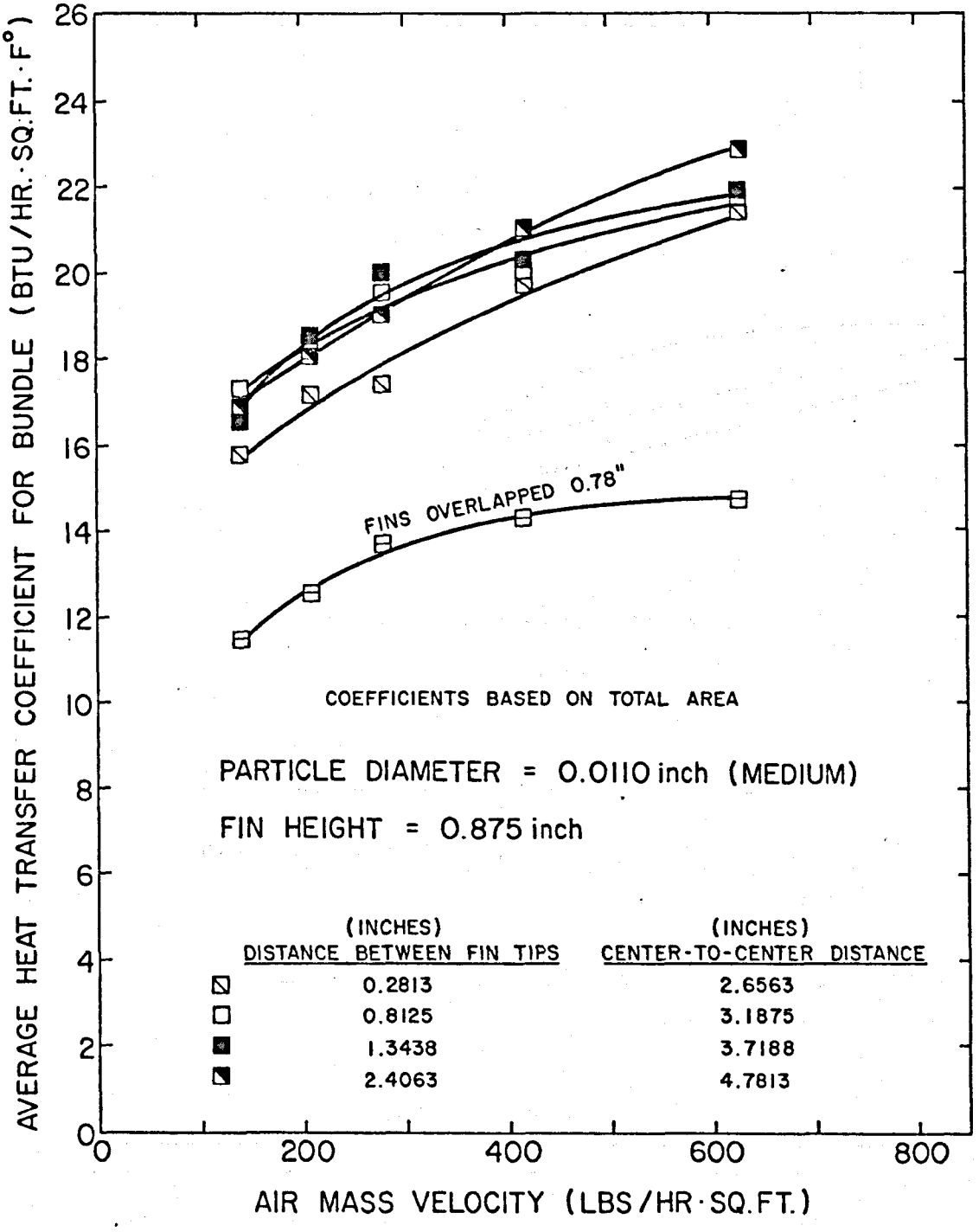


FIGURE 36. PERFORMANCE OF 0.875" FINNED TUBES

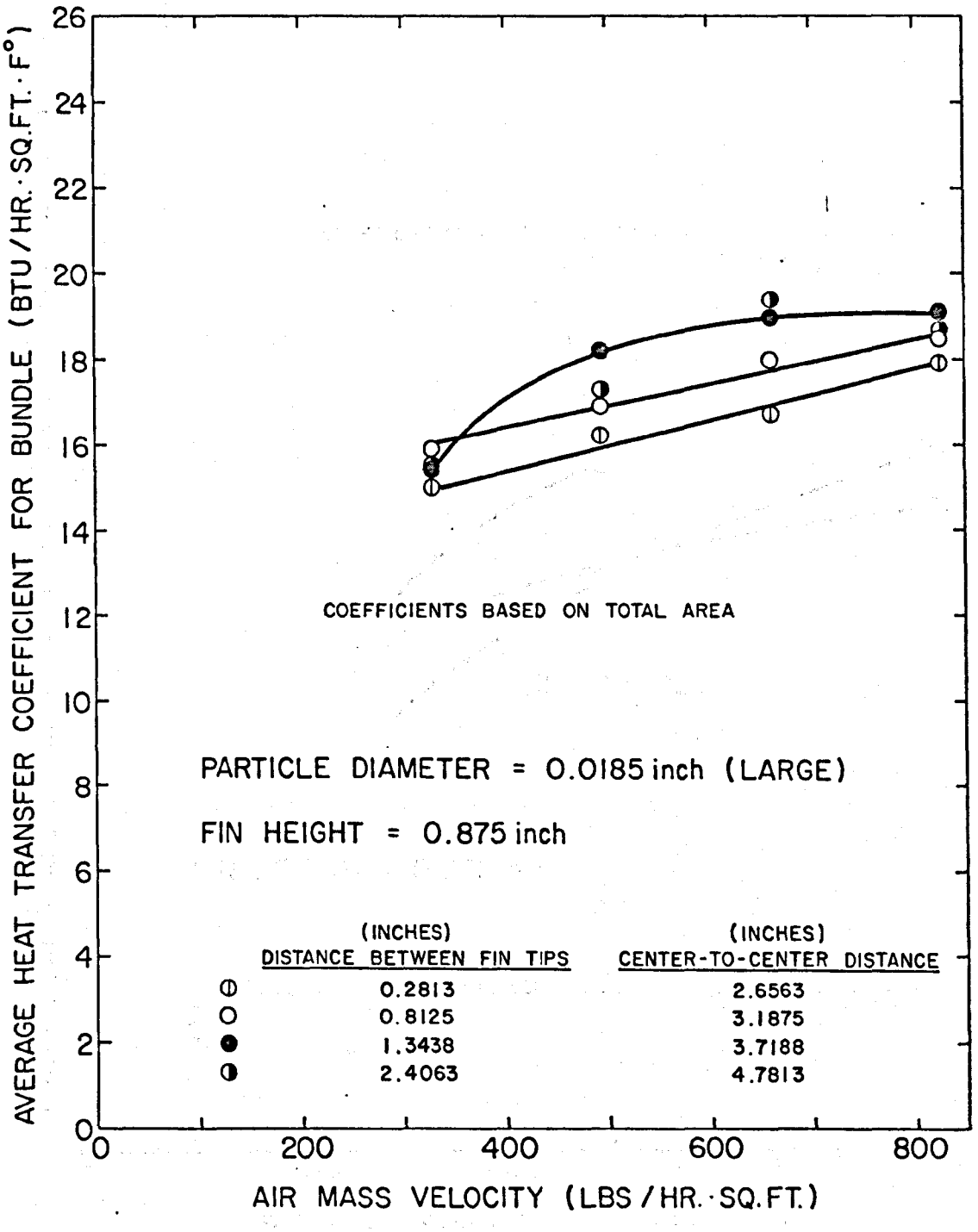


FIGURE 37. PERFORMANCE OF 0.875" FINNED TUBES

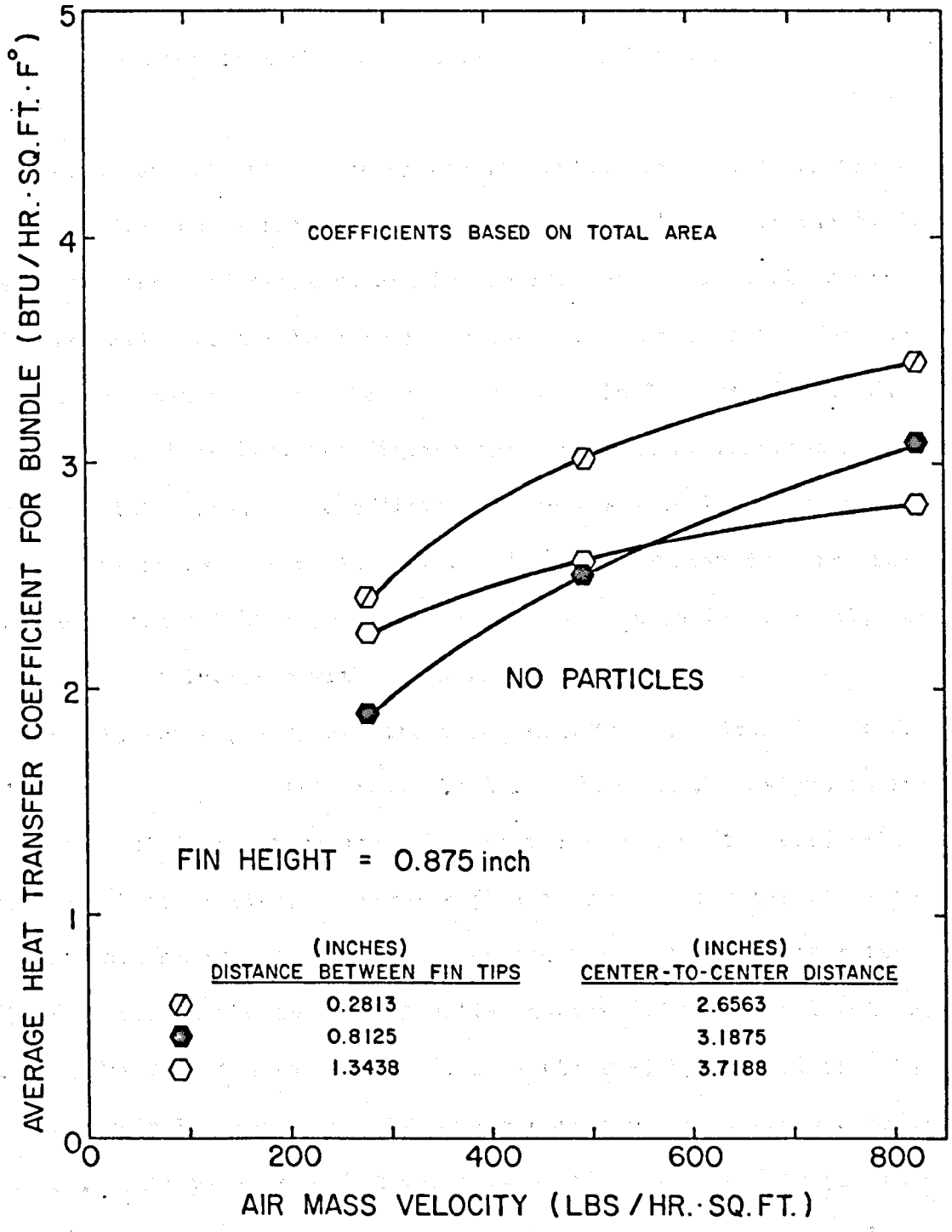


FIGURE 38. PERFORMANCE OF 0.875" FINNED TUBES

COMPARATIVE PERFORMANCE OF ALL TUBE BUNDLES

A comparison of heat transfer coefficients, based on total area, is shown in Figures 39 and 40, in which the coefficients for the bundles in the most clustered position and in the most expanded position are plotted for all 5 of the bundles investigated. Similar plots for the coefficients based on bare tube area are shown in Figures 41 and 42. It can be seen in these last two figures that when the coefficient is based on the bare tube area, the coefficient increases with increase in fin height. This is to be expected because the rate of heat transfer increases with fin height and, since the bare tube area is constant, the coefficient must increase with fin height also.

However, two opposing effects occur when the heat transfer coefficient is based on the total area. That is, when the fin height is increased the total area increases, but at the same time the coefficient decreases. This is clear in Figures 39 and 40 where the bare tube coefficients are at the top of the graphs and the coefficients for the 0.875" fins are at the bottom. A better measure of the actual rate of heat transfer from the various bundles is obtained by multiplying the coefficients in Figures 39 and 40 by the corresponding average area of the tubes. This product of h times A is equal to $q/\Delta T$ and is plotted versus fin height in Figures 43 and 44. In these figures it is clear that the rate of heat transfer from the bundles increases as the fin

height increases, but the rate of change levels off near the fin height of 0.875", so that little additional heat transfer is gained if the fin height is increased beyond this point. This is true for both the small and large particles.

Another way of comparing the change in heat transfer rate with fin height is by calculating fin effectiveness factors which were defined on page 60 as

$$\phi = q/h_b A(T_{tube} - T_{bed})$$

which is equivalent to

$$\phi = \frac{\text{heat transfer coefficient (based on total area) with finned tubes}}{\text{coefficient with bare tubes at the same operating conditions}}$$

Plots of the effectiveness factor versus fin height for small and large particles are shown in Figures 45 and 46. The curves again indicate a leveling off at the fin height of 0.875", and with the low value of the effectiveness factor at this point, there would be little additional increase in the rate of heat transfer if longer fins were used. The two figures also show that the fins are more effective at the higher air velocities (shown as solid black symbols) than at the lower velocities (shown as open symbols). Also, the effectiveness of the fins is greater, for the most part, when the bundle is in the most expanded position (squares) than when it is in the clustered position (circles). A comparison of the magnitude of the effectiveness factor on the two

figures also indicates that the fins are more effective with the large particles. This is particularly true with the shorter fins, but the difference becomes less with the longest fins.

Inspection of Figures 43 thru 46 indicates that the difference in the heat transfer rate between the bundles in the most clustered position and in the most expanded position is greatest for the bundles with shorter fins. That is, the distance between the open square and the open circle, or between the solid square and the solid circle, is largest for the 0.125" fins and then gradually decreases as the fin height increases to 0.875". This pattern is most clear for the lower air velocities (open symbols), but it is also generally true for the higher velocities. This says that the rate of heat transfer from bundles of short finned tubes is more sensitive to tube spacing than it is for bundles of tubes with long fins. This can be explained by forming an analogy with a simple kinetic model in which reaction, adsorption, and desorption are neglected. The analogy is pictured in Figure 47. In a kinetic reaction defined by this simple model, the rate of reaction could be controlled either by the rate of diffusion through the film or by the rate of diffusion in the pore. In a similar manner, the movement of particles into the region between the finned tubes can be considered analogous to film diffusion, while the particle movement from the tips of the fins toward the center tube can be considered analogous to pore diffusion. From the observation made above about the heat

transfer rate for short finned tubes being more sensitive to tube spacing, it appears that with short finned tubes the particle movement is "film diffusion" controlled, while with long fins "pore diffusion" is the controlling resistance. In other words, when a bundle of short finned tubes is expanded, particles move more easily into the region between the tubes, and since the resistance encountered by the particles in moving from the tips of the fins toward the center tube is relatively small, the rate of heat transfer is increased substantially. With long finned tubes, however, expanding the bundle and allowing particles to move more easily into the region between the tubes does not increase the rate of heat transfer noticeably because the resistance to particle movement from the fin tips to the center tube is not changed and is still the principle resistance encountered by the particles.

The final comparison of the performance of the 5 bundles investigated is shown in Figures 48 and 49, where $q/\Delta T$ is plotted against the reduced fluidizing air velocity (actual air velocity/ air velocity at minimum fluidization).

COMPARATIVE PERFORMANCE CURVES

for

ALL TUBE BUNDLES

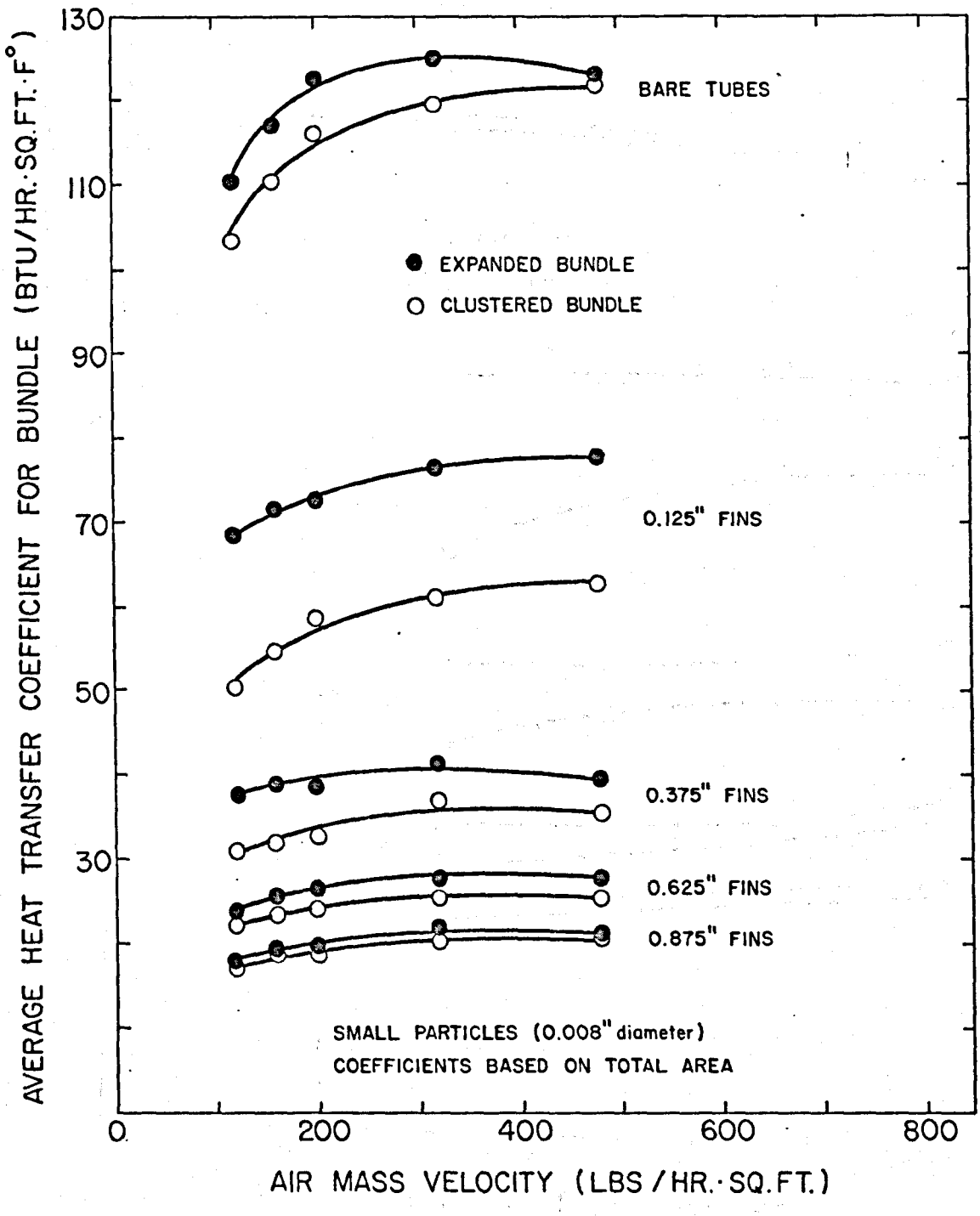


FIGURE 39. SUMMARY OF COEFFICIENTS BASED ON TOTAL AREA – SMALL PARTICLES

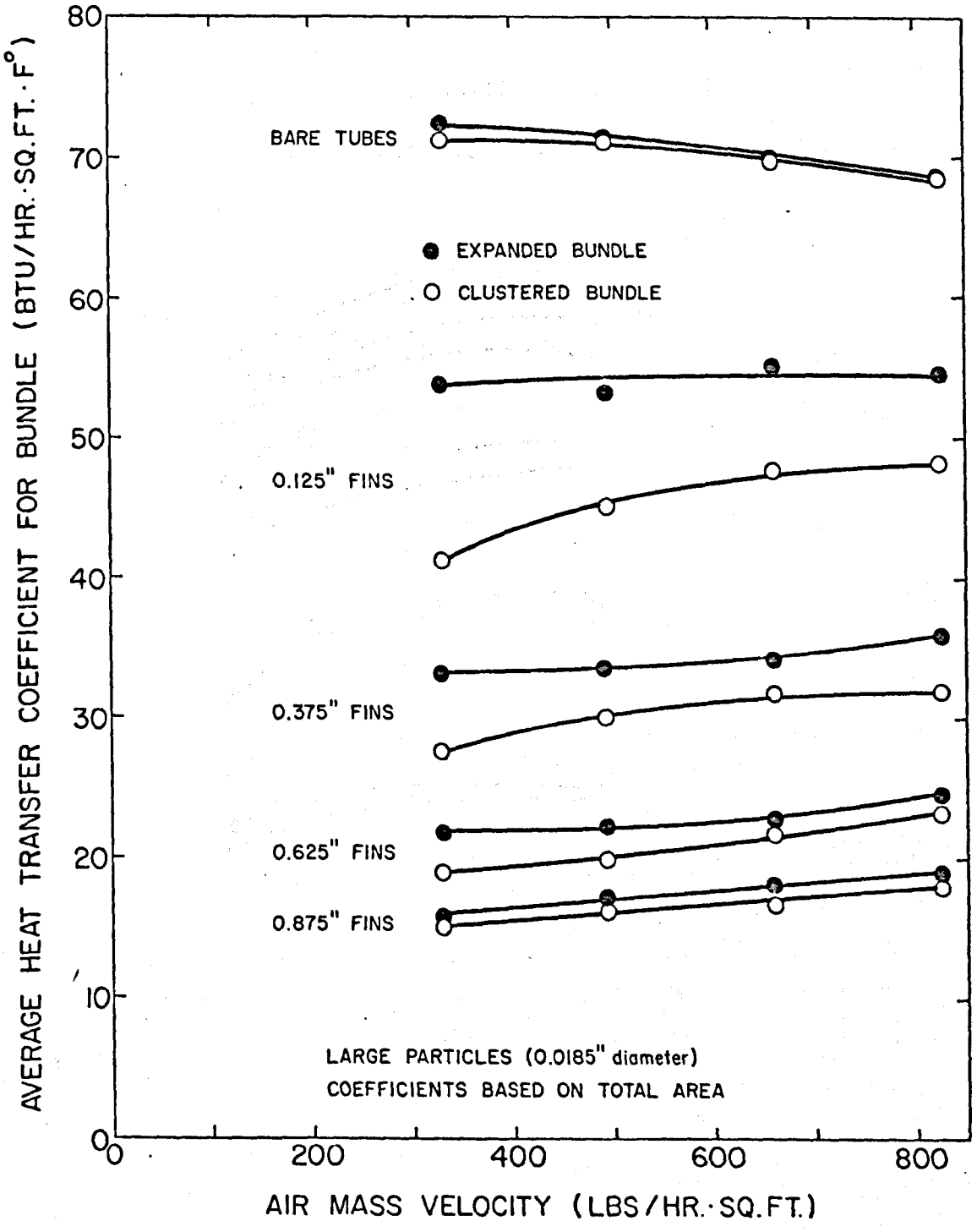


FIGURE 40. SUMMARY OF COEFFICIENTS BASED ON TOTAL AREA - LARGE PARTICLES

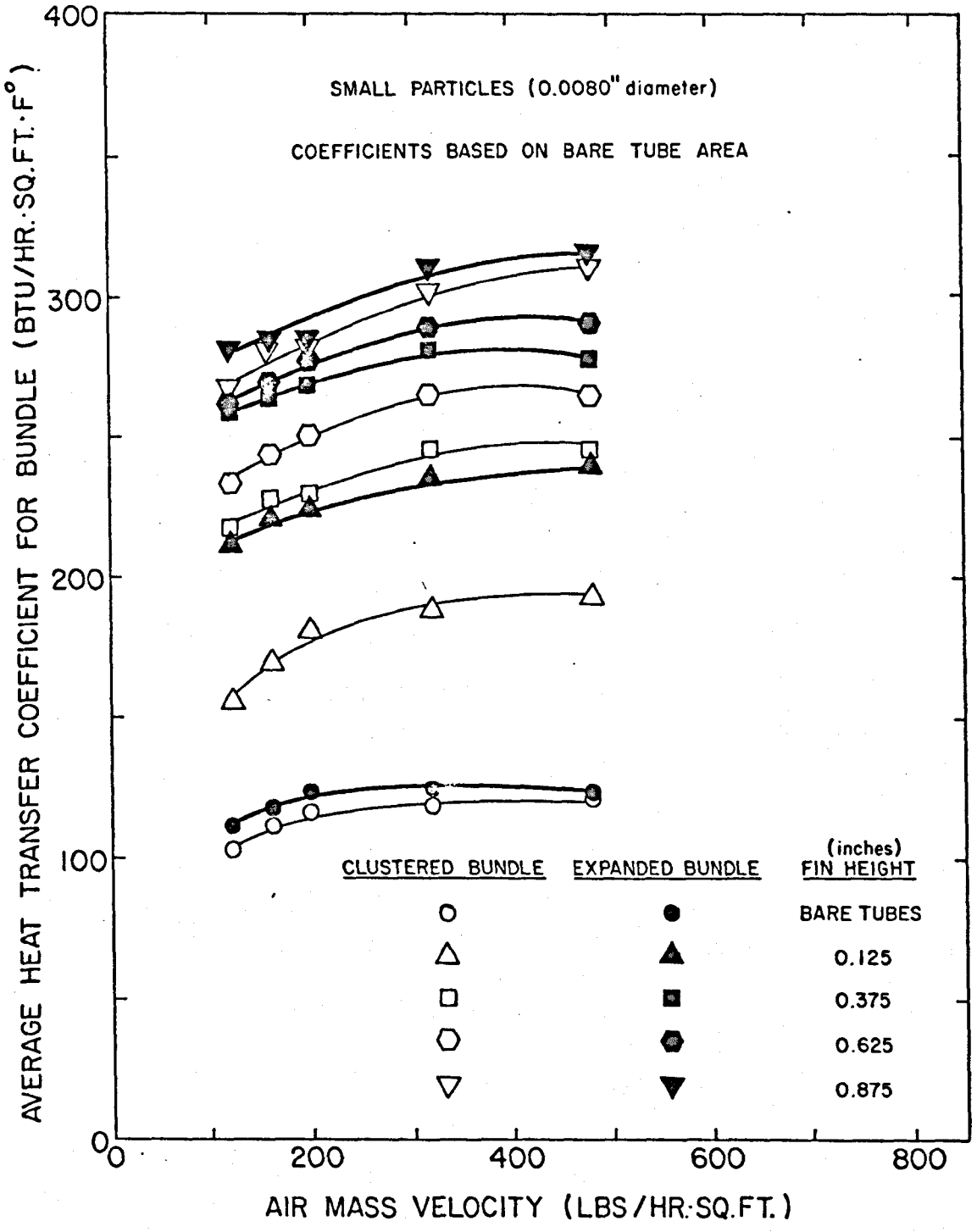


FIGURE 41. SUMMARY OF COEFFICIENTS BASED ON BARE TUBE AREA - SMALL PARTICLES

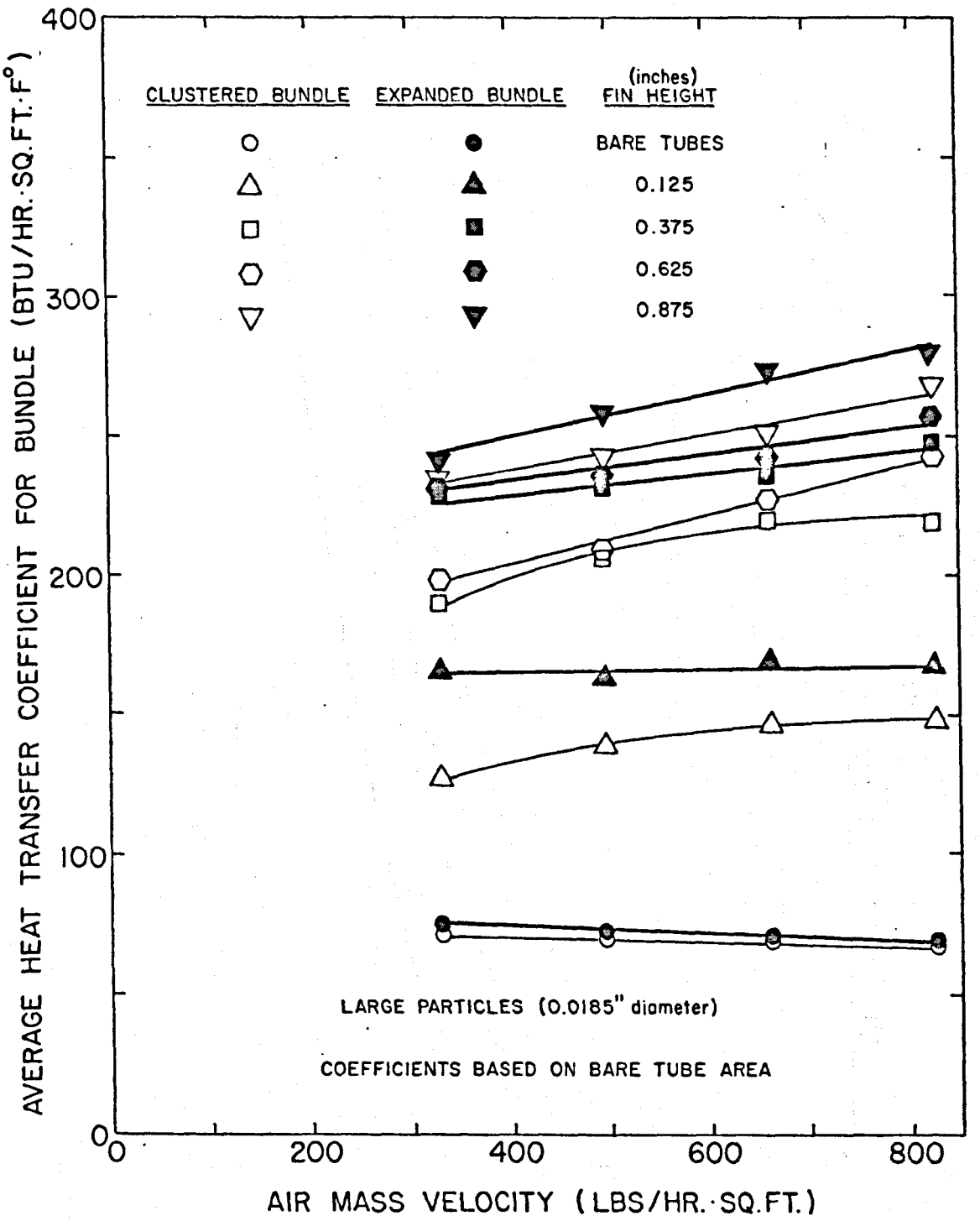


FIGURE 42. SUMMARY OF COEFFICIENTS BASED ON BARE TUBE AREA - LARGE PARTICLES

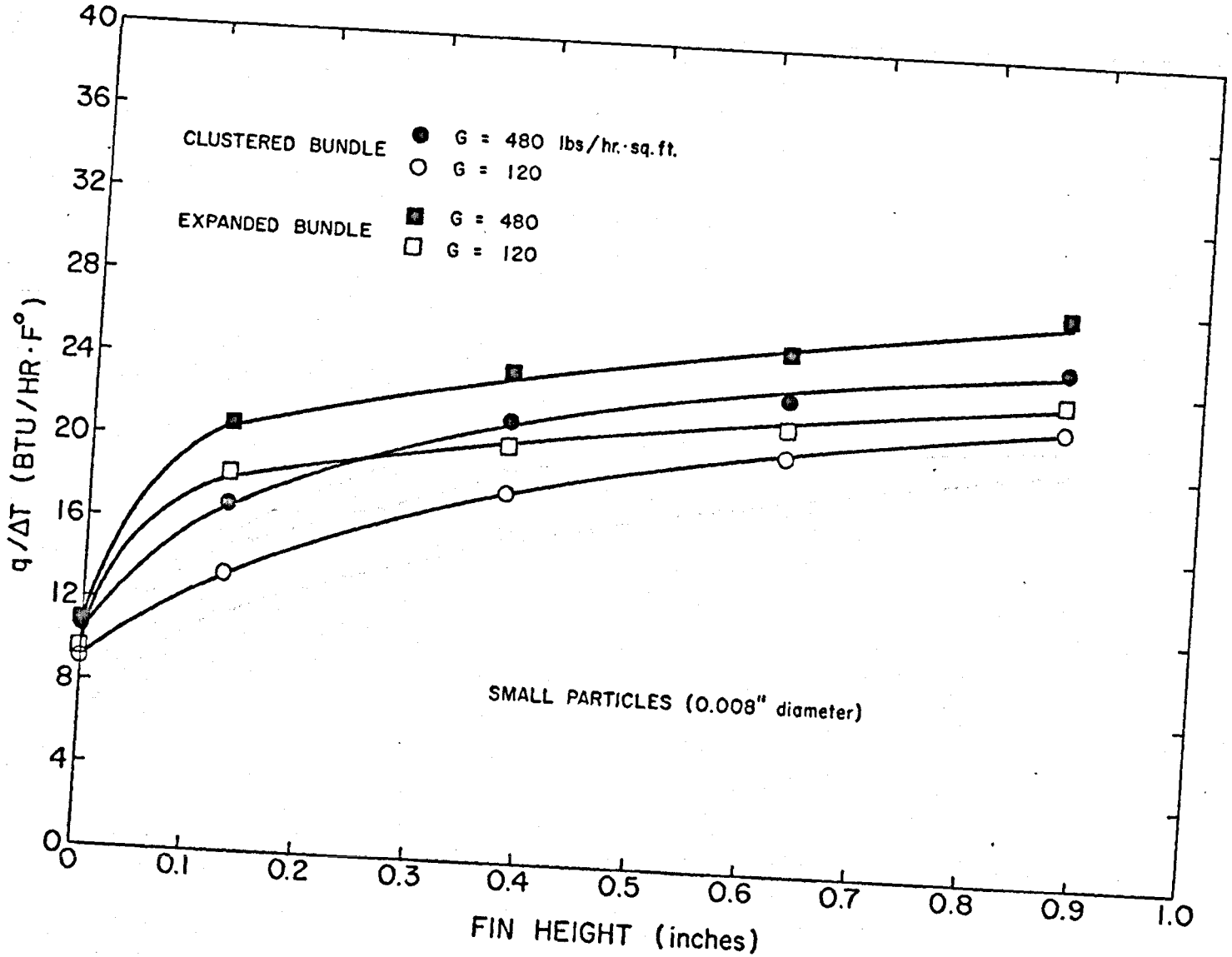


FIGURE 43. q/ΔT VERSUS FIN HEIGHT - SMALL PARTICLES

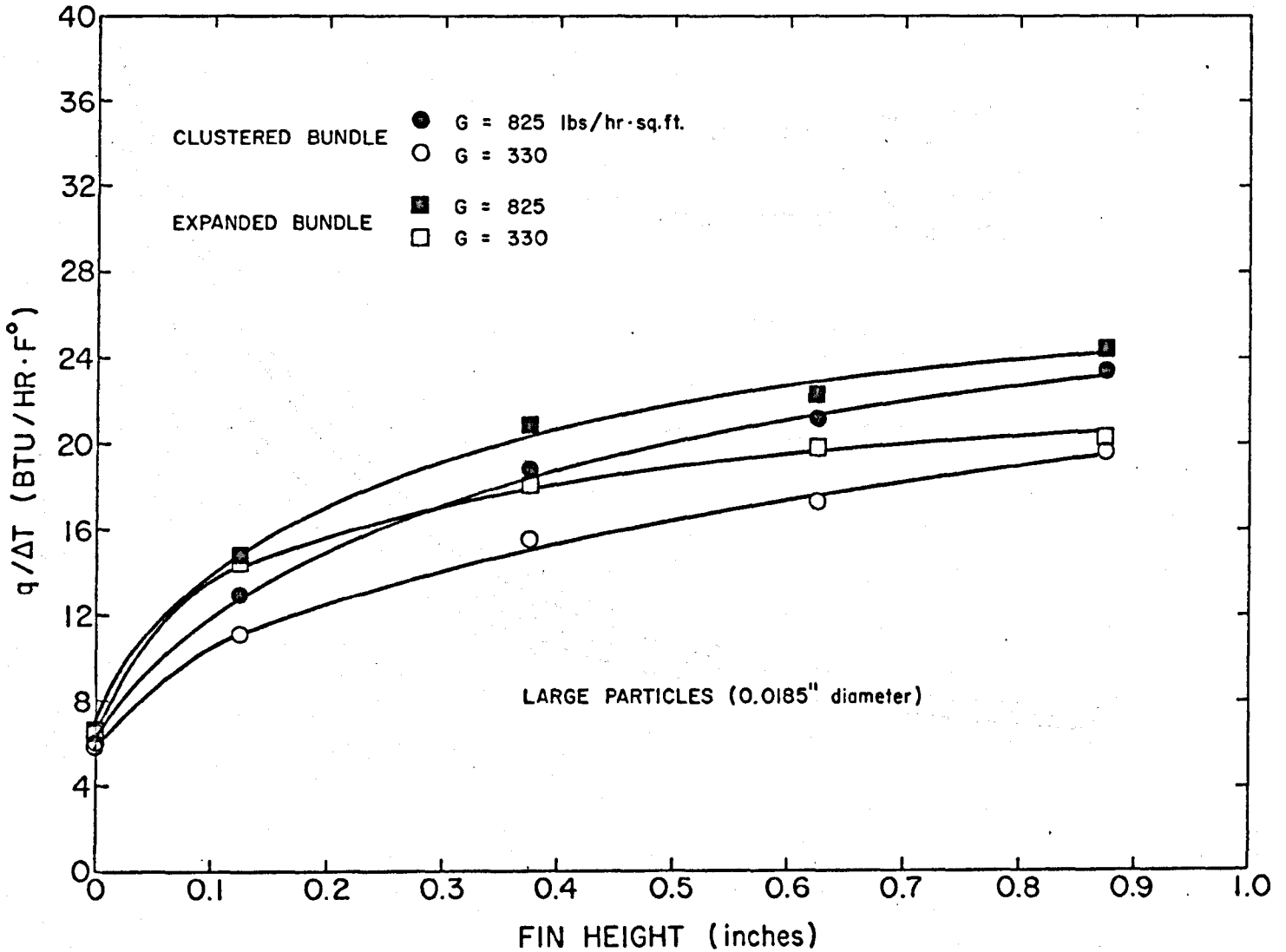


FIGURE 44. q/ΔT VERSUS FIN HEIGHT - LARGE PARTICLES

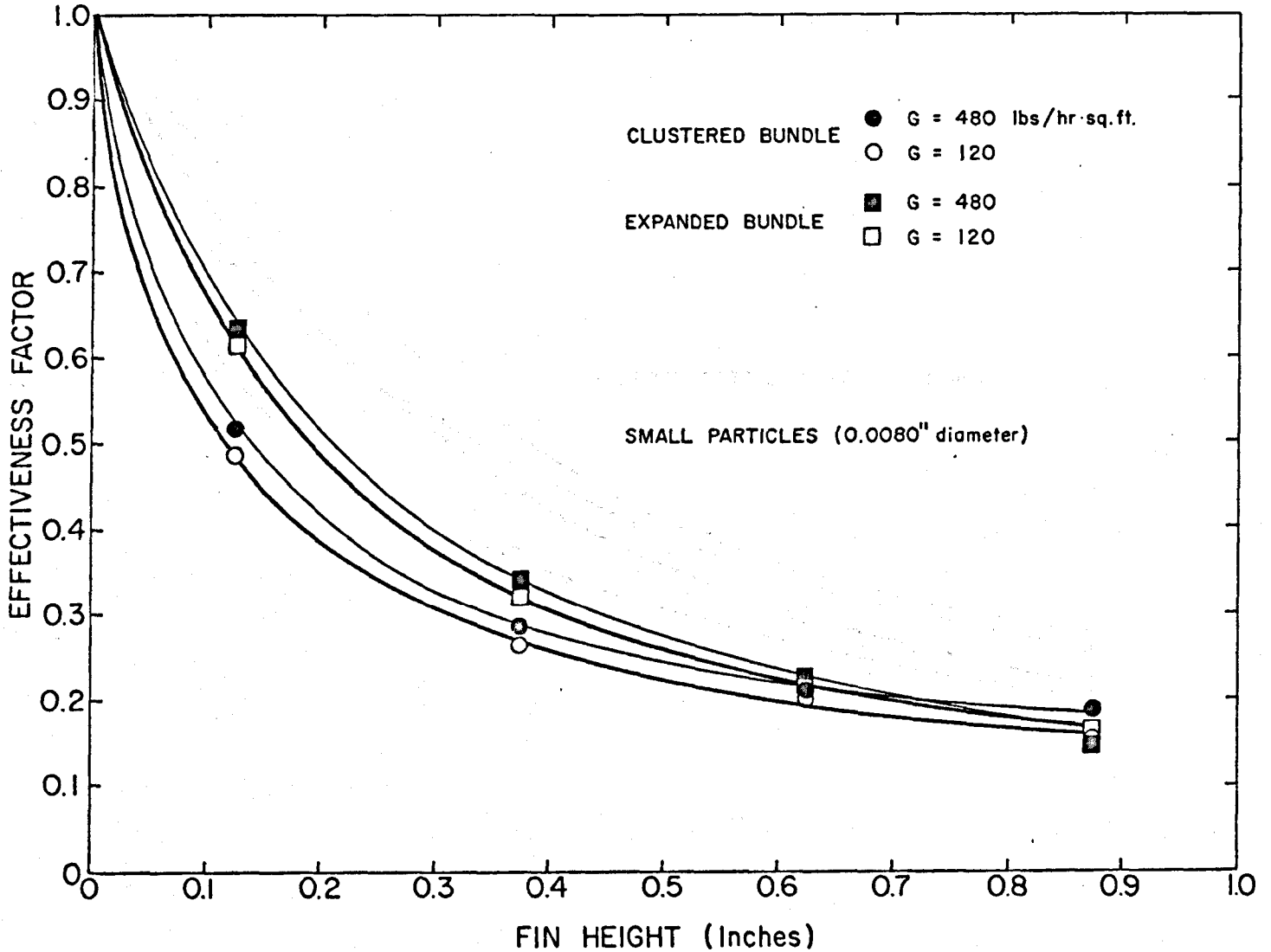


FIGURE 45. EFFECTIVENESS FACTOR VERSUS FIN HEIGHT - SMALL PARTICLES

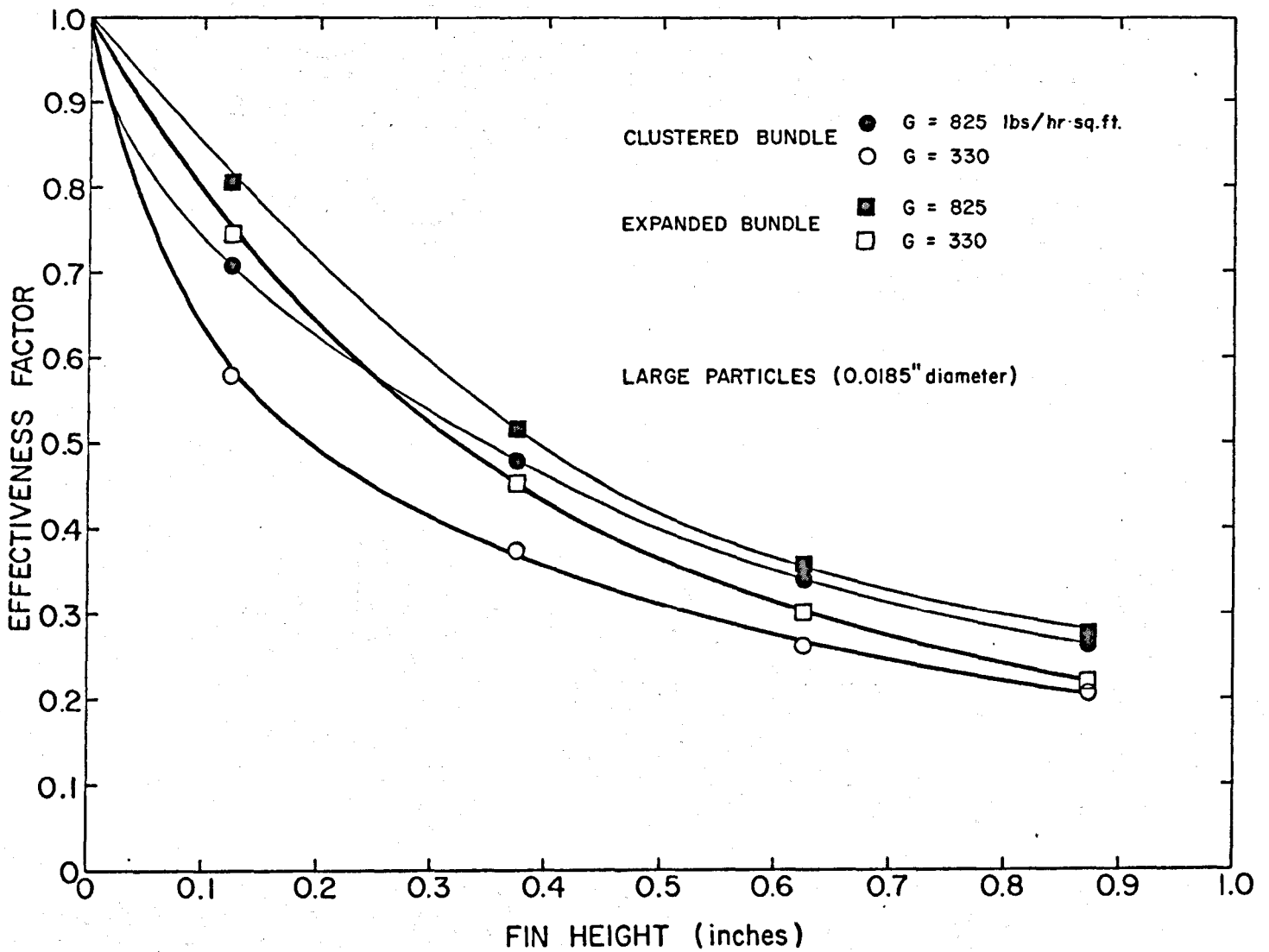
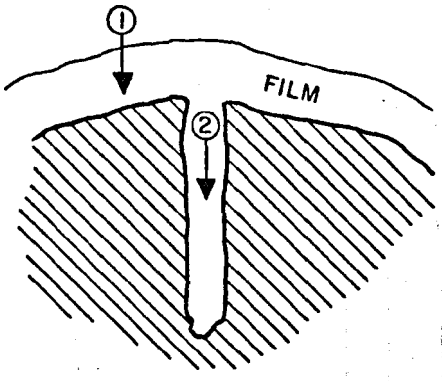


FIGURE 46. EFFECTIVENESS FACTOR VERSUS FIN HEIGHT - LARGE PARTICLES

SIMPLIFIED KINETIC MODEL

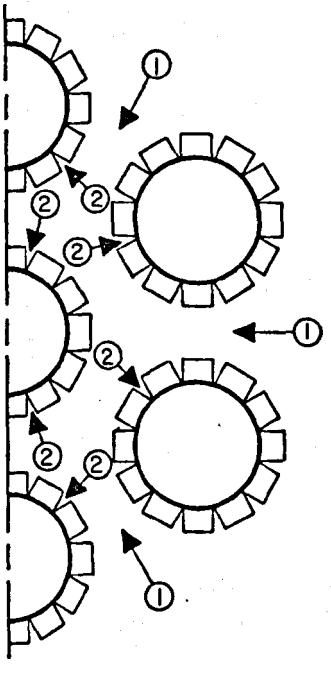


FILM DIFFUSION ①→

PORE DIFFUSION ②→

SHORT FINS

CONTROLLING RESISTANCE TO PARTICLE MOVEMENT IS SHOWN BY ①→. THEREFORE, HEAT TRANSFER COEFFICIENT IS SENSITIVE TO TUBE SPACING.



LONG FINS

CONTROLLING RESISTANCE TO PARTICLE MOVEMENT IS SHOWN BY ②→. THEREFORE, HEAT TRANSFER COEFFICIENT IS NOT SENSITIVE TO TUBE SPACING.

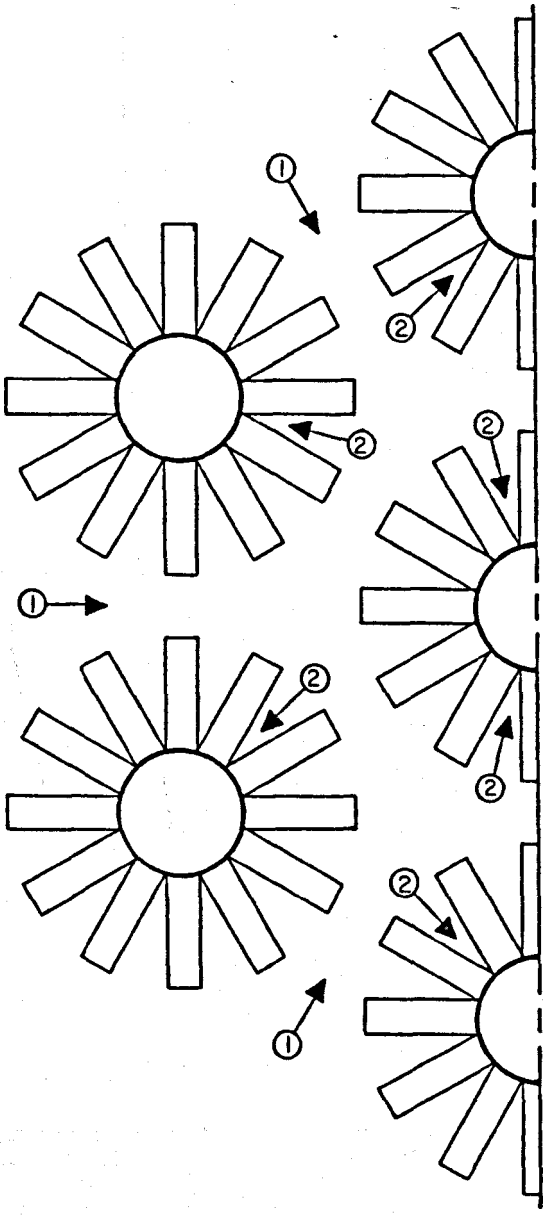


FIGURE 47. ANALOGY OF SIMPLIFIED KINETIC MODEL APPLIED TO FIN TUBES

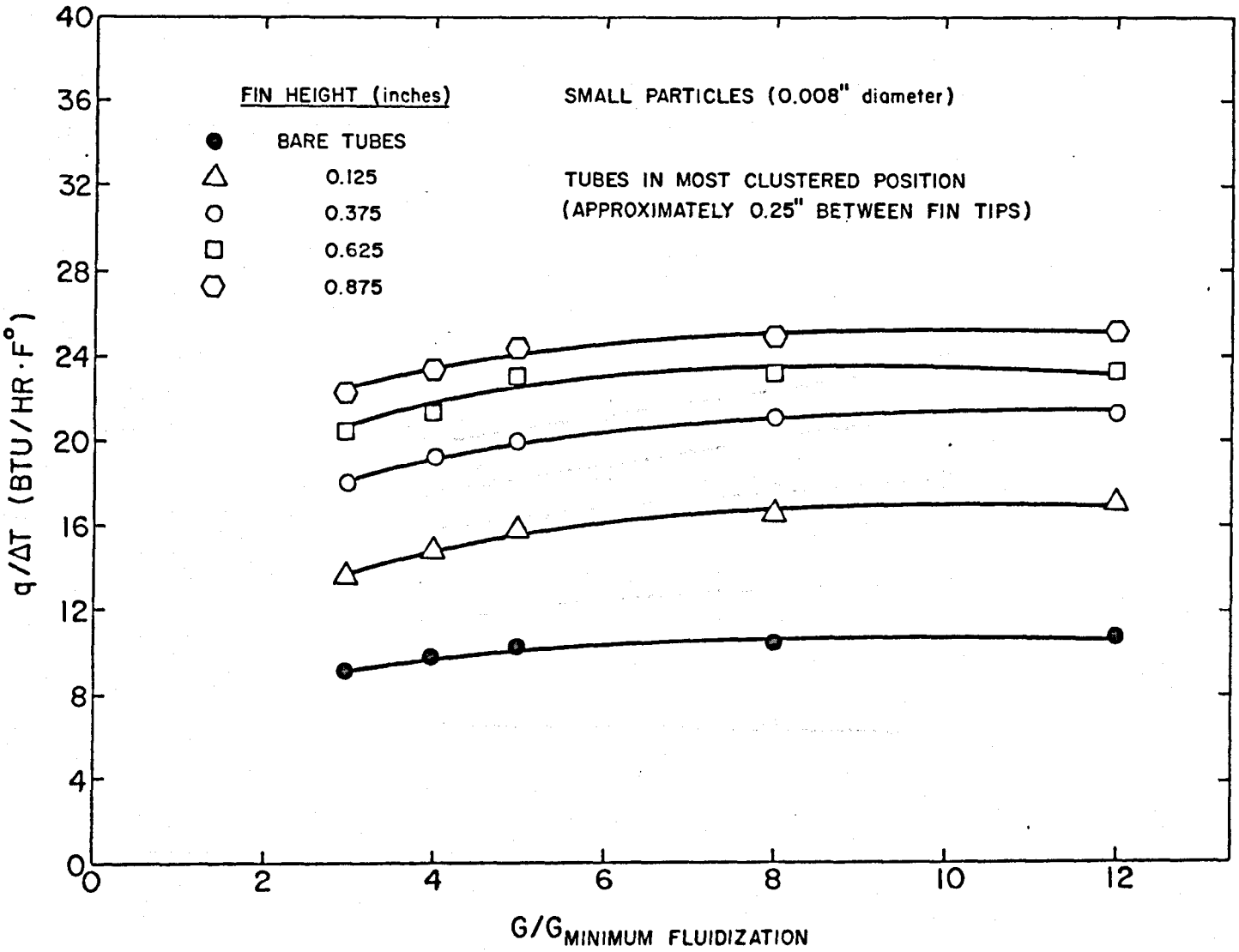


FIGURE 48. q/ΔT VERSUS REDUCED VELOCITY - SMALL PARTICLES

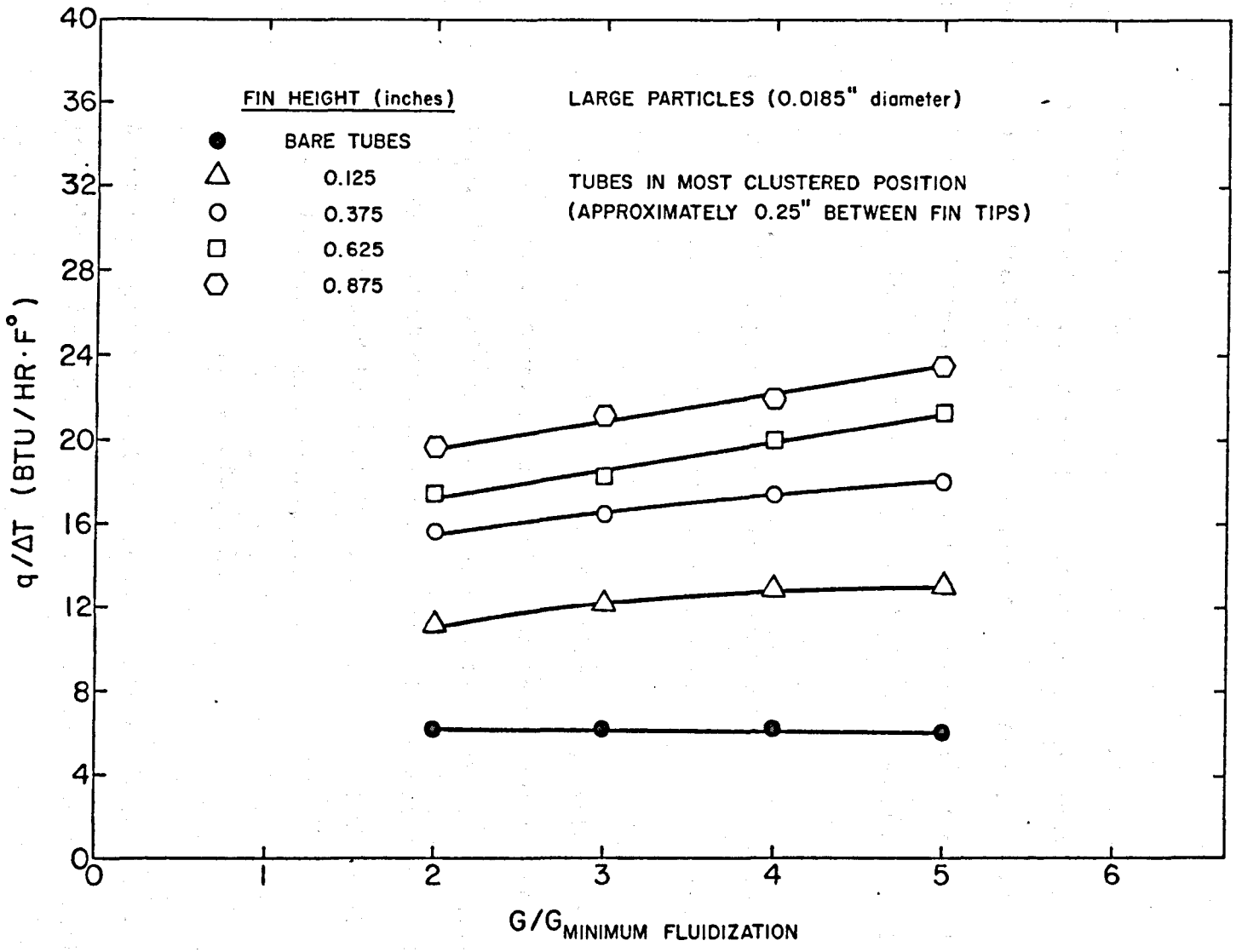


FIGURE 49. q/ΔT VERSUS REDUCED VELOCITY - LARGE PARTICLES

CORRELATION

The experimental data were correlated into a single equation, relating the heat transfer coefficient to all of the experimental variables, by using a theoretical model of heat transfer in a fluidized bed proposed by Ziegler, Koppel, and Brazelton (28), and extended by Genetti and Knudsen (8). In formulating this model the following assumptions were made:

1. The fluidized particles are spheres of uniform diameter.
2. The physical properties of the solids and the fluids are constant.
3. Particles from the bulk of the fluidized bed, having the bulk medium temperature, T_b, move adjacent to the hot transfer surface. While adjacent to the surface, the particle receives energy by convection from the fluid around the particle. This fluid is assumed to be at the arithmetic mean of the wall and the bulk medium temperature, i.e.

$$T_f = \frac{T_w + T_b}{2}$$

After some time the particle leaves the surface and returns to the bulk of the bed. This mechanism is shown for a typical particle in Figure 50.

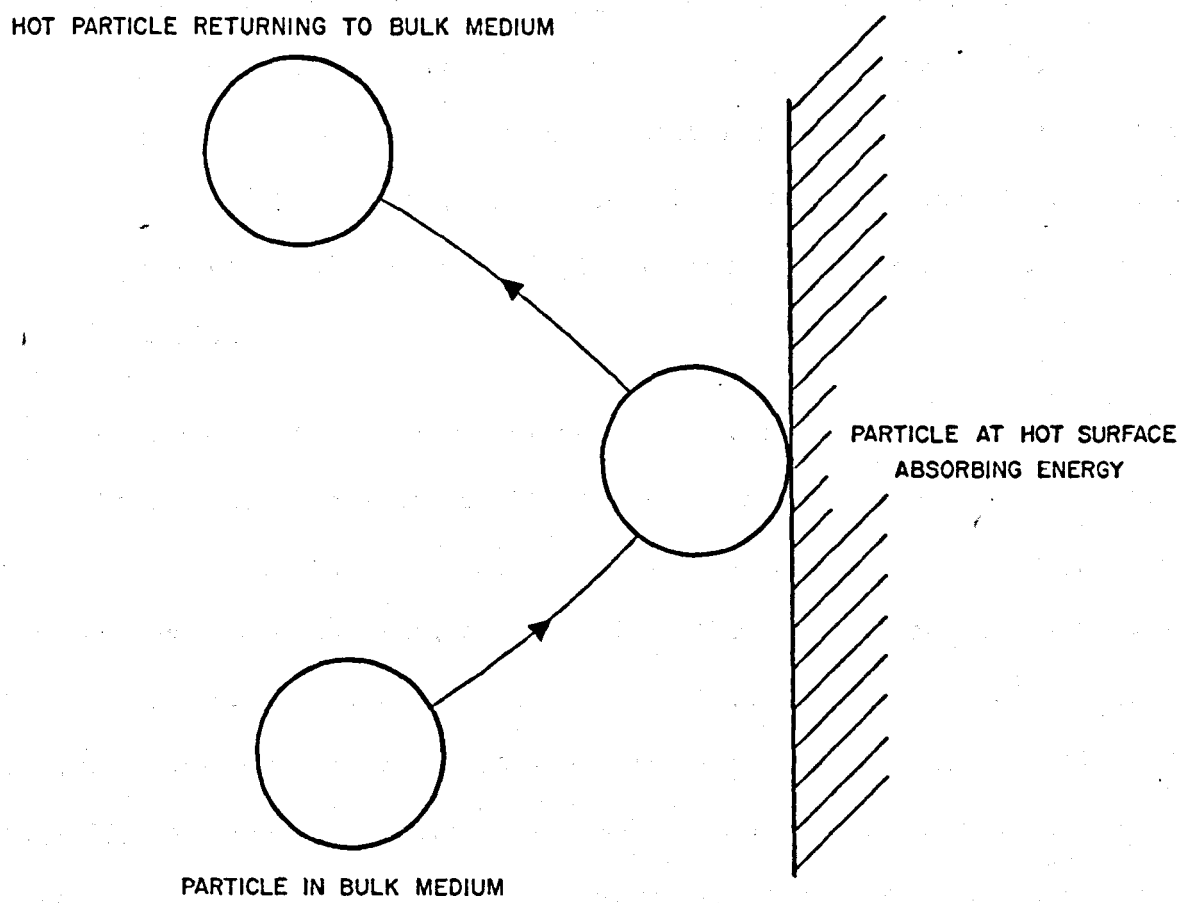


FIGURE 50. SCHEMATIC OF PROPOSED HEAT TRANSFER MECHANISM

4. The major portion of the heat transfer occurs by the mechanism described above.
5. Radiant heat transfer from the surface to the particle is neglected. Baddour and Yoon (1) have shown this effect to be negligible for packed beds at temperatures below 600°C.
6. Conduction at the point of contact between the particle and the surface is negligible. Botterill, et al., as cited by Ziegler, Koppel, and Brazelton (28), have shown that this effect is very small.

The solution to the boundary value problem describing the temperature in the particle while it is near the surface, given the above assumptions, is well known and is given by Genetti and Knudsen (8). Using various approximations, assuming that the particle residence time at the surface can be represented by the gamma distribution function, relating the number of particles at the surface to the particle fraction $(1 - \epsilon)$, and introducing dimensionless groups, it was shown that the heat transfer coefficients in a fluidized bed can be fit to the following equation:

$$Nu_p = \frac{10(1 - \epsilon)^{0.5}}{\left[1 + c/Re_p^a D_p^b\right]^2}$$

where,

Nu_p = particle Nusselt number, $hD_p/(12)(k_{air})$, dimensionless

$(1 - \epsilon)$ = particle fraction, dimensionless

Re_p = particle Reynolds number, $GD_p/(12)(\mu_{air})$, dimensionless

D_p = particle diameter, inches

k_{air} = thermal conductivity of air at bed temperature, $0.0133 + 0.000024T_b$, BTU/Hr-Ft-F°

μ_{air} = viscosity of air at bed temperature, $(0.2688)(10^{-4})\left[(2.45)(T_b - 32) + 1538.1\right]$, Lbs/Ft-Hr

h = heat transfer coefficient, BTU/Hr-Ft^2-F°

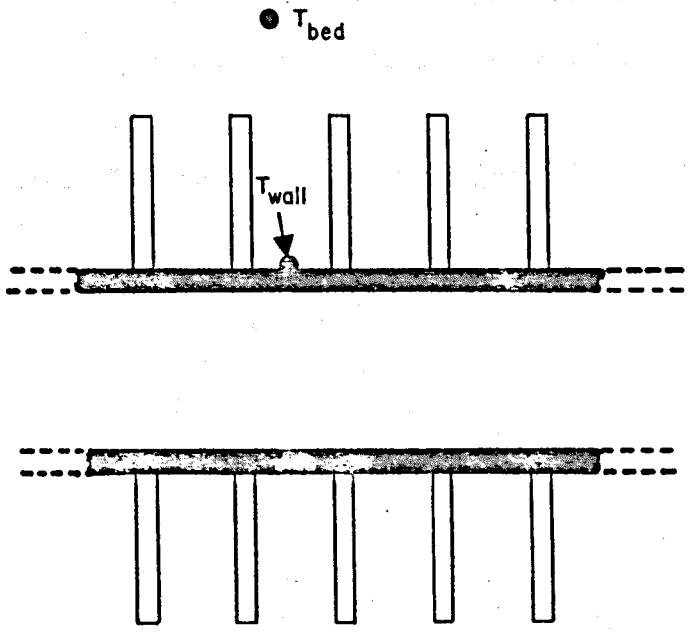
G = air mass velocity, Lbs/Hr-Ft^2

T_b = bed temperature, Fahrenheit degrees

a,b,c = functions of fin height, L, to be evaluated

The problem now is to find functions for a,b, and c which, when substituted into the equation on page 121, will produce an equation that will best fit the experimental data. However, if at this point each of the experimental values for h were substituted into Nu_p and "best fit" functions were found for a,b, and c, the correlation would only be valid for carbon steel fins, since that is the only fin material that was used in this study. To see why the correlation would be dependent on the fin material, it is necessary to recall how the heat transfer coefficient was defined in calculating all of the coefficients shown on the previous graphs. The definition and sketch are shown on the next page.

$$h = q/A(T_{wall} - T_{bed})$$



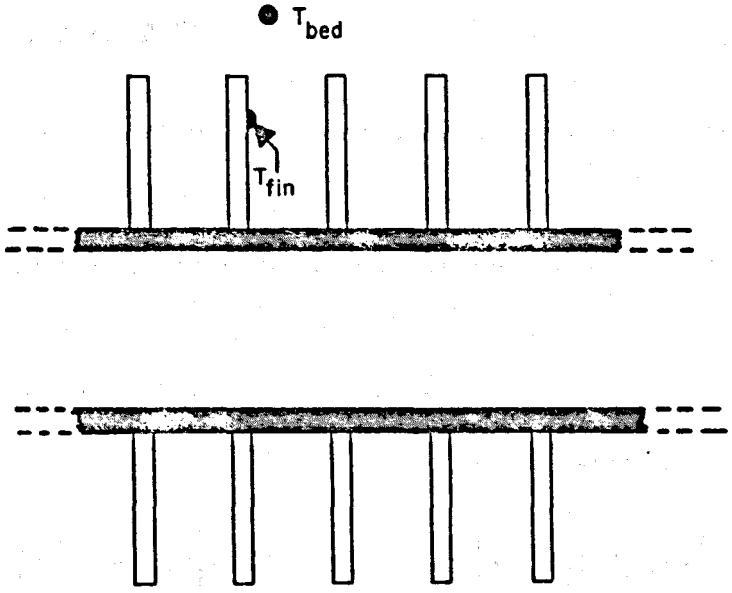
ENLARGED VIEW OF TUBE AND FINS

It can be seen from the above sketch and definition of h that the coefficient as defined in this manner is a function of the thermal conductivity of the fins. If, for example, copper fins were used, the rate of heat flow by conduction from the tube to the tip of the fins would be greater than the rate with carbon steel fins with the same value of temperature difference ($T_{wall} - T_{bed}$). Therefore, with copper fins the fin temperature would be higher and the rate of heat transfer to the bed, q, would be greater. Thus, with the same value of ($T_{wall} - T_{bed}$) a tube with copper fins would have a higher heat transfer coefficient than a

tube with carbon steel fins if the coefficient is defined as shown.

To make the correlation as general as possible, it is necessary to eliminate the dependence of h on the thermal conductivity of the fin material. This was accomplished by redefining h as shown below:

$$h_{local} = q_{local}/A_{local}(T_{fin\ local} - T_{bed})$$



ENLARGED VIEW OF TUBE AND FINS

As defined above, h_{local} is independent of the thermal conductivity of the fin and is a function only of the frequency of collisions between the particles and the fin surface. To simplify the mathematics that will be used to convert the experimental values of $q/\Delta T$ to h as defined

above, it was assumed that h is constant over the full length of the fin, so that $h_{local} = h_{average}$. This is probably not strictly true, but because of the high degree of penetration of particles into the region between the fins, particularly for the shorter fins, it is probable that there is little change in h from the base of the fin to the tip of the fin.

To evaluate the coefficient as defined in the previous equation, it is necessary to obtain an equation relating the fin temperature at any point to the distance between the tube and that point on the fin. This equation was derived as follows:

1. A sketch of a single fin of length L was made and is shown in Figure 51.
2. A heat balance was taken around the element of height Δx.

   At steady state:

   Heat into element by conduction = Heat out by conduction + Heat out by convection

$$-kw_1w_2(dT/dx) = -\left\{kw_1w_2(dT/dx) + d/dx\left[kw_1w_2(dT/dx)\right]\Delta x\right\} + h\left[2(w_1 + w_2)\Delta x(T - T_b)\right]$$

   where,

   w_1 = fin width = 0.156"/12 = 0.013'

   w_2 = fin thickness = 0.025"/12 = 0.00208'

   k = thermal conductivity of fin, BTU/Hr-Ft-F^{o}

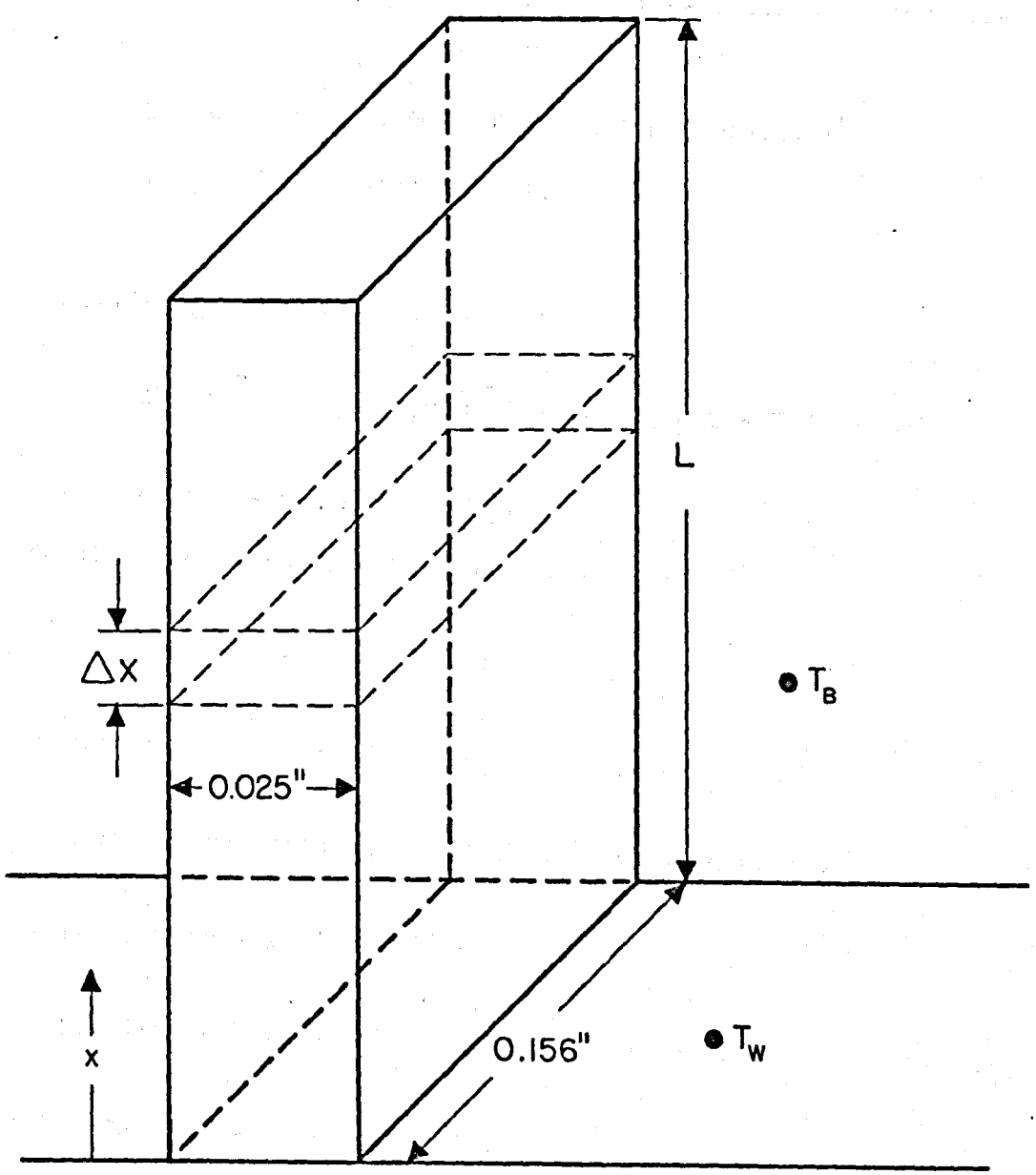


FIGURE 51. SCHEMATIC USED FOR DERIVING EQUATION FOR TEMPERATURE PROFILE IN FIN

h = heat transfer coefficient as defined on page 124, $BTU/Hr\text{-}Ft^2\text{-}F^\circ$

T = temperature at $dx/2$ on fin surface, F°

T_b = temperature of bed, F°

3. Simplifying and rearranging,

$$d^2T/dx^2 - (h/kw_1w_2)\left[2(w_1 + w_2)\right](T - T_b) = 0$$

4. Let $\Theta = (h/kw_1w_2)\left[2(w_1 + w_2)\right]$

5. Substituting into previous equation,

$$d^2T/dx^2 - \Theta T = -\Theta T_b$$

6. Solving the last equation,

Homogeneous part: $T = C_1 \text{Sinh} \sqrt{\Theta}\, x + C_2 \text{Cosh} \sqrt{\Theta}\, x$

Particular solution: $T = T_b$

Complete solution: $T = C_1 \text{Sinh} \sqrt{\Theta}\, x + C_2 \text{Cosh} \sqrt{\Theta}\, x + T_b$

7. Boundary conditions:

a. $x = 0 \qquad T = T_w$

b. $x = L \qquad -kw_1w_2(dT/dx) = h(T_L - T_b)w_1w_2$

where T_L is temperature at tip of fin

8. Applying the two boundary conditions, solving for C_1 and C_2, and substituting into the complete solution leads to the following equation which gives the surface temperature of the fin at the distance x from the base of the fin:

$$T = \frac{(T_b - T_w)\left[(k\sqrt{\theta}/h)\text{Sinh}\sqrt{\theta}\,L + \text{Cosh}\sqrt{\theta}\,L\right]}{(k\sqrt{\theta}/h)\text{Cosh}\sqrt{\theta}\,L + \text{Sinh}\sqrt{\theta}\,L}\,\text{Sinh}\sqrt{\theta}\,x + (T_w - T_b)\text{Cosh}\sqrt{\theta}\,x + T_b$$

The experimental value of $q/\Delta T$ for each run can now be related to h as defined on page 124 by using the following procedure:

Derive an equation for the rate of heat entering the base of a single fin by first taking the derivative of T, in the equation above, with respect to x. Then, from Fourier's law, if dT/dx is multiplied by $(-kw_1w_2)$, the product will be the rate of heat conduction into a single fin.

$$-kw_1w_2(dT/dx)\Big|_{x=0} = q_{\text{single fin}}$$

$$= \frac{-kw_1w_2(T_b-T_w)\sqrt{\theta}\left[(k\sqrt{\theta}/h)\text{Sinh}\sqrt{\theta}\,L + \text{Cosh}\sqrt{\theta}\,L\right]}{(k\sqrt{\theta}/h)\text{Cosh}\sqrt{\theta}\,L + \text{Sinh}\sqrt{\theta}\,L}\,\text{Cosh}\sqrt{\theta}\,x\,\Big|_{x=0} - kw_1w_2(T_w-T_b)\sqrt{\theta}\,\text{Sinh}\sqrt{\theta}\,x\,\Big|_{x=0}$$

Evaluating the right-hand side at x=0,

$$q_{\text{single fin}} = \frac{kw_1w_2(T_w - T_b)\sqrt{\theta}\left[(k\sqrt{\theta})\text{Sinh}\sqrt{\theta}\,L + h\text{Cosh}\sqrt{\theta}\,L\right]}{(k\sqrt{\theta})\text{Cosh}\sqrt{\theta}\,L + h\text{Sin}\sqrt{\theta}\,L}$$

To obtain an equation for $q/\Delta T$, both sides are first divided by $(T_w - T_b)$. Then, to find $q/\Delta T$ for the entire surface area on a tube, it is necessary to multiply the right-hand side by the ratio of (Total fin area/Area per single fin), and then to add a term for the heat transferred from the center tube to the bed. The heat transfer coefficient from the center tube to the bed was considered equal to that of the fin to the bed. The final equation relating the experimental $q/\Delta T$ values to the heat transfer coefficient, h, defined on page 124 is shown below:

$$q/\Delta T = \frac{kw_1w_2\sqrt{\theta}\left[(k\sqrt{\theta})\text{Sinh}\sqrt{\theta}\,L + h\text{Cosh}\sqrt{\theta}\,L\right]\left[A_T - A_b\right]}{\left[(k\sqrt{\theta})\text{Cosh}\sqrt{\theta}\,L + h\text{Sinh}\sqrt{\theta}\,L\right]\left[2L(w_1 + w_2) + w_1w_2\right]} + A_bh$$

where,

A_T = total area of fins and tube, ft^2

A_b = area of exposed portion of tube, ft^2

h = heat transfer coefficients as defined on page 124, $BTU/Hr\text{-}Ft^2\text{-}F^\circ$

$\theta = (h/kw_1w_2)\left[2(w_1 + w_2)\right]$, $1/ft^2$

Using the last equation, a value of h corresponding to each experimental value of $q/\Delta T$ can be found. However, since h cannot be factored out of the right-hand side of the equation and solved for explicitly, the following procedure was used:

1. Choose one of the fin heights studied, say 0.125"
2. Substitute the correct values for the constants in the equation:

   $L = 0.125"/12 = 0.0104'$

   $k = 27$ BTU/Hr-Ft-F^{o} (This value was used for the thermal conductivity for all of the carbon steel fins.)

   $w_1 = 0.013'$ (from page 126)

   $w_2 = 0.00208'$ (from page 126)

   $A_T = 0.269$ ft^2 (average of values on page 44)

   $A_b = 0.073$ ft^2 (average of values on page 44)

3. Write a computer program, containing a loop, in which h is first set equal to 5, and $q/\Delta T$ is calculated. Then, increase h by increments of 5, and print out the value for each corresponding $q/\Delta T$ until h reaches the value of 125.
4. Repeat steps 2 and 3 with the other fin lengths investigated in this study (0.375", 0.625", and 0.875").
5. Plot h versus $q/\Delta T$ for each length of fin. The plot is shown in Figure 52. The values for the bare tubes are also shown on this plot, but it should be noted that h for bare tubes is the same whether it is defined by the equation on page 123, or by the

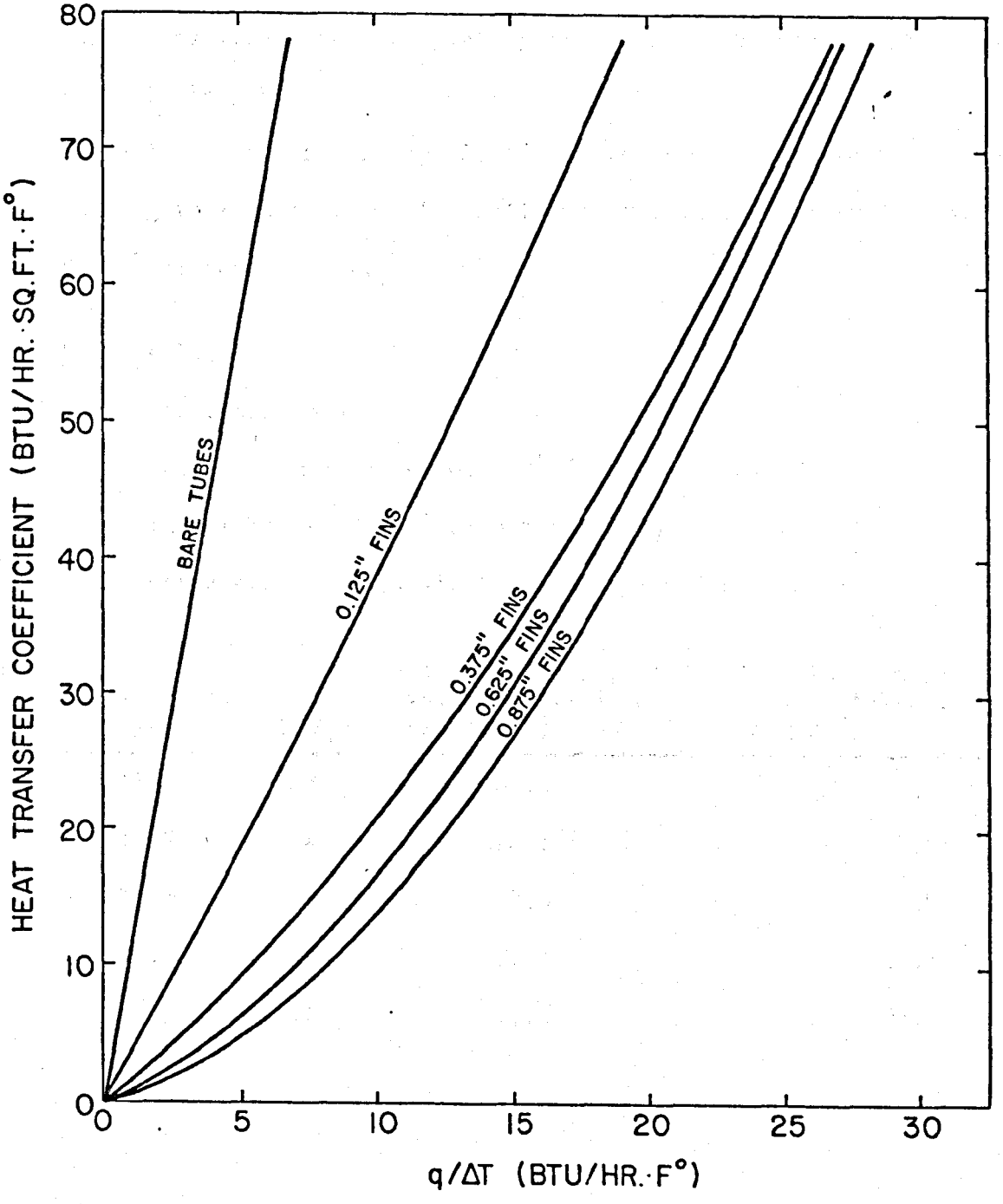


FIGURE 52. SOLUTIONS TO EQUATION RELATING q/ΔT TO h

equation on page 124. The values for the bare tubes were included only to provide a more complete picture of how h versus $q/\Delta T$ changes with fin length.

6. Using the curves in Figure 52, a heat transfer coefficient corresponding to each experimental $q/\Delta T$ can be found. Some typical values for h are shown below.

Example 1:

Operating conditions:

Particle diameter = 0.0080" (small particles)

Fin height = 0.125" (shortest fins)

Tube spacing = Bundle in most expanded arrangement

Experimental $q/\Delta T$	G/G_{mf}	h defined on page 123 (values plotted in Figure 39)	h defined on page 124 (values taken from Figure 52)
18.4	3	68.5	74.5
19.2	4	71.5	78.4
19.6	5	72.5	79.5
20.5	8	76.4	84.5
20.9	12	77.6	86.0

Example 2:

Operating conditions:

Particle diameter = 0.0080" (small particles)

Fin height = 0.875" (longest fins)

Tube spacing = Bundle in most expanded arrangement

Experimental $q/\Delta T$	G/G_{mf}	h defined on page 123 (values plotted in Figure 39)	h defined on page 124 (values taken from Figure 52)
23.8	3	18.3	59.0
24.8	4	19.0	62.7
24.9	5	19.1	62.9
26.0	8	19.9	67.8
27.9	12	21.4	76.5

It can be seen in the two examples above that the difference between the two h values at any reduced fluidizing velocity is much greater with the longest fins than it is with the shortest fins. This is to be expected, however, because of the larger temperature gradients with the longer fins.

After finding a redefined value of h, from Figure 52, for each experimental value of $q/\Delta T$, it is now possible to go back to the equation on page 121 and obtain "best fit" values for a,b, and c, to produce a correlation that is independent of the thermal conductivity of the fin material.

As the first step in fitting the experimental data to the equation on page 121, it was decided that only the data for the 5 bundles in the most expanded tube arrangement would be used. Since the tubes are performing independently when the bundle is in the most expanded arrangement, the correlated values could be compared to the correlation for a single horizontal tube developed by Bartel, Genetti, and Grimmett (2).

The following procedure was used to evaluate the functions a, b, and c in the equation on page 121:

1. Plot $10(1 - \epsilon)^{0.5}/Nu_p - 1$, which is equal to $c/Re_p^a D_p^b$, against Re_p on log-log paper using the redefined values of h for the bare tubes.
2. Draw 3 straight parallel lines through the data points, with one line drawn through the points for each particle size.
3. Write the equation for each straight line in the form

$$c/Re_p^a D_p^b = z_1 Re_p^{n_1}$$

where,

z_1 = intercept at $Re_p = 1$

n_1 = slope of all 3 parallel lines

4. Repeat steps 1 through 3, using the redefined h values for the bundles with fin heights of 0.125", 0.375", 0.625", and 0.875".

5. At this point there are 15 values for the coefficient z_1 (3 for each bundle x 5 bundles) and 5 values for the slope n_1 (1 for each bundle).

6. Plot the 5 values of n_1 against the fin height, L, and obtain the equation

$$n_1 = 0.33 + 0.40L^{9.33} = a$$

7. Plot the 15 values of z_1 against D_p on log-log paper and draw a straight line through the 3 points for each tube bundle, for a total of 5 straight lines. Write the equation for each straight line in the form $z_1 = z_2 D_p^{n_2}$.

8. Plot z_2 and n_2 against fin height and obtain the following two equations:

$$z_2 = 0.00102 + 0.047L^{0.80} = c$$

$$n_2 = 1.23 - 0.57L^{0.23} = b$$

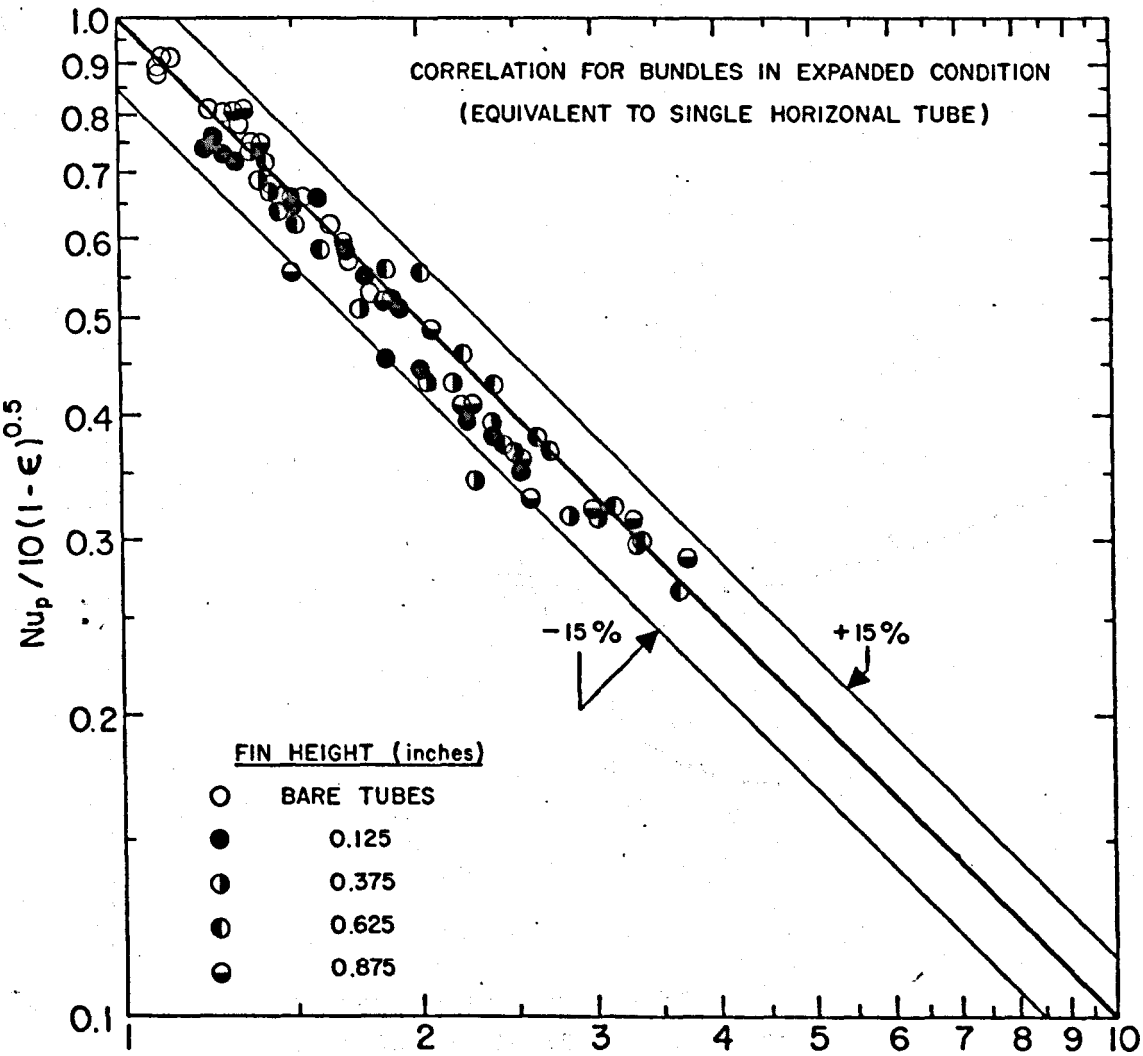
The values for a, b, and c obtained in steps 6 and 8 were then substituted into the equation on page 121, and the equation for the correlation became:

$$Nu_p = \frac{10(1 - \epsilon)^{0.5}}{\left[1 + \frac{0.00102 + 0.047L^{0.80}}{Re_p^{(0.33 + 0.40L^{9.33})} D_p^{(1.23 - 0.57L^{0.23})}}\right]^2}$$

The redefined values of h, for all of the runs in which the bundles were in the most expanded arrangement, were then substituted into Nu_p, the corresponding fin height and physical properties were also substituted into the equation, and the results for each run were plotted on Figure 53. It can be seen in this figure that the experimental data fit the correlation equation to within plus or minus 15%.

If this correlation were to be used for preliminary design calculations for a fluidizing system, it would be difficult to estimate a correct value for the particle fraction, $(1 - \epsilon)$, if no experimental data for the system were available. The particle fraction was measured for each run made in this study, and the average values for the 3 particle diameters and for the different air mass velocities are shown in figure 54. The total range of the particle fraction is 0.500 to 0.580, with corresponding square roots of 0.707 and 0.762. Since there is relatively little spread between the two extreme values of the square root, it was felt that the arithmetic average of the two, which is equal to 0.734, could be substituted into the equation so that $10(1 - \epsilon)^{0.5}$ could be held constant at 7.34.

The redefined values of h for all of the same runs were then substituted into this modified correlation equation, and the results are shown in Figure 55. There is very little difference in the position of the points in Figures 53 and 55, indicating that using a constant for $10(1 - \epsilon)^{0.5}$ does not noticeably affect the accuracy of the correlation.



$$\left[1 + \frac{0.00102 + 0.047L^{0.80}}{Re_p^{(0.33 + 0.40L^{9.33})} D_p^{(1.23 - 0.57L^{0.23})}}\right]^2$$

FIGURE 53. CORRELATION FOR EXPANDED BUNDLES, WITH VARIABLE $(1-\epsilon)$

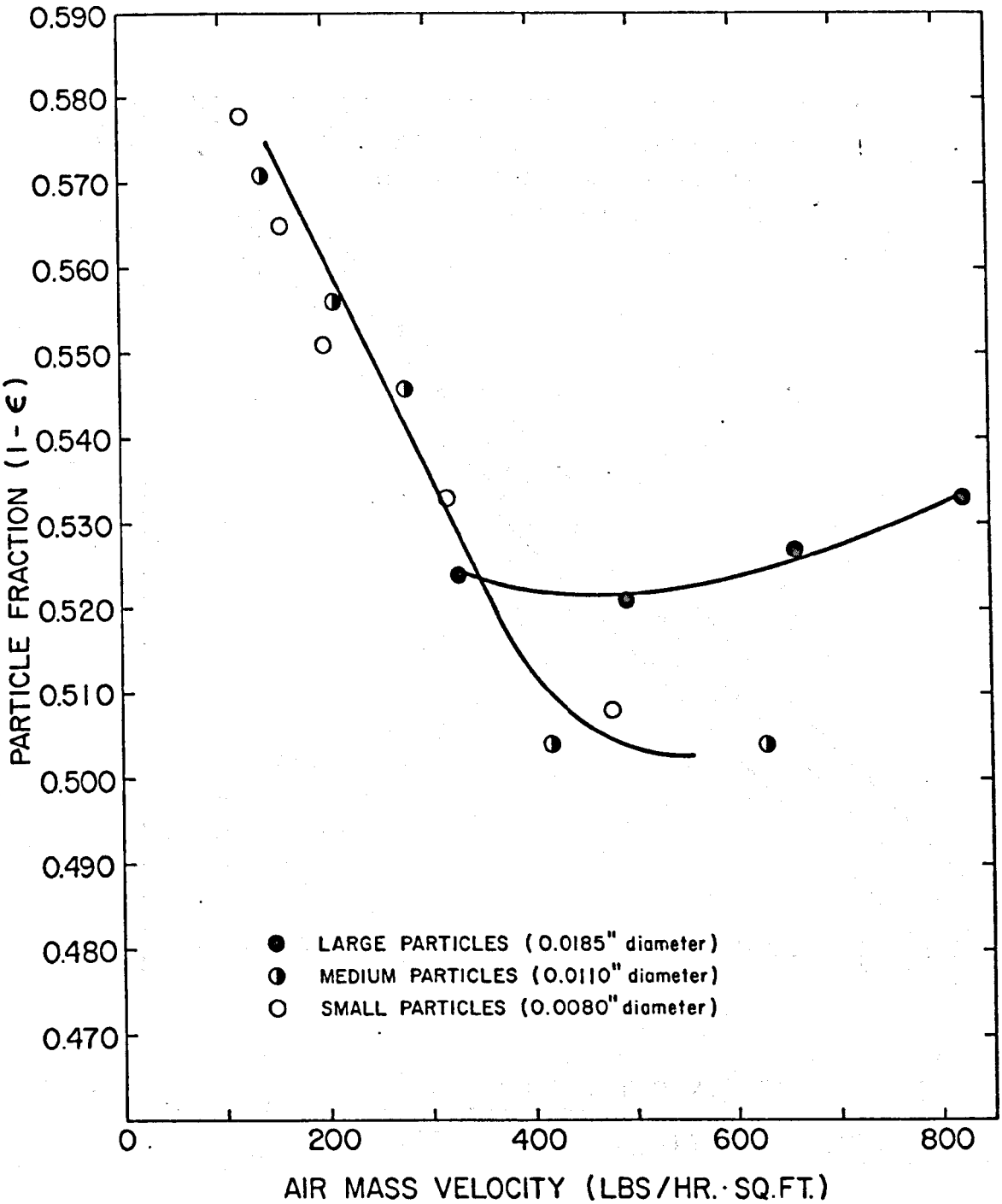
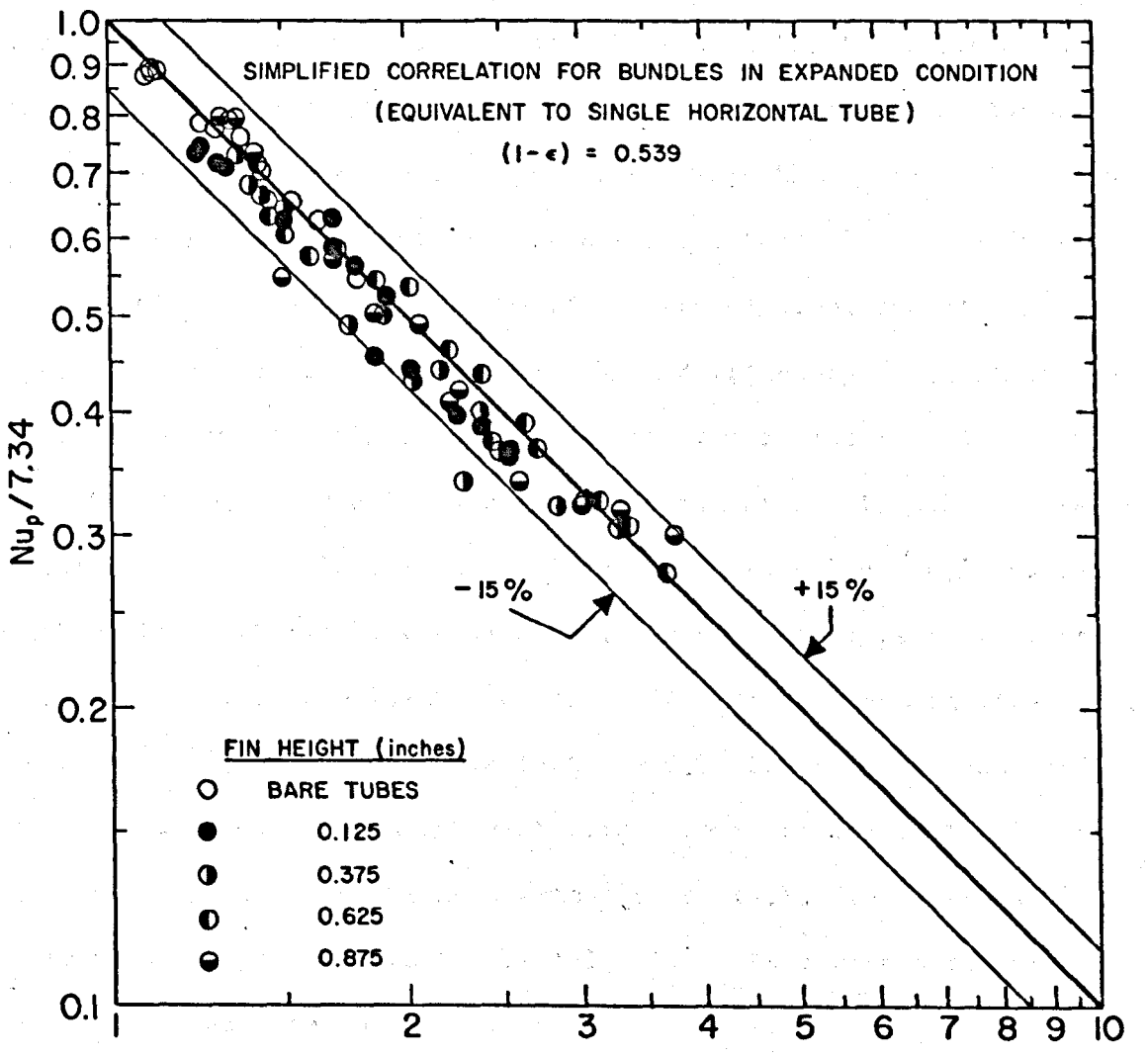


FIGURE 54. AVERAGE OF (1 - ϵ) VALUES MEASURED IN THIS STUDY



$$\left[1 + \frac{0.00102 + 0.047L^{0.80}}{Re_p^{(0.33 + 0.40L^{9.33})} D_p^{(1.23 - 0.57L^{0.23})}}\right]^2$$

FIGURE 55. CORRELATION FOR EXPANDED BUNDLES, WITH CONSTANT (1-ε)

The experimental values of $q/\Delta T$ for a single horizontal finned tube, obtained by Bartel, Genetti, and Grimmett at the Idaho Nuclear Corporation, were compared to the modified correlation by first redefining the h values with the use of Figure 52. The redefined h values and the corresponding values for the physical properties were then substituted into the modified correlation equation. It was found that all of the data points were within plus or minus 45% of the correlation, except for the data points from the 0.5" finned tube, which deviated by 75%. It is believed that the data obtained in this report is more accurate than that obtained in Idaho, because in this investigation each data point represents the average of 7 individual horizontal tubes, while the Idaho data were taken with a single horizontal tube. When the average of 7 tubes is used, much of the experimental error, and error inherent in each tube, is "averaged out". It is probable that the 0.5" finned tube mentioned above had an abnormally high inherent error, possibly due to the thermocouple attachment or to the heater-to-tube contact. The error would probably have been noticeable immediately if the tube were used with 6 other tubes as was done in this study.

Final Correlation:

As was mentioned previously, the correlation shown in Figure 53 and the modified correlation shown in Figure 55 apply only when the tubes are spaced far enough apart so that they are performing as 7 independent horizontal tubes. To make the correlation as general as possible, to include the heat transfer data for all tube spacings, it is necessary to introduce a correction factor to account for the decrease in the heat transfer coefficients as the tubes are moved closer together.

This correction factor was developed by cross-plotting various parameters against fin height, tube spacing, and fluidizing velocity in a manner similar to that described on pages 134 and 135. It was observed that the correction factor was not too strongly dependent upon the fluidizing velocity, so this factor was eliminated for the sake of simplicity, and the final expression for the correction factor is as follows:

$$\text{Correction Factor} = \left[1 - \frac{0.027 + 4.3L^{1.5}}{P(1.12 + 3.2L^{0.6})} \right]$$

where,

L = fin height, inches

P = center-to-center distance, inches

(P is defined on pages 73 and 74)

It can be seen that as P increases, the right-hand term in the brackets decreases, and the value of the correction factor approaches unity. The effect of increasing L is not so clear, but substituting various values of L into the equation for a given P value also results in a decrease in the right-hand term, so the correction factor again approaches unity. This is compatible with what was found experimentally, where the heat transfer coefficient was found to be relatively insensitive to tube spacing for long fins, but fairly sensitive for short fins.

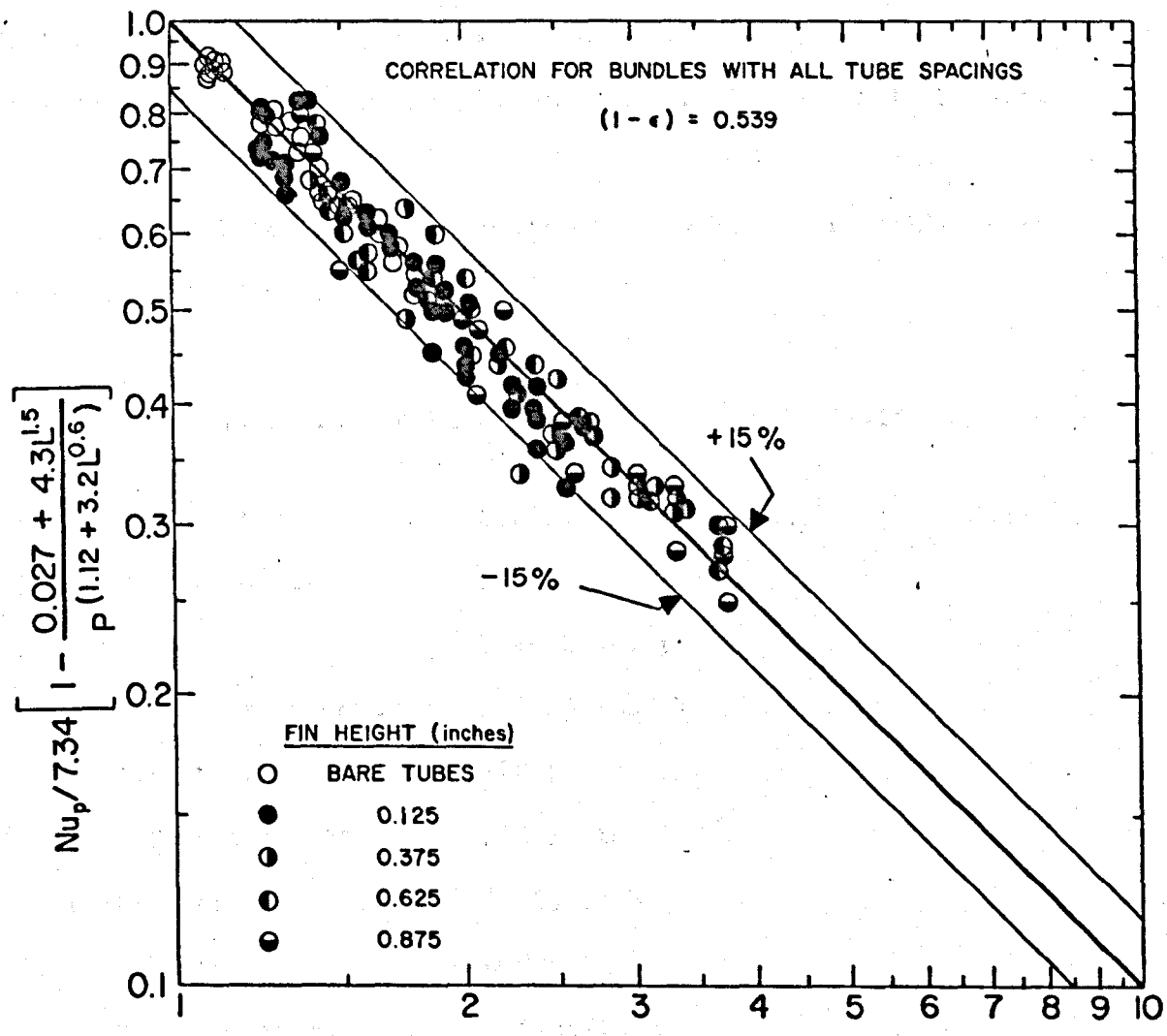
The final correlation equation, including correction factor, is shown below:

$$Nu_p = \frac{10(1-\epsilon)^{0.5}\left[1 - \frac{0.027 + 4.3L^{1.5}}{P(1.12 + 3.2L^{0.6})}\right]}{\left[1 + \frac{0.00102 + 0.047L^{0.80}}{Re_p(0.33 + 0.40L^{9.33})D_p(1.23 - 0.57L^{0.23})}\right]^2}$$

where L, D_p, and P are all expressed in inches.

As shown previously, the constant 7.34 can be substituted into the equation in place of $10(1-\epsilon)^{0.5}$ with no noticeable change in the accuracy of the correlation.

In Figure 56, Nu_p divided by the numerator in the above equation is plotted against the denominator. This leads to a straight line plot with slope of minus one, as was the case in Figures 53 and 55. It is



$$\left[1+\frac{0.00102+0.047L^{0.80}}{Re_p^{(0.33+0.40L^{9.33})}D_p^{(1.23-0.57L^{0.23})}}\right]^2$$

FIGURE 56. CORRELATION FOR BUNDLES WITH ALL TUBE SPACINGS

interesting to note that the introduction of the correction factor and the inclusion of all of the experimental data into the correlation did not expand the accuracy limits on the correlation, since most of the points are still within the plus or minus limits shown in Figures 53 and 55.

Table 2 below gives the range of experimental variables over which the correlation applies:

Table 2. Range of Correlation Applicability

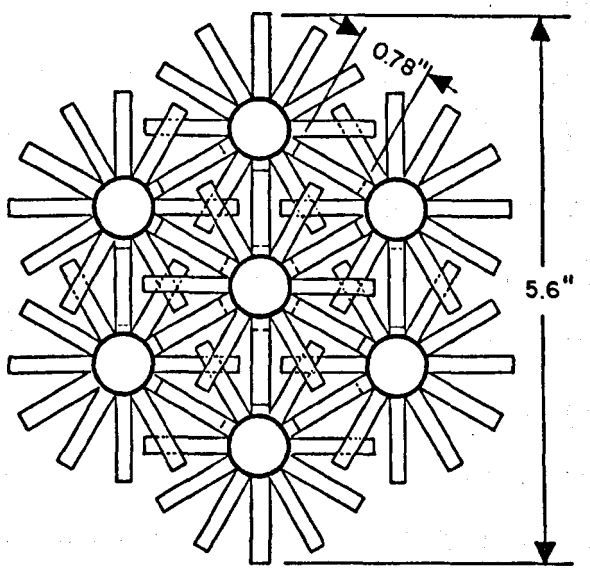
Variable	Range
Particle diameter	0.008, 0.011, and 0.0185 inch diameter
Fluidizing velocity	120 to 825 Lbs/Hr-Ft^2
Fin height	bare tubes to 0.875 inch
Center-to-center spacing	1.0625 to 4.7813 inches
Bed temperature	120°F to 220°F
Tube surface temperature	150°F to 250°F
Tube diameter	0.625 inch
Fin thickness	0.025 inch
Fin spacing on tube	8 fins/inch

MISCELLANEOUS RELATED STUDIES

Optimum Fin Length for an Overall Available Diameter

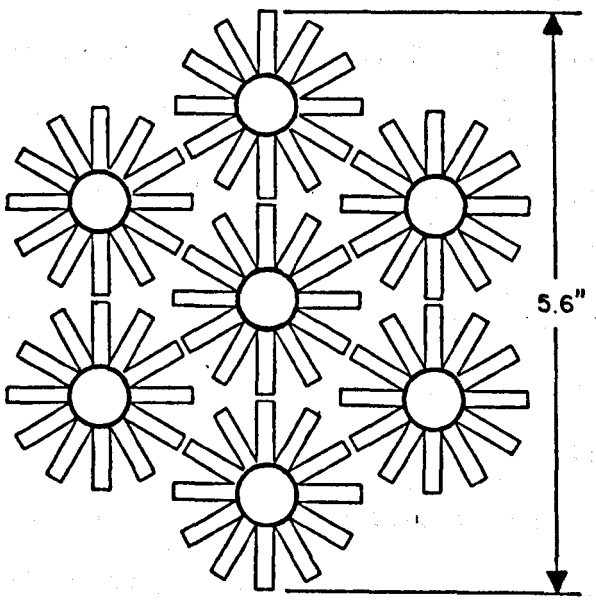
A study was made to provide information for determining how fin length and tube spacing should be selected to maximize the rate of heat transfer from a bundle of tubes contained within a restricted overall diameter. Such a situation might arise in an industrial design study where the volume or diameter available for the tubes is restricted by the column diameter or by some other geometric consideration unique to the particular design.

It was assumed in this study, for purposes of comparison, that a bundle of 7 horizontal finned tubes would be used, and that the overall diameter of the bundle could not exceed 5.6". Data had previously been obtained with 0.625" finned tubes with 0.25" between fin tips; the overall diameter for such a bundle is about 5.6". The 7 available 0.875" finned tubes were meshed tightly together so that the fins on adjacent tubes overlapped by 0.78"; this bundle also had an overall diameter of about 5.6". For this latter bundle, heat transfer data were obtained with particle diameters of 0.0080" (small particles) and 0.0110" (medium particles). The values of $q/\Delta T$ for various air velocities were then compared for the two bundles at the same operating conditions. The comparison is shown in Figure 57. It can be seen in this figure that the rate of heat transfer with the 0.625" finned tube bundle is greater than



0.875 INCH FINS

G/G_{mf}	$q/\Delta T$ PARTICLE DIAMETER 0.008	0.011
2	—	15.0
3	16.6	16.2
4	17.2	17.9
5	17.6	—
6	—	18.7
8	19.5	—
12	20.4	—



0.625 INCH FINS

G/G_{mf}	$q/\Delta T$ PARTICLE DIAMETER 0.008	0.011
2	—	20.2
3	20.7	22.5
4	21.5	23.0
5	22.2	—
6	—	24.0
8	23.7	—
12	24.2	—

FIGURE 57. COMPARISON OF RATE OF HEAT TRANSFER IN A RESTRICTED OVERALL DIAMETER

the rate with the meshed 0.875" finned tube bundle for every air velocity with both particle sizes. It is clear that the increased area with the 0.875" finned tube bundle is offset by the decrease in particle mobility. In fact, the center tube in the meshed bundle exhibited heat transfer coefficients that were between 20% and 30% lower than the average of the other 6 tubes for both particle diameters. This was the only bundle studied in which the heat transfer coefficient of any tube in the bundle was consistently different, by a large amount, from the other tubes in the bundle. This was also about twice the previous largest difference in the measured heat transfer coefficient between any two tubes in a bundle. So, for this particular problem, the 0.625" finned tube bundle would be more effective in transferring heat.

There are other optimization problems, however, that are not so straightforward. A real life optimization problem also requires economic and maintenance considerations. It is therefore difficult to discuss optimization in a general manner, unless the ground rules, including all costs and maintenance requirements, are well defined. For example, in the problem discussed above, the 0.625" finned tube bundle was shown to produce a higher heat transfer rate than the meshed 0.875" finned tube bundle. However, if the bundle is not restricted to 7 tubes, it would be possible to place 9 tubes with fin height of 0.625" in the 5.6" by 5.6" envelope, with 3 rows of 3 tubes per row. Also, 16 tubes with fin height of 0.375" (in 4 rows of 4 each) or 36 tubes with fin

height of 0.125" (in 6 rows of 6 each) could be placed in the same envelope.

The trade-off to be considered in optimizing the number of tubes and height of the fins is as follows:

1. As fin height increases, the effectiveness of the fins decreases.
2. As fin height decreases, the area decreases. This factor, however, is somewhat offset by the fact that in decreasing the fin height it may be possible to place more tubes in the envelope, and this will again increase the area.

As an approximation, the maximum rate of heat transfer, for a given envelope, can be found by using the following procedure:

1. Draw the available envelope.
2. Draw in the tubes with various fin heights and place as many tubes as possible in the envelope for each fin height. It may be possible to increase the number of tubes in the envelope by mixing tubes with short fins in between tubes with long fins.
3. Find the total area for each tube bundle.
4. Multiply the area by the effectiveness factor for the fins as shown in Figures 45 and 46 on pages 114 and 115.
5. The bundle configuration which produces the highest product of

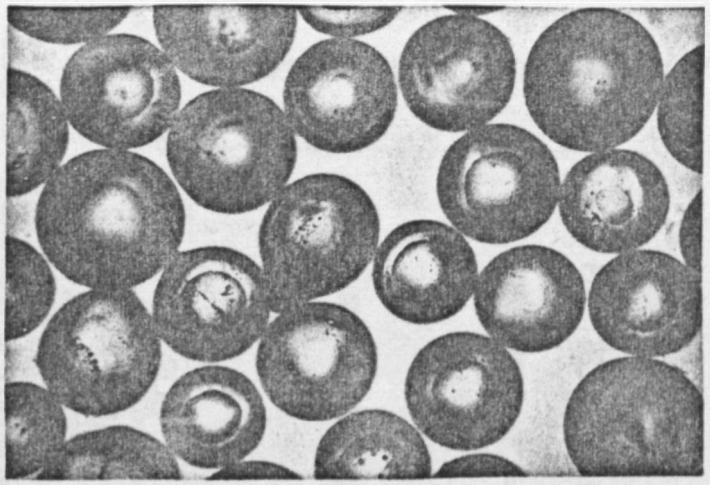
area times effectiveness factor will be the the configuration that will provide the highest rate of heat transfer for the envelope.

As was mentioned previously, however, the cost of the finned tubes, the length of time they are expected to be used, and other economic factors would have to be known before a complete optimization could be performed.

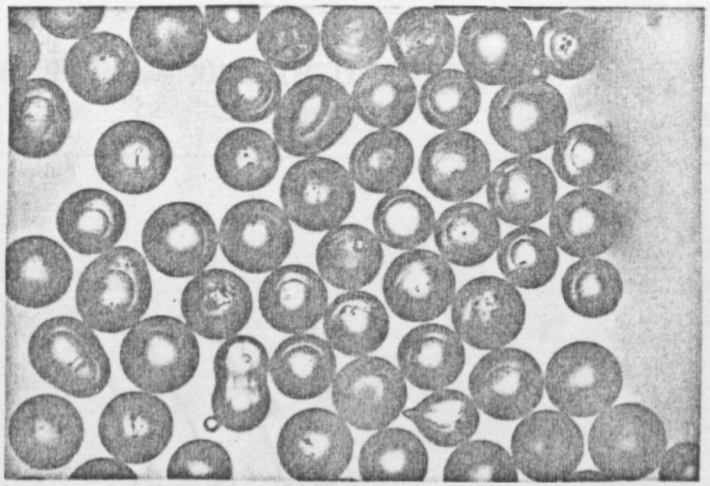
Effect of Particle Surface Area on Heat Transfer Coefficients

A study was made to check the model depicted on page 120, where a particle moves adjacent to the hot surface, absorbs energy by convection from the fluid near the surface, and then returns to the bulk of the bed. It was felt that this theoretical mechanism could be checked by fluidizing high silica sand particles in place of glass beads. If the sand particles had the same physical properties as the glass, the additional surface area on the sand particles should produce an increase in the heat transfer coefficient.

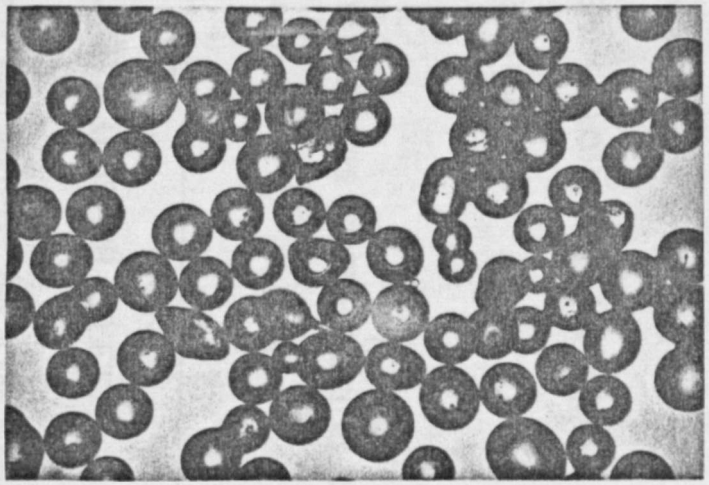
Ottawa sand, which is pure quartz sand mined near Ottawa, Illinois, was obtained and screened. It was found that the size distribution was identical to that of the 0.0110" diameter glass beads. Photomicrographs of all of the glass particles used in this study, and of the Ottawa sand, are shown in Figure 58. Heat transfer coefficients for Ottawa sand used with 0.375" finned tubes are shown in Figure 59.



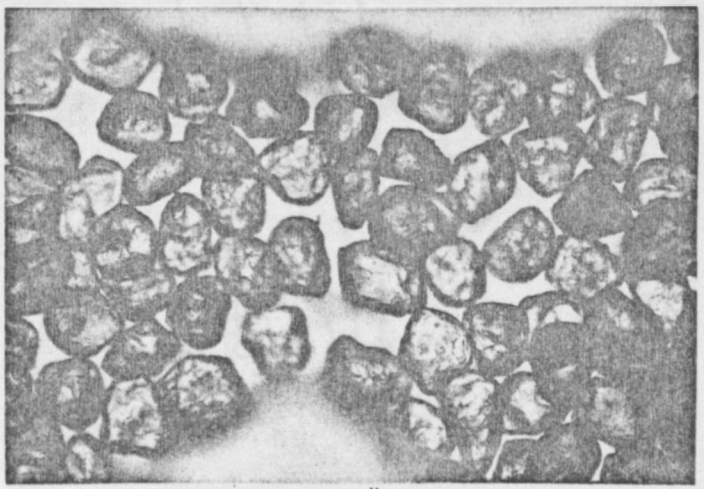
LARGE PARTICLES - 0.0185" NOMINAL DIAMETER



MEDIUM PARTICLES - 0.0110" NOMINAL DIAMETER



SMALL PARTICLES - 0.0080" NOMINAL DIAMETER



SAND PARTICLES - 0.0110" NOMINAL DIAMETER

FIGURE 58. PHOTOMICROGRAPHS OF PARTICLES

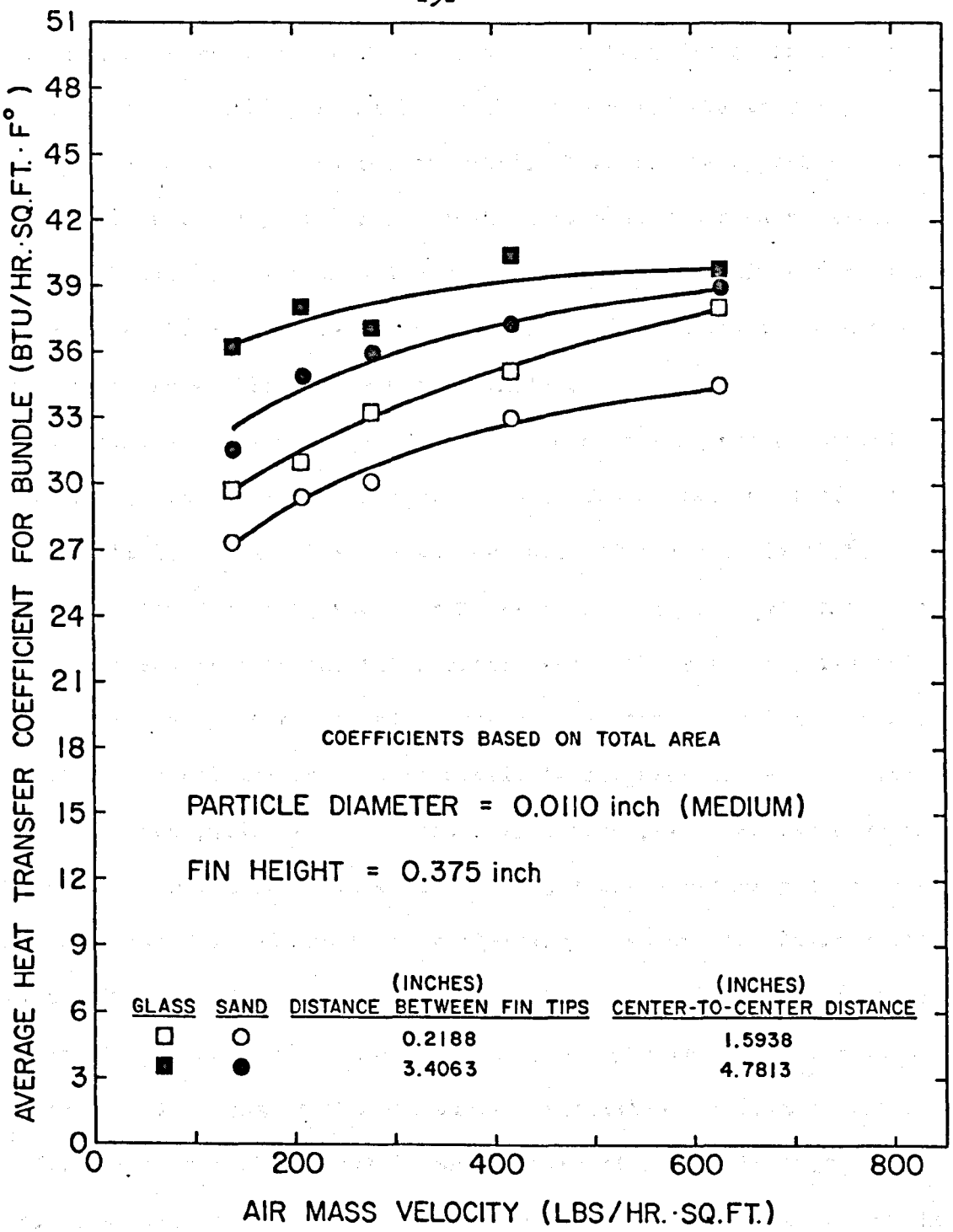


FIGURE 59. COMPARISON OF COEFFICIENTS FOR SAND PARTICLES AND GLASS PARTICLES

It can be seen in Figure 59 that the heat transfer coefficients with sand were about 10 percent lower than the coefficients for glass at all of the air velocities investigated. This is the opposite of what was expected, and the probable explanation is that the sand particles are more cubical in shape than the glass beads, and therefore the sand particles pack together more closely and reduce the total surface area of the particles available for heat transfer.

For example, consider a glass bead of diameter D_p and a cubical sand particle with edge length equal to D_p. The surface area of the glass bead is $3.14D_p^2$, while the surface area of the cube is $6D_p^2$. However, during fluidization, when the spheres are packed together in the laminar film adjacent to the hot surface, each sphere touches its neighboring spheres at only one point of contact, so that almost the entire surface area of all the spheres is available for heat transfer. With the cubical sand particles, however, neighboring particles may have one or more faces in contact with a given cube, thereby reducing or eliminating heat transfer between these contacting faces and the laminar film. In fact, if the sand particles were perfect cubes, it would be possible for five of the faces of a cube to be covered by neighboring cubes, with just the face in front of the hot surface available for heat transfer. Therefore, even though the total surface area of a cube is $6D_p^2$, the actual area available for heat transfer may easily be reduced below the area of an equivalent sphere. Though the shape of the sand particles

in not actually cubical, this type of argument still applies, since it can be seen in Figure 58 that the sand particles do have flat surfaces which can come into contact with each other during fluidization and reduce the amount of surface area free for heat transfer by convection in the laminar film.

This type of explanation can also be used to explain why there was a large increase in the rate of heat transfer in going from the large glass particles to the medium particles, but relatively little difference in the rate between the medium particles and the small particles. The explanation given for this on page 70 was that the small particles sometimes cling together by van der Wall interparticle adhesive forces, producing an effective diameter larger than the actual particle diameter. However, the theory of particle packing postulated in the paragraph above might be considered a complementary or alternate theory to explain why small particles sometimes produce coefficients that are about the same as those produced by larger particles. For simplification, consider a case where the laminar film at the hot surface is the same thickness as the diameter of a large particle. Then, consider the case where particles with diameter of one-half of the large particle diameter are packed into the same film thickness. In this second case the total surface area of the particles will be greater than that for the large particles, but the volume of the air pockets between the spheres will be less. However, the air pockets are still large enough to allow heat

transfer by convection, so the increased area effect predominates and the heat transfer coefficient will increase. If, however, the diameter of the particles is again cut in half, the surface area will again increase, but the air pockets between the spheres will now become very small and will greatly reduce the effectiveness of the convective currents. Therefore, the effect of increased surface area may only balance out the effect of decreased convection, and result in heat transfer coefficients that are the same as those for particles with twice the diameter. If the particle diameter is reduced further, the heat transfer coefficients may become smaller than the coefficients for larger particles.

The results of this second miscellaneous related study did not achieve the purpose for which it was intended, that is, to check the proposed mechanism of heat transfer, because in using sand particles another variable was introduced into the model, namely the effect of particle shape on the particle packing characteristics at the hot surface. However, it does indicate that the heat transfer coefficient is not too sensitive to particle shape, since there was only 10 percent difference between the glass and the sand at the same operating conditions. This small difference between the two types of particles makes it appear that the final correlation on page 142 can be applied to particles with an irregular shape also, since the accuracy limits on the correlation are plus or minus 15 percent. It appears that the way to

check the proposed mechanism of heat transfer is to measure heat transfer coefficients with smooth spheres of some material, and then to measthe coefficients with porous spheres of the same material. The physical properties and packing arrangement of the two types of spheres would be the same, and the difference in the magnitude of the heat transfer coefficients would then indicate the effect of the surface area of the particles on the coefficient.

CONCLUSIONS

In the Experimental Program it was stated that the primary objective of this study was to determine the effect of fin height, tube spacing, particle diameter, and fluidizing air velocity on the heat transfer coefficient of each tube in a horizontal bundle of 7 serrated, or discontinuous, finned tubes. However, in all of the runs made in this investigation the magnitude of the heat transfer coefficients for all tube positions in the bundle were within 15 percent of each other as long as there was at least 0.25" clearance between fin tips of adjacent tubes. Also, there was no consistent trend to indicate that the coefficient of any particular tube was different from the other tube coefficients because of the position of the tube in the bundle. Thus, it can be concluded that the heat transfer coefficient of any tube in a horizontal bundle in a fluidized bed is independent of the tube position in the bundle as long as there is some clearance between fin tips of adjacent tubes, as long as all of the tubes are sufficiently far from the walls of the column to avoid the "wall effects" caused by the different fluidizing patterns near the walls, and provided that all of the tubes are within the static bed and are covered with particles before fluidization is begun. Therefore, in comparing the performance of the various tube bundles, the arithmetic average of the 7 tube coefficients was used, and it was assumed that the differences in the individual tube coefficients

were caused by experimental errors or by inherent errors resulting from the method of thermocouple attachment to the tubes or from slight differences in the heater-to-tube contact for the 7 tubes.

An analysis of the various plots of experimental data presented in this report leads to the following conclusions concerning the effect of the 4 experimental variables on the heat transfer coefficients of the bundles studied:

Fin Height: The rate of heat transfer from the bundle increases with increasing fin height, but the rate of increase becomes less with longer fins, and the curves of $q/\Delta T$ versus Fin Height level off near a fin height of about 1 inch. Thus, there is little additional increase in the rate of heat transfer if the fin height is made longer than 1 inch. This effect also shows up clearly on the plots of Fin Effectiveness Factor versus Fin Height where it can be seen that the effectiveness of the fin in transferring heat decreases rapidly as the fin height approaches 1 inch.

Tube Spacing: In the investigation of the effect of tube spacing on the rate of heat transfer, it was found that the arithmetic average heat transfer coefficient for the bundle of bare tubes was independent of tube spacing if the distance between adjacent tube surfaces was about 1.5 inches or more. When the tubes were clustered closer than this distance, there was a decrease in the average coefficient.

With finned tubes, the change in the average coefficient with tube spacing depends upon the length of the fins. With short-finned tubes, the average coefficient for the bundle is sensitive to the spacing between tubes for the first inch between adjacent tube fin tips. After the fin tips are about 1 inch apart there is very little change in the average coefficient as the tubes are moved farther apart. With long-finned tubes, the average coefficient for the bundle is quite insensitive to tube spacing even in the first inch of tube movement. This behavior is most noticeable on the curves of $q/\Delta T$ versus Fin Height. It can be seen on these curves that $q/\Delta T$ for the longest fins (0.875") is about the same whether there is 0.28" or 2.4" between fin tips, while with the shortest fins (0.125") $q/\Delta T$ increases by about 40% when the distance between fin tips is increased from 0.19" to 2.3". This phenomena was explained by comparing the resistances to particle movement with the resistances encountered by molecules in a simple kinetic model.

Particle Diameter: In the study of the effect of particle diameter on the heat transfer coefficient it was found that the average heat transfer coefficient for the bundle increased by 25% to 50% when the particle diameter was decreased from 0.0185 inch to 0.0110 inch for all of the bundles investigated. However, the increase was less than 15% when the particle diameter was reduced from 0.0110 inch to 0.0080 inch.

Fluidizing Air Velocity: With both bare tubes and finned tubes the heat transfer coefficient generally increased with increasing air velocity. However, in some instances the coefficient reached a maximum value and then decreased with an additional increase in air velocity. The presence of a maximum value was explained by noting that there are two opposing conditions which arise as the air velocity is increased; the particle circulation increases with a resulting increase in the heat transfer coefficient, but the particle fraction in the vicinity of the bundle decreases as the bed expands with higher air velocities, and this produces a decrease in the coefficient. The product of these two factors sometimes leads to a maximum value in the plot of Average Heat Transfer Coefficient versus Air Mass Velocity, while at other times the curves are monotonically increasing or decreasing.

In correlating the experimental data to a theoretically developed model it was found that almost all of the data points fit the correlation within plus or minus 15% and that the correlation was quite insensitive to the particle fraction, $1 - \epsilon$. There was very little effect on the accuracy limits when the experimentally measured constant 7.34 was substituted into the correlation for the term $10(1 - \epsilon)^{0.5}$ as shown in the final correlation on page 142. This experimental constant is in close agreement with the theoretically developed value of 7.2 shown on page 15.

In the first miscellaneous related study the optimum fin length and tube spacing for a fixed overall space envelope was discussed. No quantitative values can be presented until all requirements for a given system are known, but a preliminary procedure involving the product of the total heat transfer area and the fin effectiveness factor will provide fairly accurate values for the optimum fin height and tube spacing. It was also found in this study that meshing the finned tubes closely together by overlapping the fins on adjacent tubes will lead to a decrease in the heat transfer coefficient of the center tube, and will also result in a lower rate of heat transfer from the bundle than in the case where there is a small amount of clearance between the tips of the fins on adjacent tubes.

In the second related study an attempt was made to determine the effect of particle surface area on the heat transfer coefficients by fluidizing sand particles in place of the glass beads. The study did not achieve the desired purpose because in using sand the variable of particle packing was introduced into the model. That is, since the sand particles are more cubical in shape, they can pack together more tightly and reduce the total amount of particle surface area available for heat transfer. However, the study did provide an explanation of why the coefficient increased a large amount in going from the large particles to the medium particles, while there was a relatively small change between the medium particles and the small particles.

RECOMMENDATIONS FOR FURTHER STUDY

1. It is hoped that the correlation developed in this study will be a start toward a more general correlation that will relate the heat transfer coefficient not only to the four variables studied here, but also to parameters such as tube diameter, fin spacing on the tube, fin thickness, and possibly other fin geometries (tapered fins, pin fins, etc.). Also, although it is convenient to work with glass particles, it is important that heat transfer with particles of different composition be investigated so that the correlation may be applied directly to industrial design problems in which coke, catalyst pellets, or similar materials are encountered. In short, the correlation developed in this study is of limited applicability because of the restrictions on fin thickness, fin spacing on the tube, and particle composition, and a great deal of additional study is needed to produce a general, widely applicable, correlation which will be of value in real life industrial fluidized bed heat transfer problems.

2. It was mentioned in the Experimental Program that serrated fin tubes were chosen instead of continuous helically wound fin tubes because it was felt that the openings between the serrated fins would allow greater particle movement and higher heat transfer coefficients. For comparison, a bundle of continuous helically wound fin tubes should be assembled, and heat transfer coefficients should be measured at

operating conditions identical to those used in this study with fins of the same height. The relative magnitude of the coefficients for the two types of fins might provide data which could be used to improve the design of the fins to increase the heat transfer coefficients.

For example, with short fins the fin effectiveness factor is large, so the rate of heat transfer may be increased if continuous helically wound fins are used. The separation between the fins would be eliminated and there would be more interference with particle movement, but the increase in the surface area might offset the increased particle interference and lead to a higher rate of heat transfer.

On the other hand, with long fins the effectiveness factor near the fin tips is very small, so the rate of heat transfer might be increased by tapering the fins from the present width near the center tube to almost a point at the fin tip. This would remove a lot of surface area, but most of the area would be removed near the fin tip where the effectiveness factor is small. The increased particle circulation caused by the larger separation between the fins might then offset the loss in area and produce a higher rate of heat transfer.

3. A variety of experiments can be performed in which simultaneous heat and mass transfer take place in the fluidized bed. A comparison of the rates of heat transfer and mass transfer will provide information for checking existing theoretical models, or for developing new models.

BIBLIOGRAPHY

1. Baddour, R.F. and C. Y. Yoon, Chem. Eng. Progr. Symp. Series, 32, 35(1961).

2. Bartel, W.J., W. E. Genetti, and E. S. Grimmett, to be published.

3. Botterill, J. S. M., R. Chandrasekhar, and M. van der Kolk, Fundamental Processes in Fluidized Beds, A. I. Ch. E., 66(1970).

4. Botterill, J. S. M., J. S. George, and H. Besford, Chem. Eng. Progr. Symp. Series, 62, (62), 7(1966).

5. Brötz, W., Chem.-Ing.-Tech., 28, 165, (1956).

6. Davidson, J. F. and D. Harrison, Fluidized Particles, Cambridge University Press, New York, 1963.

7. Dow, W. M. and M. Jakob, Chem. Eng. Progr., 47, 637(1951).

8. Genetti, W. E. and J. G. Knudsen, I. Chem. Eng. Symp. Series, 30, 147(1968).

9. Hiraki, I., K. Yoshida, and D. Kunii, Kagaku Kogaku (Chem. Eng. Japan), 29, 846(1965).

10. Kearns, D. L., Westinghouse Research Laboratories, Pittsburgh, Pa.

11. Kobayashi, H., F. Arai, and T. Chiba, Kagaku Kogaku (Chem. Eng. Japan), 29, 858(1965).

12. Kondukov, N. B. and collaborators, Intern. Chem. Eng., 4, 43(1964).

13. Kunii, D. and O. Levenspiel, Fluidization Engineering, John Wiley and Sons, Inc., New York, 1969.

14. Leva, M., Fluidization, McGraw-Hill Book Co., New York, 1959.

15. Leva, M., M. Weintraub, and M. Grummer, Chem. Eng. Progr., 45, 563(1949).

16. Levenspiel, O. and J. S. Walton, Chem. Eng. Progr. Symp. Series, 50, (9), 1(1954).

BIBLIOGRAPHY (Continued)

17. Mickley, H. S. and D.F. Fairbanks, A. I. Ch. E. Journal, 1, 374(1955)

18. Mickley, H. S., T. K. Sherwood, and C. E. Reed, Applied Mathematics in Chemical Engineering, McGraw-Hill Book Co., New York, 1957

19. Nazemi, A., E. B. Lancaster, and T. D. Wheelock, Fluidization Fundamentals, A. I. Ch. E., 15g(1970).

20. Parent, J. D., N. Yagol, and C. S. Steiner, Chem. Eng. Progr., 43, 429(1947).

21. Perry, J. H., Chemical Engineers' Handbook, 3rd Edition, McGraw-Hill Book Co., New York, 1950.

22. Petrie, J. C., W. A. Freeby, and J. A. Buckham, Chem. Eng. Progr., 64, 51(1968).

23. Rowe, P. N. and B. A. Partridge, Proc. Symp. on interaction between fluids and particles, Inst. Chem. Engrs., 135, June 1962.

24. Toei, R., R. Matsuno, H. Ishii, and H. Kojima, Kagaku Kogaka (Chem. Eng. Japan)29, 851(1965).

25. Vreedenberg, H. A., Chem. Eng. Science, 9, 52(1958); 11, 274(1960).

26. Weast, R. C., Handbook of Chemistry and Physics, 49th Edition, The Chemical Rubber Co., 1968.

27. Ziegler, E. N. and W. T. Brazelton, Ind. Eng. Chem. Fundamentals, 3, 94(1964).

28. Ziegler, E. N., L. B. Koppel, and W. T. Brazelton, Ind. Eng. Chem. Fundamentals, 3, 324(1964).

29. Fluid Meters - Their Theory and Operation, 5th Edition, A.S.M.E., 1959.

NOMENCLATURE

Symbol	Definition	Dimension
a, b, c	functions of fin height in correlation equation	various dimensions
A	surface area of tube and fins	ft^2
A_c	inside cross-sectional area of column	ft^2
C	coefficient of discharge	dimensionless
C_{ps}	specific heat of solids	BTU/lb-F°
c_p	heat capacity at constant pressure	BTU/lb-F°
c_v	heat capacity at constant volume	BTU/lb-F°
D_p	mean particle diameter	ft or inch
D_t	tube diameter	ft or inch
G	air mass velocity	$lbs/hr-ft^2$
G_{mf}	air mass velocity at minimum fluidizing conditions	$lbs/hr-ft^2$
g	gravitational constant, 4.18×10^8	ft/hr^2
g_c	dimensional constant	lb_m-ft/lb_f-sec^2
h	heat transfer coefficient	$BTU/hr-ft^2-F°$
h_b	heat transfer coefficient for bare tubes at same operating conditions as for finned tubes	$BTU/hr-ft^2-F°$
k	thermal conductivity of fin	BTU/hr-ft-F°
k_{air}, k_f	thermal conductivity of fluidizing gas at bed temperature	BTU/hr-ft-F°
k_r	ratio of c_p/c_v	dimensionless
L	fin height	inches

NOMENCLATURE (Continued)

Symbol	Definition	Dimension
L_t	distance between pressure taps	ft
Nu_p	particle Nusselt number = hD_p/k_{air}	dimensionless
P	center-to-center distance	inches
p_1	pressure upstream of orifice	lb/ft^2
p_2	pressure downstream of orifice	lb/ft^2
ΔP	pressure drop in bed between two pressure taps	lb/ft^2
q	rate of heat transfer	BTU/hr
N_{Pr}	Prandtl number for fluidizing air	dimensionless
Re_p	particle Reynolds number = D_pG/μ_f	dimensionless
S	distance between fin tips	inches
S_c	cross-section area of orifice opening	ft^2
T	temperature	^oF
T_{bed}, T_b	bed temperature	^oF
T_f	temperature of fluid near surface wall	^oF
T_L	temperature at tip of fin	^oF
$T_{lower\ bed}$	temperature near bottom of static bed	^oF
$T_{middle\ bed}$	temperature near middle of static bed	^oF
$T_{upper\ bed}$	temperature near top of static bed	^oF
T_w, T_{tube}	temperature on outer surface of tube	^oF
$\bar{t}$	mean residence time of solids on surface	hr

NOMENCLATURE (Continued)

Symbol	Definition	Dimension
u_b	velocity of bubble rising through a bed	ft/sec
u_e	velocity of gas through the emulsion phase	ft/sec
u_{mf}	superficial fluid velocity at minimum fluidizing conditions	ft/sec
u_s	mean downward velocity of solids in the emulsion phase	ft/sec
V	potentiometer reading	millivolts
w_1	fin width, 0.156 inch	
w_2	fin thickness, 0.025 inch	
Y	expansion factor	dimensionless
β	ratio of orifice diameter to inside pipe diameter	dimensionless
ϵ_{mf}	void fraction in the bed at minimum fluidizing conditions	dimensionless
$(1 - \epsilon)$	particle fraction	dimensionless
θ	$(h/kw_1w_2)\left[2(w_1 + w_2)\right]$	$1/ft^2$
μ	viscosity of fluidizing gas at bed temperature	centipoises
μ_f	viscosity of fluidizing gas at bed temperature	lbs/hr-ft
ρ_1	density at upstream temperature and pressure	lbs/ft^3
ρ_F	density of fluidizing gas at bed temperature	lbs/ft^3
ρ_s	density of solids	lbs/ft^3
ϕ	effectiveness factor	dimensionless

MONTANA STATE UNIVERSITY LIBRARIES
stks D378.B28
Heat transfer from a horizontal bundle o
3 1762 00186231 5
RL

[redacted]
D378 Bartel, William J
B28 Heat transfer from a
cop.2 horizontal bundle of
tubes in an air
fluidized bed

NAME AND ADDRESS
APR 18 197[illegible] Kurt Greis - 3 4/12 Hang Loan

[redacted]
D378
B28
Cop. 2